

Organic Superconductors

Michael Lang and Jens Müller

1 Introduction

Over the past twenty years the research on organic conductors has developed into a most active branch of modern condensed-matter physics. The main difference of molecular conductors compared to conventional metals is that the former are made up of building blocks constructed from carbon atoms and their combinations with other elements such as sulfur, selenium or oxygen. As a result, when forming a crystal, these molecular units preserve to a large extent their specific features such as the molecular orbitals, the ionization energy and the intramolecular vibrational modes. Molecular materials thus have the potential of providing a flexible building-block system where the physical properties can be tuned by small modifications in the arrangements and bridging of these functional units.

In contrast to the molecular crystals formed by weakly van der Waals-bond neutral entities, organic conductors consist of open-shell molecular units which are the result of a partial oxidation and reduction of the donor and acceptor molecules in the crystal-growth process. It is the unpaired electron residing in the π -molecular orbital (π -hole) of the donor unit which is responsible for the electronic properties of these charge-transfer salts. Due to a π -orbital overlap between adjacent molecules, the π -holes can delocalize throughout the crystal giving rise to metallic conductivity.

The unique chemistry of carbon, which, on the one hand, provides a rich basis of potential organic donor molecules, and the manifold possibilities of combining them with charge-compensating acceptor units, on the other, have enabled the synthesis of an enormous number of conducting organic charge-transfer salts. The geometry of the building blocks and the way they are packed together in the crystal determine the effective dimensionality of the electronic structure of the compound. The planar shape of the TMTSF (tetramethyltetraselenafulvalene) molecule - a derivative of the prototype TTF (tetrathiafulvalene) - permits an infinite stacking of these units in the crystal structure. As a consequence, a significant intermolecular overlap of the π -orbitals occurs only along the stacking axis giving rise to a quasi-one-dimensional conduction band. In contrast, packing of the larger BEDT-TTF (bisethylenedithio-tetrathiafulvalene) molecules often results in a quasi-two-

dimensional electronic structure.

These low-dimensional organic conductors constitute a peculiar class of materials which has gained strong interest among scientists due to the wealth of interesting phenomena that have been observed over the last two decades or so. Above all it was the discovery of superconductivity in pressurized $(\text{TMTSF})_2\text{PF}_6$ by Jérôme et al. in 1979 [1] which created much excitement among both solid-state chemists and physicists. Indeed, this finding was a result of interdisciplinary efforts in synthesizing and characterizing organic conductors - activities which started up in the early 1950's by the pioneering work of Akamatu et al. [2] and which received a fresh impetus in 1964 thanks to the work of Little [3]. He proposed that in a suitably designed one-dimensional conductor embedded in a polarizable medium, superconductivity at high temperatures should be possible. Although it soon became clear that the nature of the superconducting state in the $(\text{TMTSF})_2\text{PF}_6$ salt is of a fundamentally different type from what had been discussed in Little's model, this finding set the stage for the discovery of a large number of conducting charge-transfer salts including up to the latest count, more than 80 superconductors. Many of these systems superconduct even at ambient pressure with the highest T_c value of about 12K received in the quasi-two-dimensional BEDT-TTF-based systems. Besides superconductivity, the organic charge-transfer salts reveal a variety of other interesting collective phenomena including spin-Peierls and density-wave states as well as phases with localized charges and commensurate-type antiferromagnetic order. These states have been found to depend most sensitively on factors such as the acceptor ions, the magnetic field or external pressure.

One of the key features underlying the above phenomena is the low dimensionality of the materials. The confinement of the carrier motion to one or two spatial dimensions together with the low charge-carrier concentration enhance the effect of the interactions between the electrons. Another important feature specific to these molecular systems is a considerably strong coupling of the charge carriers to the lattice degrees of freedom. For molecular crystals, this coupling includes both the interactions with high-frequency intramolecular modes and the low-lying intermolecular vibrations. The present organic metals thus represent ideal model systems for exploring the interplay of strong electron-electron and electron-phonon interactions in reduced dimensions. In particular, the close proximity of superconductivity to a magnetically-ordered state encountered not only in the organic materials but also in other strongly-correlated electron systems such as the heavy-fermion metals and high-temperature superconductors continues to challenge our understanding of superconductivity. While for the latter systems evidence is growing that, indeed, the magnetism and superconductivity are intimately related to each other, the nature of the superconducting state for the present materials is far

from being understood.

The discussion of the superconducting-state properties for the present organic materials is complicated by the existence of contradictory experimental evidences. In some cases, this controversy even encompasses results on the same quantity when the measurements have been carried out by different groups. While about one half of the data seem to support an anisotropic superconducting state, with a *d*-wave order parameter being the most favored one, the other half are consistent with an order parameter which is finite everywhere on the Fermi surface.

Closely related to the issue of superconductivity in the proximity to antiferromagnetic order is the nature of the state above T_c . For the quasi-two-dimensional organic conductors, for example, unusual metallic properties have been observed posing the question whether this phenomenon is related to the equally unusual behavior seen in the other class of quasi-two-dimensional superconductors, the high- T_c cuprates [4].

This article will give an overview on the normal- and superconducting-state properties of organic superconductors. There are a number of review articles on this subject [5–10] - most of them focus on either the quasi-one-dimensional or two-dimensional materials. The intention of the present review is therefore to provide a discussion which covers aspects common to both families on the same footing. Instead of reviewing the whole diversity of behaviors found among the various compounds with all their structural and chemical modifications, we will mainly focus on selected compounds of both families. These are the most extensively studied and best characterized $(\text{TMTSF})_2\text{X}$ and $(\text{BEDT-TTF})_2\text{X}$ salts whose properties are representative for a wide class of materials. Special attention is paid to the more recent developments including the controversial discussions of some aspects, in particular the discussion on the nature and symmetry of the superconducting state.

2 Characteristics of organic charge-transfer conductors

2.1 Molecular building blocks

The prerequisites of forming conducting molecular solids are essentially (i) the creation of unpaired electrons and (ii) their delocalization throughout the crystal. For the organic superconductors discussed in this article, condition (i) is satisfied by a partial transfer of charge between the two constituent parts of a charge-transfer complex: an organic electron-donor molecule D is combined with an - in most cases inorganic - electron-acceptor complex X according to the reaction $[D_m] + [X_n] \rightarrow [D_m]^{+\delta} + [X_n]^{-\delta}$, where m and n are integers. Since the π -electrons of the D molecule with orbits extending perpendicularly to the planes of the molecules have low binding energies - much lower than those of the σ -electrons - they can easily be excited which can be seen in the charge-transfer process. Accordingly, the so created charge carriers have a π -electron (hole) character. In most cases, the negatively charged anions $[X_n]^{-\delta}$ adopt a closed-shell configuration and thus do not contribute to the electrical conductivity. When the crystal is formed, a delocalization of the charge carriers (ii) may be obtained by a dense packing of the donor molecules. As a result, the π -orbitals of the partially filled outer molecular shells overlap and an electronic band structure is formed.

The conductivity of solids depends on both the number of free carriers and their mobility in the crystal. In organic charge-transfer salts, the carrier concentration is determined by the electronegativity of the donor, the electron affinity of the acceptor molecule and the chemical bonds. A high mobility is obtained by a relatively large bandwidth which is the result of a considerably strong overlap of the π -orbitals from adjacent molecules.

Organic superconductors have been derived from a variety of different organic electron-donor molecules, where most of them are derivatives of the archetype TTF molecule. Its combination with the electron acceptor TCNQ (tetracyanoquinodimethane) in 1973 led to the synthesis of the first quasi-one-dimensional (quasi-1D) organic conductor TTF-TCNQ [11,12]. This material and its derivatives served for a long time as model systems for exploring the physical properties of quasi-1D conductors.

In the vast majority of D_mX_n salts, the donor-acceptor molecular ratio $m : n$ is fixed to 2 : 1, i.e., two donor molecules transfer one electron to the acceptor X. Organic and organometallic chemistry have provided an enormous number of donor molecules which may serve as building blocks for organic conductors and superconductors. The main examples are the TTF derivatives TMTSF, TMTTF¹, BEDT-TTF (commonly abbreviated as ET) and BEDT-TSF² (or simply BETS), see Fig. 1. The TMTSF differs from TMTTF in that the four sulfur atoms of the latter have been replaced by selenium. In the same way, BEDT-TSF is derived from BEDT-TTF. It is interesting to note that

¹ TMTTF stands for tetramethyltetrathiafulvalene

² BEDT-TSF stands for bisethylenedithio-tetraselenafulvalene

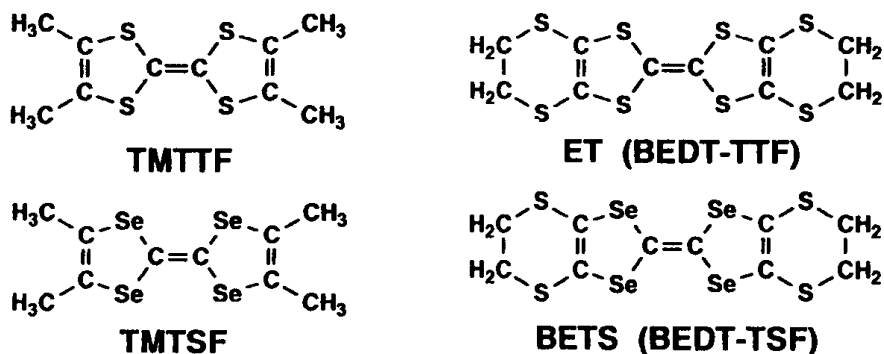


Fig. 1. Principal structures of donor molecules that furnish organic superconductors.

organic superconductors have been synthesized not only by using these symmetric molecules, but also on the basis of asymmetric complexes. These are the DMET (dimethylethylenedithio-diselenedithiafulvalene) [13,14], which is a hybriide of TMTSF and BEDT-TTF, MDT-TTF (methylenedithio-TTF) [13,14] and BEDO-TTF (bisethylenedithioxy-TTF) [15], see [5] for an overview.

The TMTSF molecule provides the basis for the so-called Bechgaard salts $(\text{TMTSF})_2\text{X}$ which form with a variety of inorganic monovalent acceptor molecules X. Indeed, it was $(\text{TMTSF})_2\text{PF}_6$ where in 1979 superconductivity had been observed for the first time in an organic compound [1]. At ambient-pressure conditions, the material was found to undergo a metal-to-insulator transition around 12 K which had been identified as a spin-density-wave (SDW) ordering [6]. By the application of hydrostatic pressure of 12 kbar the SDW instability can be suppressed and superconductivity forms below $T_c = 0.9\text{ K}$ [16,1]. A replacement of PF_6 by ClO_4 has resulted in the first and - till now - only member of the quasi-1D salts which becomes superconducting at ambient pressure [17].

Apparently, the strong tendency of the Bechgaards salts to undergo a metal-insulator transition, inherent to quasi-1D electron systems, counteracts with their ability to become superconducting. In order to achieve ambient-pressure superconductivity in these organic complexes with possibly even higher transition temperatures it is necessary to increase their dimensionality. According to this strategy, in 1982 the first metallic compound based on the new electron donor molecule BEDT-TTF [18], cf. Fig. 1, was synthesized by Saito et al. [19]. The underlying idea was to enhance the overlap between π -orbitals of adjacent molecules by enlarging the π -electron system on each molecule. This has been accomplished by adding rings of carbon and sulfur atoms at the outer ends of the TTF skeleton. In contrast to the Bechgaard

salts where the donor molecules form infinite stacks, steric effects specific to the BEDT-TTF molecules prevent such an infinite face-to-face stacking in the (BEDT-TTF)₂X salts. As a consequence, the side-by-side overlap between π -orbitals of adjacent molecules becomes stronger and, in some cases, comparable to the face-to-face interaction resulting in a quasi-2D electronic structure of the BEDT-TTF-based salts. The combination of BEDT-TTF with the monovalent anion $X = \text{Cu}(\text{NCS})_2$ achieved in 1988 led to the discovery of the first ambient-pressure superconductor in this class of materials - the second generation of organic superconductors - with transition temperatures in the range of 10 K [20].

The quasi-1D and -2D systems tend to grow in needle- and plate-like shapes, with the latter usually showing well developed smooth and shiny metallic surfaces. The synthesis of organic molecular conductors can be divided into two steps: (1) the synthesis of the neutral donor and acceptor molecules and (2) the oxidation and reduction of the donors and acceptors to radical cations and radical anions. For step (1) several independent methods have been discussed and used even for selected donor and acceptor molecules, see e.g. [18]. Conversely, to perform step (2), the redox process, the electrocrystallization technique has proved to be the method of choice for synthesizing high-quality crystals. For details on the chemical synthesis and crystal growth techniques, the reader is referred to [21,18,5] and references cited therein.

2.2 Structural aspects

Figure 2 shows exemplarily the crystal structure of (TMTSF)₂PF₆ viewed almost perpendicular to the stacking axis (a -axis) - the direction of highest conductivity. All members of the (TM)₂X family, where TM stands for TMTSF and TMTTF, are isostructural with triclinic symmetry. The conducting stacks are separated by the anions which are located at inversion centers of the lattice. The donor molecules which are nearly planar and almost perpendicular to the chain axis are arranged in a zigzag-type manner along the chains with two slightly different intrachain distances corresponding to a weak dimerization. The fairly close Se...Se distance of 3.87 Å along the b -axis being smaller than the sum of the van der Waals radii of 4 Å results in a weak interchain overlap [6] and thus a weakly 2D electronic character. An important structural aspect of the (TM)₂X compounds is related to the symmetry of the anion X. Where these anions are centrosymmetric such as the octahedral $X = \text{PF}_6$, AsF_6 , SbF_6 or TaF_6 complexes, their orientation is fixed in the structure. In contrast, (TM)₂X salts formed with non-centrosymmetric tetrahedral anions such as ClO_4 or FeO_4 undergo a structural transition from a disordered high-temperature state to an ordered low-temperature phase [22].

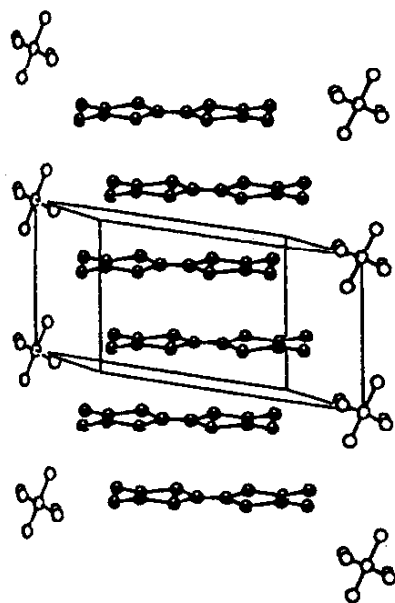


Fig. 2. Crystal structure of $(\text{TMTSF})_2\text{PF}_6$ (side-viewed tilted). The axis with the highest conductivity is the vertical a' -axis, the one with the lowest conductivity the horizontal c -axis. a' is the projection of the a -axis onto the direction perpendicular to the bc -plane.

While all members of the $(\text{TM})_2\text{X}$ family share the same crystal structure, the rather loose intra-stack coupling of the $(\text{BEDT-TTF})_2\text{X}$ salts gives rise to a variety of polymorphic phases (packing motifs) which are distinguished by Greek characters; the most important amongst them are the α -, β -, and κ -phases, see e.g. [23] for a comprehensive review of the structural properties of these salts. In some cases, as for instance realized in the compound with the linear anion $\text{X} = \text{I}_3$, various structural modifications exist even for the same anion, cf. Fig. 3. The α -type structure consists of stacks arranged in a herring-bone pattern. The ET molecules are connected via $\text{S} \cdots \text{S}$ contacts being shorter than the sum of the van-der-Waals radii of 3.6 \AA . The β -type packing is reminiscent of the stacking arrangement found in the Bechgaard salts. However, the smaller inter-stack distances in β -(ET) $_2\text{I}_3$ lead to a more two-dimensional electronic structure. The κ -phase is unique in that it does not consist of interacting stacks but rather of interacting dimers formed by two face-to-face aligned ET molecules. Adjacent dimers are arranged almost orthogonal to each other so that the *intra*- and *inter*-dimer interactions are of the same size. This results in a quasi-2D electronic structure with a small in-plane anisotropy. The κ -type compounds with polymere-like anions are of particular interest with respect to their superconducting properties as they exhibit the highest transition temperatures.

In forming the crystal, apart from the ethylene $[(\text{CH}_2)_2]$ groups at the outer ends of the molecules, the charged ET molecules $\text{C}_6\text{S}_8[(\text{CH}_2)_2]_2$ untwist at their centre and become planar. As shown schematically in Fig. 4, the rel-

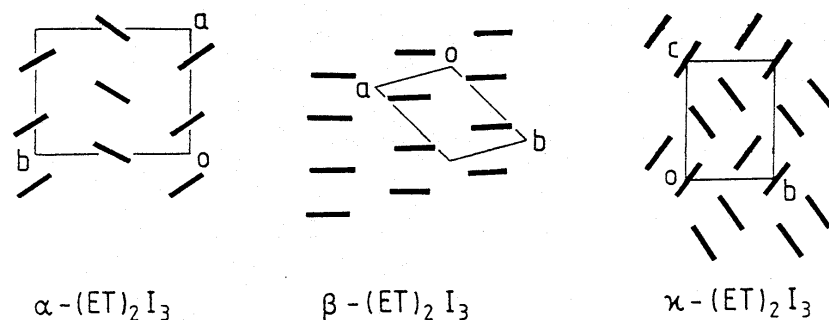


Fig. 3. Schematic packing motifs of the ET molecules in the α -, β - and κ -phases of $(\text{ET})_2\text{I}_3$ viewed along the long axis of the ET molecules.

ative orientation of the outer C—C bonds can either be parallel (eclipsed) or canted (staggered). At high temperatures, the ethylene endgroups become disordered due to the strong thermal vibrations. Upon cooling to low temperatures, the endgroups adopt one of the two possible conformations, depending on the anion and the crystal structure. As will be discussed in section 3.4 for the κ -(ET) $_2$ X salts, disorder in the conformation of the $[(\text{CH}_2)_2]$ groups can have a severe influence on the electronic properties in these compounds, in particular the superconductivity.

The planar C_6S_8 skeleton of the ET molecules permits a rather dense packing with a variety of possible packing arrangements. As a result, the interdimer interaction becomes comparable to that within the dimers giving rise to a quasi-2D electronic structure. Besides the intermolecular $\text{S} \cdots \text{S}$ contacts, i.e. the donor-donor interaction, the donor-acceptor couplings also play an important role for the physical properties of these multilayer systems. The latter interaction is provided by electrostatic forces as a consequence of the charged molecules and the hydrogen bonds joining between the carbon atoms at the donor site and the sulfur, carbon or nitrogen atoms being located at the acceptor site. The relative strength of these different interactions, the conformational degrees of freedom of the ethylene groups along with the flexibility

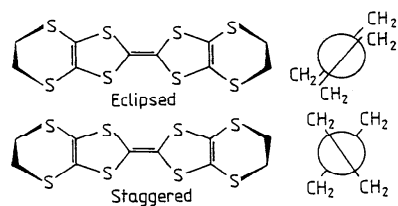


Fig. 4. Schematic view of the relative orientations of the ethylene endgroups $[(\text{CH}_2)_2]$ of the ET molecule. Right side shows the view along the long axis of the molecule.

of the molecular framework give rise to a variety of different ET complexes [5,23].

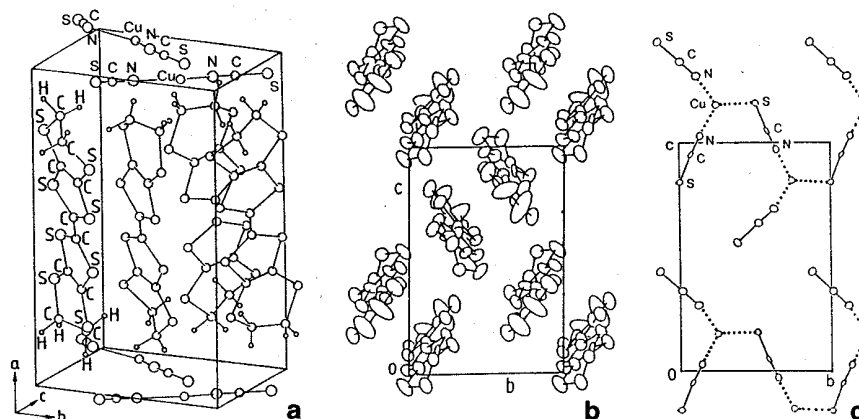


Fig. 5. (a) Crystal structure of κ -(BEDT-TTF)₂Cu(NCS)₂. The arrangement of the ET molecules (b) and the Cu(NCS)₂ anions (c) when viewed along the a^* direction, i.e. perpendicular to the conducting planes. The a -axis is slightly tilted from the a^* -axis which is normal to the conducting bc -plane.

Despite their complex crystal structure with rather low symmetry (cf. Table 1) it is convenient to think of the (ET)₂X compounds as layered systems consisting of conducting sheets formed by the ET molecules which are intersected by more or less thick insulating anion layers. Prime examples are the κ -phase (ET)₂X salts with X=Cu(NCS)₂, Cu[N(CN)₂]Br and Cu[N(CN)₂]Cl which are the most intensively studied and best characterized members of this class of materials. These compounds are of particular interest not only because of their relatively high superconducting transition temperatures but also owing to certain similarities in their normal- and superconducting-state properties with those of the high-temperature cuprate superconductors [9,4]. Figures 5 and 6 display the crystal structures of κ -(ET)₂Cu(NCS)₂ and κ -(ET)₂Cu[N(CN)₂]Z. In both cases the layered structure consists of conducting planes with the characteristic κ -type arrangement of the ET molecules separated by insulating anion layers. While the crystal structure of κ -(ET)₂Cu(NCS)₂ has monoclinic symmetry with two dimers, i.e. two formula units per unit cell, the κ -(ET)₂Cu[N(CN)₂]Z salts are orthorhombic with a unit cell containing four dimers, see Table 1. Due to the particular arrangement of their polymeric anions, these crystals lack a center of inversion symmetry.

Subtle changes in the intermolecular spacing or relative orientation of the ET molecules as e.g. induced by either external pressure or anion substitution may significantly alter the π -electron overlap between adjacent molecules.

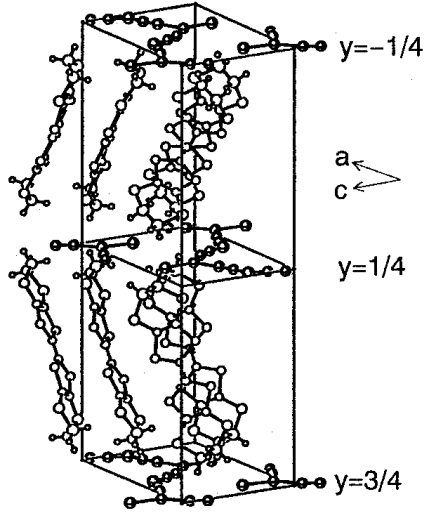


Fig. 6. Crystal structure of κ -(BEDT-TTF) $_2$ Cu[N(CN) $_2$]Z, with Z = Br and Cl. Here the direction perpendicular to the conducting plane is the crystallographic b -axis. The anion layers are parallel to the ac -plane at $y = -1/4$, $1/4$ and $3/4$. The polymeric-like anion chains are running along the a direction.

This can have a severe influence on the electronic properties as demonstrated for the κ -(ET) $_2$ Cu[N(CN) $_2$]Z system for various Z: while the compound with Z=Br is a superconductor with $T_c = 11.2$ K [24], replacement of Br by the slightly smaller Cl results in an antiferromagnetic insulating ground state. On the other hand, the application of hydrostatic pressure of only about

Table 1. Room-temperature crystallographic data of some (ET) $_2$ X superconductors including the space group SG, lattice parameters a, b and c , unit-cell volume V , number of formula units per unit cell z as well as T_c values. In the case of quasi-2D (ET) $_2$ X salts the lattice parameter perpendicular to the conducting planes is underlined.

	SG	a (Å)	b (Å)	c (Å)	V (Å 3)	z	T_c (K)
(TMTSF) $_2$ PF $_6$	$P\bar{1}$	7.297	7.711	13.522	713.14	1	1.1 (6.5 kbar)
κ -(ET) $_2$ Cu(NCS) $_2$	$P2_1$	<u>16.248</u>	8.440	13.124	1688	2	10.4
κ -(ET) $_2$ Cu[N(CN) $_2$]Br	$Pnma$	12.949	<u>30.016</u>	8.539	3317	4	11.2
κ -(ET) $_2$ Cu[N(CN) $_2$]Cl	$Pnma$	12.977	<u>29.977</u>	8.480	3299	4	12.8 (300 bar)
β'' -(ET) $_2$ SF $_5$ CH $_2$ CF $_2$ SO $_3$	$P\bar{1}$	9.260	11.635	<u>17.572</u>	1836	2	5.3
α -(ET) $_2$ NH $_4$ Hg(SCN) $_4$	$P\bar{1}$	10.091	<u>20.595</u>	9.963	2008	2	1.1
κ -(ET) $_2$ I $_3$	$P2_1/c$	<u>16.387</u>	8.466	12.832	1688	2	3.5
λ -(BETS) $_2$ GaCl $_4$	$P\bar{1}$	16.141	18.58	6.594	1774	2	6

300 bar drives the latter system to a superconductor with a T_c of 12.8 K [25–27], the highest transition temperature found among this class of materials so far.

A new class of materials which has recently gained considerable interest is based on the donor molecule BETS and its combination with the discrete anions MX_4 ($M = \text{Fe, Ga, In}$; $X = \text{Cl, Br}$). Two structural modifications have been found. These are the orthorhombic κ -type structure (Pnma) which results in plate-like crystals and the triclinic ($P\bar{1}$) λ -type variant which grow in a needle-like manner [28–30]. The λ -(BETS) $_2$ GaCl $_4$ salt is a superconductor with $T_c = 6$ K [31]. Upon substituting Ga by Fe in λ -(BETS) $_2$ Fe $_x$ Ga $_{1-x}$ Cl $_4$ superconductivity becomes continuously suppressed with increasing x [32] and, for $x \geq 0.5$, replaced by an antiferromagnetic insulating ground state.

Some structural data for a selection of organic superconductors are summarized in Table 1.

3 Normal-state properties

3.1 Electronic structure

As for ordinary metals, the electronic properties of organic charge-transfer salts are determined by the quasiparticles at the Fermi surface (FS).³ The energy-band structures for both the quasi-1D (TM) $_2$ X and the quasi-2D (ET) $_2$ X salts have been calculated employing a tight-binding scheme with a few simplifications [34]. The calculations are based on the assumption that the *intramolecular* interactions are much stronger than the interactions *between* adjacent molecules reducing the complexity of the problem enormously. In a first step, σ - and π -molecular orbitals are constructed using linear combinations of atomic s - and p -orbitals of the constituent atoms. In the molecular-orbital (MO) approximation, the electrons (holes) are considered to be spread over the whole molecule and only those electrons (holes) near the Fermi surface in the highest occupied (HOMO) and lowest unoccupied molecular orbitals (LUMO) are taken into account. Due to the overlap between molecular orbitals of adjacent molecules, the corresponding π -electrons (holes) are delocalized. Using available structural data, the overlap integrals and transfer energies can be obtained from quantum chemistry. These are input parameters for a standard tight-binding calculation based on molecular orbitals obtained by the extended Hückel approximation (EHA) from which the band structure and Fermi surfaces are derived [35–37,23].

Based on the above approximations, Grant et al. have calculated a model band structure for the quasi-1D materials (TM) $_2$ X [38], see upper panel of Fig. 7. The FS consists of two open sheets which are slightly corrugated

³ This implies the applicability of the Fermi-liquid concept which is questionable for the most anisotropic (TM) $_2$ X salts, see e.g. [33].

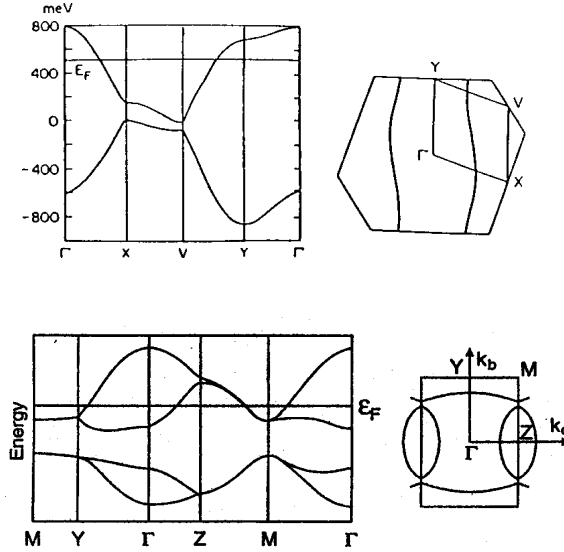


Fig. 7. Calculated energy dispersion and Fermi surface of $(\text{TMTSF})_2\text{X}$ [38] (upper panel) and $\kappa-(\text{ET})_2\text{Cu}(\text{NCS})_2$ [42,43] (lower panel).

due to weak interactions perpendicular to the stacking axis. While the standard magnetic-quantum-oscillation studies cannot be used for these quasi-1D metals, some important information on the FS can still be derived from angular-dependent magnetoresistance measurements, see e.g. [39]. Of crucial importance are the topological aspects of the FS, i.e. the nesting properties, and the band filling. The conduction band can accommodate four electrons per $(\text{TM})_2$ unit. Due to the weak structural dimerization which is more pronounced in the TMTTF compared to the TMTSF salts, a dimerization gap splits the conduction band into two parts. Therefore, removing one electron per unit cell in the charge-transfer process results in a half-filled conduction band.

The FS topology of the quasi-2D materials has been studied in great detail employing measurements of the de Haas-van Alphen (dHvA) and Shubnikov-de Haas (SdH) effect, the angular-dependent magnetoresistance (AMRO) and the cyclotron resonance, see [40,41]. These results clearly demonstrate the presence of a well-defined Fermi surface and quasiparticle excitations in accordance with the Fermi-liquid theory.

The lower panel of Fig. 7 shows the results of EHA band-structure calculations for the superconductor $\kappa-(\text{ET})_2\text{Cu}(\text{NCS})_2$. Since any *interlayer* electron transfer has been neglected in these calculations, the resulting FS is strictly two dimensional. Despite the various simplifications employed, the main features of the so-derived FS are generally found to be in remarkable agreement with the experimental results [40], although a more elaborated analysis reveals certain details which are not adequately described [44,10].

The four bands correspond to the four ET molecules in the unit cell, each

represented by its HOMO. Due to the lack of a center-of-inversion symmetry, an energy gap opens at the Z-M zone boundary. As a consequence, the FS consists of closed hole-like quasi-2D orbits (α -pockets) and a pair of open quasi-1D corrugated sheets. According to a charge transfer of one electron per pair of ET molecules, the conduction band is three quarters filled. Due to the strong dimerization of the ET molecules in the κ -type structure, the conduction bands split up so that the upper band becomes half filled. Band-structure calculations based on high-temperature crystallographic data reveal FS topologies which are very similar among the various κ -(ET)₂X systems [36,37], except for the degeneracy of the upper two bands along the Z-M zone boundary for the linear anion X = I₃. While the α - and κ -phase (ET)₂X salts still combine quasi-1D and -2D bands, the FS of β -type salts is even more simple. It is of almost cylindrical shape and closed within the first Brillouin zone, reflecting the isotropic in-plane interactions between adjacent ET molecules.

Fermi-surface studies In a magnetic field B , the transverse motion of electrons becomes quantized and their allowed states in \mathbf{k} -space are confined to so-called Landau levels. Periodic oscillations in magnetization and resistivity as a function of $1/B$ arise from the oscillatory behavior of the density of states at the Fermi level E_F as the Landau levels pass through the Fermi surface. From the oscillation period $\Delta(1/B)$ the extremal area of the FS cross section, S_F , perpendicular to the magnetic-field direction can be derived [45]:

$$S_F = \frac{2\pi e}{\hbar} \frac{1}{\Delta(1/B)}, \quad (1)$$

where $-e$ is the electron charge and \hbar the Planck constant. A quantitative description of the oscillatory magnetization was given by Lifshitz and Kose-

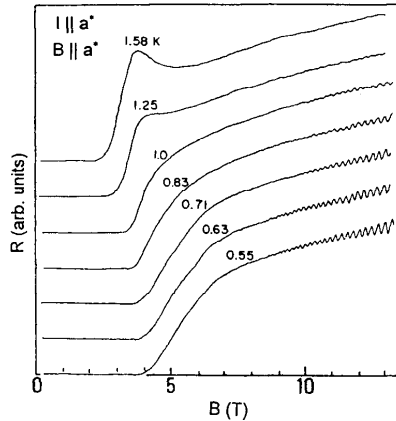


Fig. 8. Magnetoresistance of κ -(ET)₂Cu(NCS)₂ at different temperatures. Electrical current and magnetic field were applied along the a^* -axis, i.e. perpendicular to the conducting planes. Shubnikov-de Haas oscillations start to become visible below 1 K. Taken from [42].

vich [46]. According to their work, the amplitude of the oscillations is given by:

$$A \propto \frac{T}{\sqrt{B}} \frac{\exp(-\frac{\lambda m_c^* T_D}{m_e B})}{\sinh(\frac{\lambda m_c^* T}{m_e B})}, \quad (2)$$

where the effect on the electron spin has been neglected. m_e denotes the free electron mass and m_c^* the cyclotron effective mass, $\lambda = 2\pi^2 m_e k_B / (e\hbar)$ with k_B being the Boltzmann constant. $T_D = \hbar / (2\pi k_B \tau)$ is the Dingle temperature which accounts for the broadening of the Landau levels due to scattering of the electrons where τ is the relaxation time averaged over a cyclotron orbit. For state-of-the-art crystals of the (ET)₂X salts, the Dingle temperatures are usually far below about 1 K, as e.g. $T_D \sim 0.5$ K as reported for κ -(ET)₂Cu(NCS)₂ [47], which reflect the high quality of these materials.

Figure 8 shows early magnetoresistance data on κ -(ET)₂Cu(NCS)₂ [42]; see also [41] for more recent data. At the low-field side of the data sets, the transition from the superconducting to the normal state is visible. With increasing the field and at temperatures below 1 K, Subnikov-de Haas (SdH) oscillations caused by the closed α -orbits of the FS are superimposed. As expected from the simple FS topology (lower panel of Fig. 7), a single frequency according to only one extremal orbit (α -orbit) dominates the oscillatory behavior at lower fields. At higher magnetic fields, however, a second high-frequency component becomes superimposed [48,49]. The latter corresponds to the so-called magnetic breakdown effect which is due to tunnelling of charge carriers across the energy gaps at the FS. It is common to refer to the magnetic-breakdown orbit which encompasses the whole FS as the β -orbit. For a detailed description of the FS studies on quasi-1D and quasi-2D charge-transfer salts, see [40,41] and references therein.

Effective masses and renormalization effects The experimentally derived effective cyclotron masses m_c^* for the various (ET)₂X salts are significantly larger than the band masses m_b predicted by the above band-structure calculations, which are of the order of the free-electron mass m_e (see below). For the κ -(ET)₂Cu(NCS)₂ salt, for example, experiments reveal $m_c^* = (3.5 \pm 0.1) m_e$ for the α -orbit and (6.9 ± 0.8) for the magnetic-breakdown β -orbit [48]. A mass enhancement of comparable size is observed also for the thermodynamic effective mass m_{th}^* as determined by measurements of the specific heat $C(T)$. For a quasi-2D material consisting of stacks of metallic planes with interlayer spacing s , the Sommerfeld coefficient $\gamma^{2D} = C/T$ is given by:

$$\gamma^{2D} = \frac{\pi k_B^2}{3} \frac{m_{th}^*}{\hbar^2} \frac{1}{s}. \quad (3)$$

For κ -(ET)₂Cu(NCS)₂ one finds $\gamma = (23 \pm 1)$ mJ/mol K² [50,51] which corresponds to $m_{th}^* = (4.7 \pm 0.2) m_e$. Both m_c^* and m_{th}^* are renormalized com-

pared to the band mass m_b . The latter takes into account the fact that the electrons are moving in a periodic potential associated with the crystal lattice. The band masses estimated from tight-binding calculations and interband optical measurements are of the order of the free electron mass: Caulfield et al. applied the effective dimer model to κ -(ET)₂Cu(NCS)₂ and found $m_b^\alpha = 0.64 m_e$ and $m_b^\beta = 1.27 m_e$ [47] corresponding to a width of the conduction band of $W = 0.5 \sim 0.7$ eV. These values have to be compared with $m_b^\alpha = (1.72 \pm 0.05) m_e$ and $m_b^\beta = (3.05 \pm 0.1) m_e$ as derived from first-principles self-consistent local-density calculations [52]. For a discussion on the band masses derived from band-structure calculations and their relation to the cyclotron effective masses, see e.g. [53]. The substantial enhancement of the cyclotron masses compared to the band masses suggest an appreciable quasiparticle renormalization due to many-body effects, i.e. electron-electron and electron-phonon interactions. It has been proposed that a direct tool to determine the relative role of electron-electron correlations in the mass enhancement is provided by cyclotron resonance measurements [54]. According to the Kohn theorem the effective mass determined by cyclotron resonance experiments, m_{cr}^* , is independent of the electron-electron interactions. As a consequence, the experimental finding of $m_{cr}^* \approx m_b$ has been attributed to a dominant role of the Coulomb interaction for the mass renormalization [47]. However, recent studies on different (ET)₂X systems along with theoretical calculations showed that the general applicability of the Kohn theorem for the quasi-2D organic superconductors is questionable, see [41,10].

On the other hand, various experiments such as optical studies [55–60], thermal conductivity [61,62,51] as well as inelastic neutron scattering experiments [63] indicate a substantial coupling of the charge carriers to the lattice vibrations. Taken together, it is likely that for the present molecular conductors both electron-electron as well as electron-phonon interactions are responsible for the mass-renormalization.

By means of pressure-dependent Shubnikov-de Haas experiments a striking interrelation between the suppression of superconductivity and changes in the effective masses have been found [47]. Figure 9 shows the hydrostatic-pressure dependence of the effective masses for κ -(ET)₂Cu(NCS)₂ [47]. As the pressure increases, m_c^* rapidly decreases, an effect which has been observed also for other (ET)₂X compounds [64]. Above some critical pressure of about 4 ~ 5 kbar the rate of suppression of m_c^* becomes much weaker. As this is about the same pressure value above which superconductivity becomes completely suppressed (see inset of Fig. 9), an intimate interrelation between mass enhancement and superconductivity has been suggested [47]. This is consistent with recent results of reflectivity measurements which showed that the pressure dependence of the 'optical masses', which are closely related to the bare band masses, do not show such a crossover behaviour [65]. Consequently, the pressure-induced reduction of the effective cyclotron masses

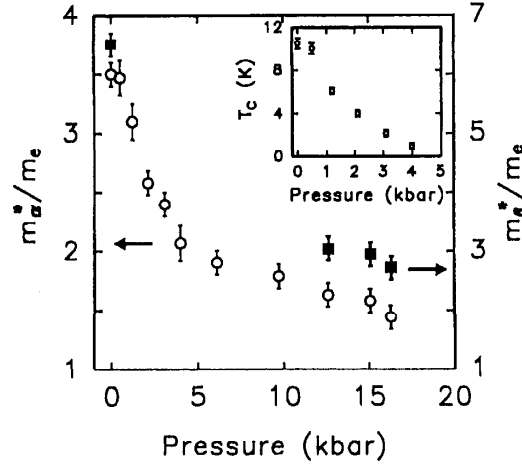


Fig. 9. Cyclotron effective masses of the α - (open circles, left scale) and β - (full squares and right scale) orbits as a function of hydrostatic pressure for κ -(ET) $_2$ Cu(NCS) $_2$. The inset shows T_c against pressure. Taken from [47].

has to be associated with a decrease in the strength of the electron-electron and/or electron-phonon interactions.

3.2 Transport and optical properties

Electrical resistivity The organic superconductors discussed in this article are fairly good metals at room temperature with resistivities that vary over wide ranges depending on the particular compound and the current direction in respect to the crystal axes. The pronounced anisotropies found in the electrical properties are direct manifestations of the strongly directional-dependent overlap integrals.

For the (TM) $_2$ X series (cf. Fig. 2) one typically finds $\rho_a : \rho_b : \rho_c$ of the order of 1 : 200 : 30.000, where a is along the stacking axis. These numbers correspond to a ratio of the overlap integrals $t_a : t_b : t_c$ of about 10 : 1 : 0.1 with $t_a \approx 0.1 \sim 0.24$ eV and 0.36 eV for the TMTTF and TMTSF compounds, respectively [6,33].

Figure 10 compiles temperature profiles of the resistivity for various (TM) $_2$ X compounds. Below a temperature T_ρ , depending on the anion, the resistivity of the sulfur-containing (TMTTF) $_2$ X compounds changes from a metallic-like high-temperature into a thermally-activated low- T behavior. Upon further cooling through $T_{SP} \simeq 20$ K $< T_\rho$ (not shown), the (TMTTF) $_2$ PF $_6$ salt undergoes a phase transition into a spin-Peierls (SP)-distorted nonmagnetic ground state, see e.g. [66] and references cited therein. With the application of moderate pressure both T_ρ and T_{SP} were found to decrease. By increasing the pressure to $p \geq 10$ kbar, the spin-Peierls ground state becomes replaced by an antiferromagnetic Néel state similar to the one found at normal conditions in (TMTTF) $_2$ Br.

In the selenium-containing (TMTSF) $_2$ PF $_6$ salt the metallic range extends

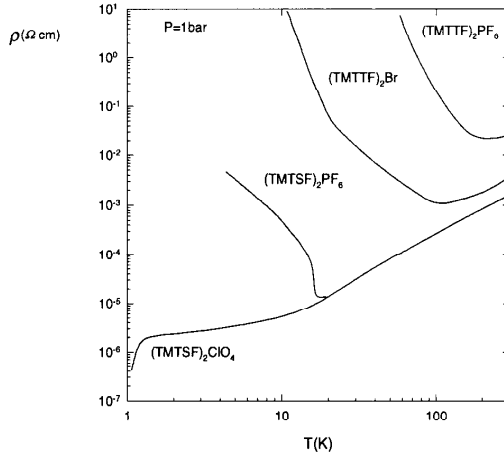


Fig. 10. Resistivity vs temperature for various $(\text{TMTTF})_2\text{X}$ and $(\text{TMTSF})_2\text{X}$ salts at ambient-pressure conditions in a double-logarithmic plot [66].

down to lower temperatures until the sudden increase in the resistivity indicates the transition into an insulating SDW ground state. Above a critical pressure of about 6 kbar, the SDW state of $(\text{TMTSF})_2\text{PF}_6$ becomes unstable giving way to superconductivity at lower temperatures, cf. the phase diagrams Figs. 21 and 22 in section 3.5.

Interestingly enough, when the spin-Peierls salt $(\text{TMTTF})_2\text{PF}_6$ is exposed to sufficiently high pressure in excess of 43.5 kbar, a superconducting state can be stabilized [67,68] which completes - for a single compound - the sequence of ground states indicated in the generic phase diagram in Fig. 21.

In their metallic regime the resistivity of the $(\text{TM})_2\text{X}$ salts along the most conducting direction decreases monotonically with a power-law temperature dependence $\rho \propto T^\alpha$, where the exponent α , depending on the temperature interval, varies between 1 and 2, see e.g. [69,33]. For $(\text{TMTSF})_2\text{PF}_6$ for example, $\alpha \approx 1.8$ between 300 and 100 K and approaches approximately 2 at lower temperatures down to the metal-SDW transition [33]. A T^2 dependence in the resistivity has been frequently observed not only in the quasi-1D [69] but also for the various $(\text{ET})_2\text{X}$ salts, see below.

A question of high current interest for the present quasi-1D conductors concerns the nature of their low-energy excitations. Is a Fermi-liquid approach still adequate or do we have to treat these materials within the framework of a Tomonaga-Luttinger liquid - a concept which has been proposed for dimensionality $D = 1$ [70–72]. Arguments in favor of a Luttinger-liquid behavior have been derived from various observations, not all of which have been generally accepted. Undisputed are, however, the non-Fermi-liquid features in the sulfur compounds $(\text{TMTTF})_2\text{X}$: these materials undergo a charge localization at elevated temperatures $T_p = 250$ K for $\text{X} = \text{PF}_6$ and 100 K for $\text{X} = \text{Br}$ (cf. Fig. 10) which leaves the static magnetic susceptibility unaffected

[6,33]. This apparent separation of spin and charge degrees of freedom is one of the hallmarks of a Luttinger liquid, see e.g. [73]. Indications for a spin and charge separation have been reported also for other $(\text{TM})_2\text{X}$ salts from optical- and thermal-conductivity experiments [74,75]. The other signatures of a Luttinger liquid are (ii) a power-law decay at long distances of the spin or charge correlation functions which suppresses long-range order in 1D systems and (iii) the absence of any discontinuity in the distribution function for electron states at the Fermi energy. Indications for (ii) and (iii) have been reported from NMR [33], photoemission [76,77] as well as transverse (c -axis) dc-resistivity [78] measurements.

The resistivity for the various $(\text{ET})_2\text{X}$ and related compounds can be roughly classified into two distinct types of temperature dependences. While some of the materials show a more or less normal metallic-like T behavior, i.e. a monotonic decrease of $\rho(T)$ upon cooling, a pronounced $\rho(T)$ maximum above about 80 K has been found for a number of $(\text{ET})_2\text{X}$ compounds. Among them are the κ -($\text{ET})_2\text{X}$ salts with polymere-like anions such as $\text{X} = \text{Cu}(\text{NCS})_2$ or $\text{Cu}[\text{N}(\text{CN})_2]\text{Br}$ [24,79–81], the α -($\text{ET})_2\text{NH}_4\text{Hg}(\text{SCN})_4$ [82] as well as the κ - and λ -type BETS salts [29]. The occurrence of the same kind of $\rho(T)$ anomaly in $(\text{DMET})_2\text{AuBr}_2$ [83] demonstrates that (i) this feature is not a property specific to ET- or BETS-based salts and (ii) does not rely on the presence of Cu ions. Fig. 11 shows the in-plane resistivity of κ -($\text{ET})_2\text{Cu}(\text{NCS})_2$ as a function of temperature at various pressures [79]. With decreasing temperatures, $\rho(T)$ first increases to a maximum at around 100 K before a metallic behavior sets in at lower temperatures. Under hydrostatic pressure, the maximum shifts to higher temperatures and becomes progressively suppressed. This is accompanied by a significant reduction of T_c (see also inset of Fig. 9). The origin of the anomalous $\rho(T)$ hump has been discussed by many authors and various explanations have been suggested including the formation of small polarons [84], a metal-metal phase transition [85], a valence instability of Cu [86], an order-disorder transition of the terminal ethylene groups of the ET molecules [87–89] as well as a crossover from localized small-polaron to coherent large-polaron behavior [90]. In this context it is interesting to note that for the κ -($\text{ET})_2\text{Cu}[\text{N}(\text{CN})_2]\text{Br}$ system this maximum has been found to be sample dependent: using a different synthesis route, Thoma et al. [91] and Montgomery et al. [92] succeeded in preparing superconducting crystals which lack the anomalous resistance hump.

A closer look on the resistivity of κ -($\text{ET})_2\text{Cu}(\text{NCS})_2$ below the maximum discloses an abrupt change in the slope at temperatures around $45 \sim 50$ K [93]. A similar behavior is found for κ -($\text{ET})_2\text{Cu}[\text{N}(\text{CN})_2]\text{Br}$ [94] and has been interpreted as a crossover from a regime of antiferromagnetic fluctuations of localized spins at high temperatures to a low- T Fermi-liquid regime [95,96]. More recent results, however, suggest that this temperature marks a density-wave-type *phase transition* [97–99], see section 3.3 for a detailed discussion.

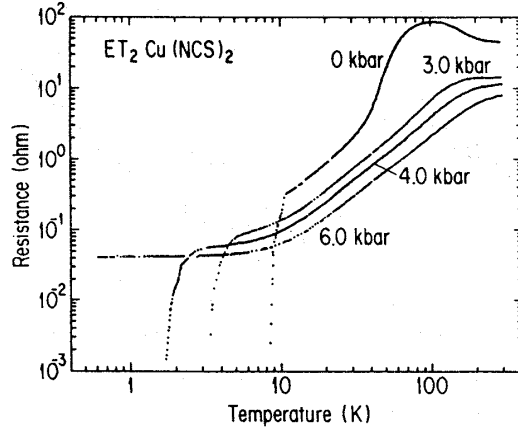


Fig. 11. Temperature dependence of the resistivity measured along the in-plane b -axis of κ -(ET) $_2$ Cu(NCS) $_2$ at various pressures. Taken from [79].

At temperatures below the inflection point, the resistivity turns into an approximate $\rho(T) = \rho_0 + AT^2$ behavior until superconductivity sets in around 10 K. As mentioned above, a resistivity roughly following a T^2 law - even at elevated temperatures - is not an exception in the present molecular conductors, see e.g. [5]. In some high-quality crystals of β - and κ -type (ET) $_2$ I $_3$, it has been observed over an extraordinarily wide temperature range up to temperatures as high as 100 K [100]. It has been argued that the T^2 dependence of the resistivity indicates a dominant role of electron-electron scattering in these materials [7]. On the other hand, for such a mechanism to predominate the resistivity at temperatures as high as 45 K for the X = Cu(NCS) $_2$ and even 100 K for the X = I $_3$ salt implies that there is only a minor contribution from electron-phonon scattering. In light of the considerable electron-phonon coupling in these materials as proved by various experiments, such a scenario appears questionable. Alternatively, the T^2 law has been attributed to the scattering of electrons by phonons via electron-libron [101] or a novel electron-phonon scattering mechanism proposed for the high- T_c cuprates [100] which invokes electron-electron interactions [102,103]. For the discussion of the temperature dependence of the resistivity, it is important to bear in mind, however, that due to the large pressure coefficients of the resistivity of about $\partial \ln \rho / \partial p \simeq -20\%/\text{kbar}$ at room temperature together with the extraordinary strong thermal contraction, it is difficult to make a comparison with theoretical predictions. Since the theory usually describes the temperature dependence at constant volume, a detailed comparison is meaningful only after transforming the constant-pressure into constant-volume profiles by taking into account the thermal expansion of the material.

Similar to the quasi-1D (TM) $_2$ X salts, the room-temperature resistivities of the quasi-2D (BEDT-TTF) $_2$ X materials are generally rather high. For the κ -(ET) $_2$ Cu(NCS) $_2$ salt for example, one finds $\rho_b \approx 6 \cdot 10^4 \mu\Omega\text{cm}$ and $\rho_c \approx 3 \cdot 10^4 \mu\Omega\text{cm}$ [104], which exceed the values for Cu by several orders of

magnitude. This is partly due to the relatively low charge-carrier concentration of only about 10^{21} cm^{-3} .

In accordance with their quasi-2D electronic structure, a pronounced in-plane vs out-of-plane anisotropy has been observed which amounts to $10^{-3} \sim 10^{-5}$ [41]. In this respect it is interesting to ask whether under these conditions the interlayer transport is coherent or not, i.e. whether there is a coherent motion of band states associated with well-defined wave vectors or if the motion from layer to layer is diffusive and a Fermi velocity perpendicular to the layers cannot be defined [105]. This question has been addressed in recent magnetoresistance studies on the κ -(ET) $_2$ Cu(NCS) $_2$ salt [106]. Here the interlayer-transfer integral has been estimated to be $t_\perp \approx 0.04 \text{ meV}$ [106] as compared with $t_\parallel \sim 150 \text{ meV}$ for the intralayer transfer [47]. According to this work, the Fermi surface is extended along the interlayer direction corresponding to a coherent transport.

Optical conductivity Optical investigations by means of infrared and Raman measurements provide important information on the electronic parameters such as the plasma frequency, the optical masses and also the bandwidths and collision times for the carriers. In addition, they permit an investigation of vibrational properties and their coupling to the charge carriers. Using polarized light it is also possible to look for anisotropies in these quantities, as e.g. in the effective masses. The optical properties of quasi-1D and -2D organic conductors have been reviewed by several authors [6,33,107–110], see also [5,10]. For a detailed discussion on the normal- and superconducting-state optical properties of the (ET) $_2$ X salts see [111]. A summary of Raman results on (ET) $_2$ X salts is given in [112,113].

First extensive optical studies of the electronic properties of (TM) $_2$ X by Jacobsen et al. [114] provided information on the energy of charge-transfer processes and on the electron-phonon coupling: the large absorption features observed in the optical conductivity of the TMTTF salts have been assigned to intra- and intermolecular vibrations [115]. These studies have been supplemented by a series of more detailed investigations covering also the low frequency range, see [110] and references therein. In accordance with the expectations for a strongly anisotropic material with open Fermi surface, the optical response of the Bechgaards salts (TMTSF) $_2$ X was found to deviate strongly from that of a simple metal. The main features are a gap-like structure around 25 meV for X = PF $_6$ and a zero-frequency mode which grows upon decreasing the temperature. The latter contribution, having only a small spectral weight corresponding to 1 % of the carriers, is responsible for the metallic conductivity of the compound [110]. At high frequencies, i.e. at energies in excess of the interchain transfer integral t_b but below the intraband width $4t_a$, the data for the optical conductivity follow a $\sigma_1(\omega) \propto \omega^{-\gamma}$ dependence with $\gamma = 1.3$ [110]. Here $\gamma = 4n^2K_\rho - 5$, where K_ρ is the Luttinger-liquid-correlation parameter and n the degree of commensurability. From the experimentally derived

γ value and assuming $n = 2$, i.e. a dominant quarter-filled band Umklapp scattering, $K_\rho \simeq 0.23$ has been determined which agrees reasonably well with photoemission [76,116,117] and transport data [78]. These observations are consistent with a dimensional crossover in $(\text{TMTSF})_2\text{PF}_6$ from a high-temperature Luttinger-liquid phase to a low-temperature (anisotropic) 3D Fermi liquid induced by interchain coupling.

For the various ET salts, the reflectance spectra are generally characterized by intensive sharp features due to molecular vibrations superimposed on a broad electronic background with the plasma edge at a frequency of about $4500 \sim 5000 \text{ cm}^{-1}$. Fig. 12 shows optical conductivity data of superconducting deuterated $\kappa\text{-(D}_8\text{-ET)}_2\text{Cu(NCS)}_2$ (left panel) and insulating $\kappa\text{-(ET)}_2\text{Cu[N(CN)}_2\text{]Cl}$ (right panel) at various temperatures obtained from reflectivity measurements after a Kramers-Kronig analysis [118,119]. The far-infrared conductivities have been found to agree reasonably well with the dc-conductivities in showing a rapid increase below 50 K for $\kappa\text{-(ET)}_2\text{Cu(NCS)}_2$. The low-frequency feature has been interpreted as a Drude peak which increases with decreasing temperature or increasing pressure, i.e. when the metallic character of the material increases. The data are in good agreement with results of other studies, see [111,90,10] and references cited therein. However, the interpretation of the spectra may vary from author to author: Kornelsen et al. attributed the mid-infrared peak ($1000 \sim 4000 \text{ cm}^{-1}$) to interband transitions superimposed on the free-carrier tail [118]. Wang et al. [90] argued that the sharp Drude peak in the conductivity that develops at low temperature, together with the large mid-infrared spectral weight indicate polaronic effects. According to this interpretation, the change from non-metallic to metallic behavior around $90 \sim 100 \text{ K}$ as observed in the

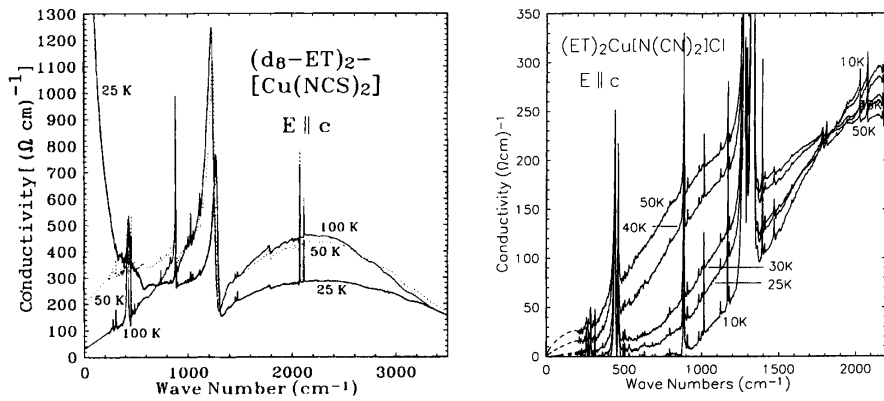


Fig. 12. Optical conductivity of $\kappa\text{-(D}_8\text{-ET)}_2\text{Cu(NCS)}_2$ (left panel) and $\kappa\text{-(ET)}_2\text{Cu[N(CN)}_2\text{]Cl}$ (right panel) at various temperatures for $E \parallel c$. Taken from [118] and [119], respectively.

resistivity is due to a crossover from localized small-polaron to coherent large-polaron behavior [90]. In contrast to the metallic/superconducting κ -(ET)₂Cu(NCS)₂ salt, the optical conductivity in the low-energy region for insulating κ -(ET)₂Cu[N(CN)₂]Cl rapidly decreases below 50 K, indicating a large temperature-dependent semiconducting energy gap with a value of about 900 cm⁻¹ at 10 K [119].

Electron-phonon coupling Infrared reflectivity measurements can also be used to obtain information on the electron-phonon interaction. In molecular crystals, the coupling between the conduction electrons and the phonons is twofold. One kind of interaction, the so-called electron-molecular-vibration (EMV) coupling, involves the *intramolecular* vibrations which are characteristic of the molecular structure. This has to be distinguished from the electron-*intermolecular*-vibration coupling which refers to the interaction of the charge carriers with motions of almost rigid molecules around their equilibrium positions and orientations (translational and librational modes).

Electron-molecular-vibration coupling It is well known [120] that electrons in the HOMO's of the TTF molecule and its derivatives couple strongly to the totally symmetric (A_g) molecular vibrations via the modulation of the HOMO energy, E_{HOMO} , by the atomic displacements. The linear EMV coupling constant g_i for mode i is defined as:

$$g_i = \frac{1}{h\nu_i} \frac{\partial E_{\text{HOMO}}}{\partial Q_i}, \quad (4)$$

where Q_i is an intramolecular normal coordinate and ν_i the mode frequency. The effective electron-intramolecular-phonon coupling constant λ_i can then be calculated using $\lambda_i = 2g_i^2 h\nu_i N(E_F)$ where $N(E_F)$ is the density of states at the Fermi level.

The sharp features superimposed on the electronic background in Fig. 12 can be attributed to molecular vibrations. An assignment of these features to the various vibrational modes [121] is feasible by comparing spectra of different isotopically labelled salts with calculations based on a valence-force-field model by Kozlov et al. [124,125]. For the ET molecule, the modes with the strongest coupling constants are those involving the central carbon and sulfur atoms [124–126] at which the HOMO's have the largest amplitudes [35]. The frequencies of these C=C stretching and ring-breathing modes are $\nu_2 = 1465 \text{ cm}^{-1}$ ($g_2 = 0.165$), $\nu_3 = 1427 \text{ cm}^{-1}$ ($g_3 = 0.746$) and $\nu_9 = 508 \text{ cm}^{-1}$ ($g_9 = 0.476$), where the calculated coupling constants are given in the brackets. Despite these sizable coupling constants, several studies - especially those of the mass isotope shifts on T_c for the ET salts [127] - indicate that the EMV coupling seems to play only a minor role in mediating the attractive electron-electron interaction, cf. section 4.5.

Electron-intermolecular-vibration coupling While much experimental data are available on the EMV coupling, relatively little is known about the coupling of the charge carriers to the low-lying intermolecular phonons. This interaction is provided by the modulation of the charge-transfer integrals t_{eff} between neighbouring molecules during their translational or librational motions. Within the Eliashberg theory, the dimensionless electron-intermolecular-phonon coupling constant λ is given by

$$\lambda = 2 \int \frac{\alpha^2(\omega)}{\omega} F(\omega) d\omega, \quad (5)$$

where $\alpha(\omega)$ is the electron-phonon-coupling constant, ω the phonon frequency and $F(\omega)$ the phonon density of states. The Eliashberg function $\alpha^2(\omega)F(\omega)$ can, in principle, be derived from tunneling characteristics of strong-coupling superconductors or via point-contact measurements. The latter experiments have been carried out by Nowack et al. on the β -type $(\text{ET})_2\text{X}$ salts with $\text{X} = \text{I}_3$ and AuI_2 [128,129] yielding $\lambda \simeq 1$. Some of the frequencies of the intermolecular modes have been determined by employing Raman and far-infrared measurements [130–132,60]. More recent studies including inelastic-neutron [63] and Raman-scattering [57–60] have focused on investigation of the role of intermolecular phonons for superconductivity. These experiments yielded quite sizable superconductivity-induced phonon-renormalization effects which clearly indicate a significant coupling of the superconducting charge carriers to the intermolecular phonons and suggest an important role of these modes in the pairing interaction, cf. section 4.5.

3.3 Thermal and magnetic properties

Common to both the quasi-1D and -2D charge-transfer salts is the variety of ground states the systems can adopt depending on parameters such as the chemical composition or external pressure. Most remarkable is the fact that for both families the superconducting phase shares a common phase boundary with a long-range magnetically ordered state.

For the $(\text{TMTSF})_2\text{PF}_6$ salt, cooling at ambient pressure leads to a metal-insulator transition at $T_{MI} \sim 12$ K. The insulating ground state in the $(\text{TMTSF})_2\text{X}$ series has been identified via NMR [133,134] and susceptibility [135] measurements as a spin-density-wave ordering whose wave vector $\mathbf{q} = 2 \mathbf{k}_F$ is determined by the optimum nesting condition of the quasi-1D Fermi surface [6]. The application of hydrostatic pressure to the $\text{X} = \text{PF}_6$ salt suppresses the magnetic state by destroying the nesting properties and instead stabilizes superconductivity below about $T_c = 1.1$ K at 6.5 kbar [136]. As has been shown again by NMR experiments, short-range spin-fluctuations with the same wave vector \mathbf{q} remain active up to ~ 100 K, i.e. far above the SDW ordering in this salt. Moreover, these fluctuations are present also in the normal state of the ClO_4 compound despite its superconducting ground

state [137].

For the quasi-2D κ -phase $(\text{ET})_2\text{X}$ compounds, the nesting properties are expected to be less strongly pronounced, cf. the Fermi surface in Fig. 7. Nevertheless, as in the case of the quasi-1D salts, superconductivity lies next to an antiferromagnetic insulating state in the pressure-temperature phase diagram, see section 3.5. While the compounds with the complex anions $\text{X}=\text{Cu}(\text{NCS})_2$ and $\text{Cu}[\text{N}(\text{CN})_2]\text{Br}$ are superconductors with T_c values of 10.4 K and 11.2 K, respectively, $\kappa\text{-(ET)}_2\text{Cu}[\text{N}(\text{CN})_2]\text{Cl}$ is an antiferromagnetic insulator with $T_N = 27$ K which can be transformed into a superconductor with $T_c = 12.8$ K by the application of a small hydrostatic pressure of only 300 bar [25]. Likewise seen in the quasi-1D salts, the metallic state above T_c in these quasi-2D systems reveals indications for magnetic fluctuations. This has been demonstrated by NMR measurements on the various $\kappa\text{-(ET)}_2\text{X}$ salts [138–142]. As shown in Fig. 13 the spin-lattice relaxation rate divided by temperature, $(T_1T)^{-1}$, for the superconductors $\kappa\text{-(ET)}_2\text{Cu}(\text{NCS})_2$ and $\kappa\text{-(ET)}_2\text{Cu}[\text{N}(\text{CN})_2]\text{Br}$ behaves quite differently from what would be expected for a simple metal and realized to a good approximation in some other organic superconductors as, e.g. $\alpha\text{-(ET)}_2\text{NH}_4\text{Hg}(\text{SCN})_4$ [140,96]. For both κ -phase compounds, the $(T_1T)^{-1}$ values at higher temperatures are enhanced by a factor 5 \sim 10 compared to a conventional Korringa-type behavior. Upon cooling, $(T_1T)^{-1}$ gradually increases down to a temperature $T^* \simeq 50$ K, below which a steep decrease sets in. Both the overall enhancement of $(T_1T)^{-1}$ along with its anomalous peak around 50 K have been assigned to the effect of strong antiferromagnetic spin fluctuations with a finite wave vector [138,143,140,96]. The latter might be related to the ordering wave vector that characterizes the AF phase of $\kappa\text{-(ET)}_2\text{Cu}[\text{N}(\text{CN})_2]\text{Cl}$ [138,143,96]. It has been emphasized by these authors that despite the rapid drop below $T^* \simeq 50$ K the overall enhancement of $(T_1T)^{-1}$ persists until the onset of

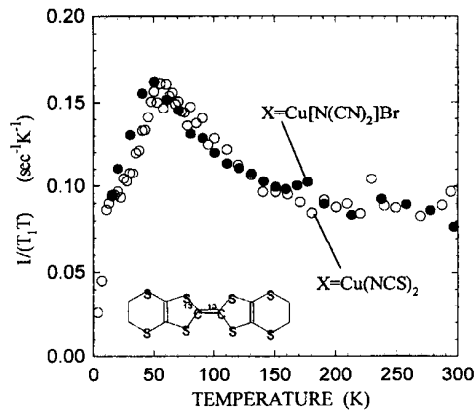


Fig. 13. Spin-lattice relaxation rate divided by temperature, $(T_1T)^{-1}$, for $\kappa\text{-(ET)}_2\text{Cu}(\text{NCS})_2$ and $\kappa\text{-(ET)}_2\text{Cu}[\text{N}(\text{CN})_2]\text{Br}$ as a function of temperature, taken from [140]. For the ^{13}C -NMR measurements, the ^{12}C atoms of the central $\text{C}=\text{C}$ double bond in the ET molecule have been replaced by ^{13}C .

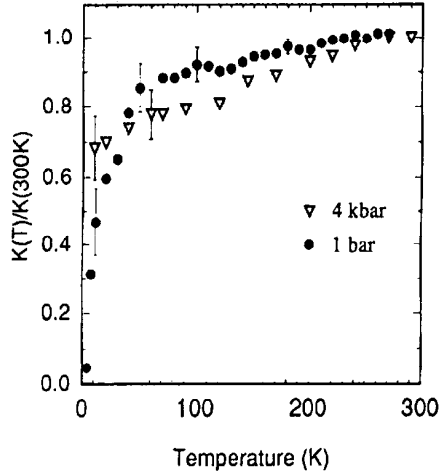


Fig. 14. Knight-shift, K_S , for κ -(ET) $_2$ Cu[N(CN) $_2$]Br as a function of temperature at ambient pressure and $p = 4$ kbar, taken from [138].

superconductivity indicative of the highly-correlated nature of the metallic state in these compounds [140,96]. NMR investigations performed at various pressures revealed that with increasing the pressure, the maximum at T^* shifts to higher temperatures while its size becomes progressively reduced. At pressures above 4 kbar the peak is replaced by a normal Korringa-type behavior, i.e. $(T_1T)^{-1} = \text{const.}$ [138,139]. In [95,96] the abrupt reduction of $(T_1T)^{-1}$ below $T^* \simeq 50$ has been linked phenomenologically to a spin-gap behavior as discussed also in connection with the high- T_c cuprates. Indeed, the formation of a pseudogap was first proposed by Kataev et al. [144] on the basis of their ESR measurements. These authors observed a reduction of the spin susceptibility around 50 K, indicating a decrease of the electronic density of states at the Fermi level $N(E_F)$ near T^* . The same conclusion has been drawn from results of the static magnetic susceptibility [140] and Knight-shift (K_S) measurements [138]. Figure 14 shows K_S as a function of temperature for the κ -(ET) $_2$ Cu[N(CN) $_2$]Br salt. While the data at ambient pressure reveal a clear drop below about 50 K, a rather smooth behavior with a gradual reduction upon cooling was found at 4 kbar [138]. The variation of the spin susceptibility in the high-temperature region has been attributed to the lattice contraction [143]. Although these experiments show clear evidence for a reduction of the density of states at E_F below $T^* \simeq 50$, the nature of this phenomenon and its interrelation to superconductivity are still unclear.

Cooling through $T^* \simeq 50$ does not only cause anomalies in the above magnetic properties but also leads to clear signatures in transport, acoustic, optical and thermodynamic quantities. As mentioned above, for both superconducting compounds a distinct peak shows up in the temperature derivative of the electrical resistivity $d\rho/dT$ [93,94] indicating a change in the density of states at E_F . A pronounced softening of ultrasound modes

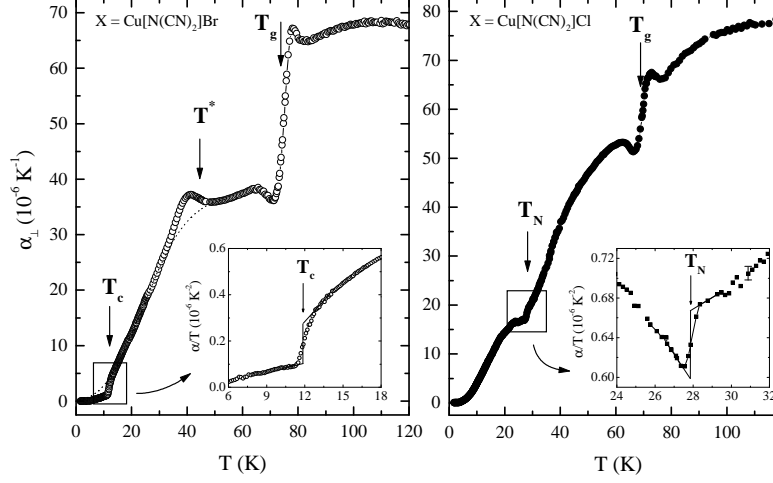


Fig. 15. Linear thermal expansion coefficient perpendicular to the planes of highest conductivity, α_{\perp} , as a function of temperature for superconducting $\kappa\text{-(ET)}_2\text{Cu}[\text{N}(\text{CN})_2]\text{Br}$ (left panel) and insulating $\kappa\text{-(ET)}_2\text{Cu}[\text{N}(\text{CN})_2]\text{Cl}$ (right panel). The inset shows details of α_{\perp} for both salts as α_{\perp}/T vs T at the superconducting ($X=\text{Cu}[\text{N}(\text{CN})_2]\text{Br}$) and antiferromagnetic ($X=\text{Cu}[\text{N}(\text{CN})_2]\text{Cl}$) phase transition. Arrows indicate different kinds of anomalies as explained in the text. Taken from [97].

for $\kappa\text{-(ET)}_2\text{Cu}[\text{N}(\text{CN})_2]\text{Br}$ and $\kappa\text{-(ET)}_2\text{Cu}(\text{NCS})_2$ with distinct minima at $T^* \simeq 38 \text{ K}$ and 46 K , respectively, have been attributed to a coupling between acoustic phonons and antiferromagnetic fluctuations [145,146]. An interaction between the phonon system and magnetism has also been suggested by Lin et al. based on their Raman scattering experiments [147,113]. Recent theoretical studies have attempted to explain both the acoustic and Raman experiments by a correlation-induced crossover from a coherent Fermi liquid at low temperatures to an incoherent bad metal at high temperatures [148,149]. According to this work, pronounced phonon anomalies as well as anomalous transport and thermodynamic properties are expected to occur at the crossover temperature T^* . Based on their NMR results, Kawamoto et al. [141] and Kanoda [95,96] argued that T^* marks the crossover temperature from a region of antiferromagnetic fluctuations of localized spins at high T to a Fermi-liquid regime at low temperatures. This differs from the interpretation given by the Orsay group [138,139,143] who analyzed their NMR results in terms of strong antiferromagnetic fluctuations enhanced by Coulomb repulsion and the nesting properties of the Fermi surface.

More insight into the nature of the anomaly at T^* and its interrelation with superconductivity can be obtained by studying the coupling to the lattice degrees of freedom. This has been done by employing high-resolution thermal expansion measurements which also allow for studying directional-

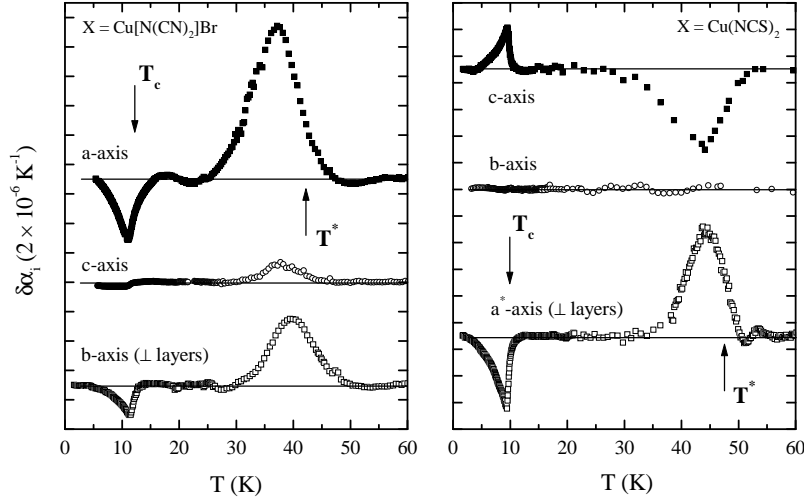


Fig. 16. Anomalous contributions, $\delta\alpha_i(T) = \alpha_i(T) - \alpha_{ib}(T)$, to the uniaxial thermal expansion coefficients, $\alpha_i(T)$, along the three principal axes for the superconducting salts κ -(ET) $_2$ Cu[N(CN) $_2$]Br (left panel) and κ -(ET) $_2$ Cu(NCS) $_2$ (right panel). Taken from [98].

dependent effects [88,150,97]. Figure 15 compares the linear coefficient of thermal expansion, $\alpha(T) = \partial \ln l(T) / \partial T$, where $l(T)$ is the sample length, perpendicular to the planes for the superconducting κ -(ET) $_2$ Cu[N(CN) $_2$]Br (left panel) with that of the non-metallic κ -(ET) $_2$ Cu[N(CN) $_2$]Cl salt (right panel). For both compounds, various anomalies have been observed as indicated by the arrows [97,151]. These are (i) large step-like anomalies at $T_g = 70 \sim 80$ K which are due to a kinetic, glass-like transition associated with the ethylene endgroups, cf. section 3.4 and (ii) a distinct peak in $\alpha(T)$ at T^* . The latter feature, also observed for the superconductor κ -(ET) $_2$ Cu(NCS) $_2$ (not shown) is absent in the non-metallic κ -(ET) $_2$ Cu[N(CN) $_2$]Cl salt, cf. right panel of Fig. 15 [97]. As demonstrated in the insets of Fig. 15, the transitions into the superconducting ($T_c = 11.8$ K) and antiferromagnetic ($T_N = 27.8$ K) ground states for the X=Cu[N(CN) $_2$]Br and X=Cu[N(CN) $_2$]Cl salts, respectively, are accompanied by distinct second-order phase transition anomalies in the coefficient of thermal expansion.

Figure 16 shows the anomalous contribution, $\delta\alpha_i(T) = \alpha_i(T) - \alpha_{ib}(T)$, to the uniaxial thermal expansion coefficients along the principal axes, $\alpha_i(T)$, at T_c and T^* for the superconducting salts X=Cu[N(CN) $_2$]Br (left panel) and X=Cu(NCS) $_2$ (right panel) obtained after subtracting a smooth background α_{ib} (dotted line in the left panel of Fig. 15) [98]. Judging from the shape of the anomalies at T^* , i.e. their sharpness and magnitude, it has been suggested that this feature be assigned to a second-order phase transition [98]. Figure 16 uncovers an intimate interrelation between the phase-transition anomalies

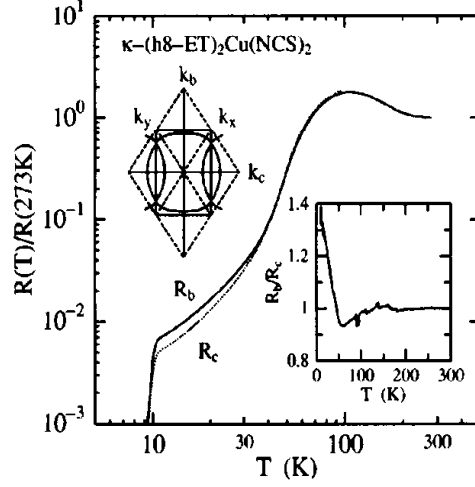


Fig. 17. Temperature dependence of the normalized resistance along the in-plane b - and c -axis of κ -(ET) $_2$ Cu(NCS) $_2$. The top left inset shows the FS and the Brillouin zone. Taken from [99].

at T_c and T^* : while both features are correlated in size, i.e. a large (small) anomaly at T_c complies with a large (small) one at T^* , they are anticorrelated in sign. A positive peak at T_c goes along with a negative anomaly at T^* and vice versa. According to the Ehrenfest relation

$$\left(\frac{\partial T^*}{\partial p_i}\right)_{p_i \rightarrow 0} = V_{\text{mol}} \cdot T^* \cdot \frac{\Delta\alpha_i}{\Delta C}, \quad (6)$$

which relates the uniaxial-pressure dependence of a second-order phase-transition temperature T^* to the discontinuities in α_i , $\Delta\alpha_i$, and that of the specific heat, ΔC , the above findings imply that the uniaxial-pressure coefficients of T_c and T^* are strictly anticorrelated. In [97,98] it has been argued that the transition at T^* is not of structural but of electronic origin and related to the Fermi-surface topology. Based on the above uniaxial-pressure results, it has been proposed that T_c and T^* mark competing instabilities on disjunct parts of the Fermi surface [97,98]: while the instability at T^* most likely involves only the minor quasi-1D fractions (see Fig. 7 and [138]), the major quasi-2D parts are subject to the superconducting instability at lower temperatures. As a result, these studies hint at the opening of a real gap associated with T^* on the small 1D-parts of the FS as opposed to a pseudogap on the major quasi-2D fractions. The condensation of parts of the FS into a density-wave below T^* would imply the onset of anisotropies in magnetic and transport properties. In fact, this has been found in recent orientational-dependent studies on both compounds [99]: cooling through T^* is accompanied by the onset of a small but distinct anisotropy in the magnetic susceptibility. As can be seen in Fig. 17, T^* affects also the charge degrees of freedom where below T^* the b -axis transport becomes more resistive compared to that along

the c -axis [99]. These authors proposed that below T^* a static or fluctuating charge-density-wave (CDW) on minor parts of the FS coexists with the metallic phase on the remaining quasi-2D fractions.

The above discussion on the nature of the anomalies at T^* for the superconducting salts κ -(ET)₂Cu[N(CN)₂]Br and κ -(ET)₂Cu(NCS)₂ poses the question whether this phenomenon is related to the magnetic signatures found in the non-metallic κ -(ET)₂Cu[N(CN)₂]Cl. Earlier magnetization measurements on κ -(ET)₂Cu[N(CN)₂]Cl revealed a shallow decrease below 45 K which was interpreted as the onset of an antiferromagnetic order [152]. In addition, indications were found for a weak ferromagnetic state at 22 K with a small saturation moment of $8 \cdot 10^{-4} \mu_B/\text{dimer}$. However, according to more recent NMR experiments, the spins order in a commensurate antiferromagnetic structure below $T_N \approx 27$ K with a sizable magnetic moment of $(0.4 - 1.0) \mu_B/\text{dimer}$ [153]. From these measurements, along with magnetization studies, it has been inferred that the easy magnetic axis is aligned perpendicular to the planes and that a small canting of the spins causes a weak ferromagnetic moment parallel to the planes below about $22 \sim 23$ K, see also [154]. Recent ¹³C-NMR experiments confirmed the commensurate character of the magnetic structure yielding a moment of $0.45 \mu_B/(\text{ET})_2$ [155]. Three different proposals have been put forward on the origin of the magnetic moments and the nature of the antiferromagnetic insulating state in κ -(ET)₂Cu[N(CN)₂]Cl: (i) electron localization due to lattice disorder accompanied by an incomplete compensation of their spins, i.e. an inhomogeneous frozen-in magnetic state [156], (ii) an itinerant SDW-type magnetism associated with the good nesting properties of the quasi-1D parts of the Fermi surface [119,143,157] and (iii) a correlation-induced Mott-Hubbard type metal-insulator transition leading to a magnetic state characterized by localized spins [153].

Although proposal (i) has been ruled out by a recent thermal expansion study providing clear thermodynamic evidence for a phase transition at T_N [97] (see inset of the right panel of Fig. 15), the nature of the ordered state is still unclear. So far the results of optical, thermal and magnetic properties seem to indicate that certain elements of the models (ii) and (iii) would be applicable to κ -(ET)₂Cu[N(CN)₂]Cl.

3.4 Anion ordering and glassy phenomena

In discussing molecular conductors and superconductors, an important issue which should not be overlooked is disorder and its possible implications on the electronic properties. In this respect we have to distinguish between different kinds of imperfections. The *extrinsic* disorder, i.e. impurity concentrations, contaminations or crystal defects can be vastly controlled in the preparation process although some aspects remain puzzling, see e.g. the discussion on the resistivity maximum in section 3.2. In a study of the alloy series β -(ET)₂X with $X = (\text{I}_3)_{1-x}(\text{IBr}_2)_x$ ($0 \leq x \leq 1$) - where the salts with the two limiting

compositions with $x = 0$ and $x = 1$ are superconductors - a clear correlation between the residual-resistivity ratio (RRR) and T_c was found [158]. These experiments show that superconductivity is very sensitive to the induced random potentials which lead to electron localization. The effect of random potentials created by radiation damage effects - resulting in a suppression of superconductivity - has been studied for the Bechgaard salts as well as for β -(ET) $_2$ I $_3$. For more details, the reader is referred to [5] and references therein.

(TM) $_2$ X salts However, certain kinds of *intrinsic* disorder are unavoidable and can be of particular importance for experiments attempting to explore superconducting-state properties. The latter type of imperfections concerns materials where, by symmetry, certain structural elements can adopt one of two possible orientations which are almost degenerate in energy [159,160]. This can be seen in the (TM) $_2$ X salts with non-centrosymmetric anions such as tetrahedral ClO $_4$. As a result, these anions are disordered at room temperature with an equal occupation for both orientations. Upon cooling, entropy is gained by a more or less perfect ordering of the anions, depending on how fast the system is cooled through the ordering temperature T_{AO} . A perfect long-range anion ordering, realized to a good approximation when cooled sufficiently slowly, then introduces a new periodicity of the lattice. Depending on the anion this can have quite different implications on the electronic properties: for the (TMTSF) $_2$ ClO $_4$ salt, for example, the anion ordering below 24 K is accompanied by a doubling of the periodicity along the b -axis, i.e. perpendicular to the stacking axis which leaves the conducting properties almost unaffected. In contrast, the anion ordering for (TMTSF) $_2$ ReO $_4$ opens up a large gap at the Fermi level leading to an insulating ground state. If the compound had been cooled quickly through T_{AO} , a disordered "quenched" state is adopted at low temperatures whose properties are quite different from the "relaxed" state obtained after slow cooling.

The left panel of Fig. 18 shows the effect of anion ordering on (TMTSF) $_2$ ClO $_4$. For a slowly cooled system, the anion-ordering phase transition occurs at $T_{AO} = 24$ K. This is accompanied by a decrease of the resistivity due to the reduction of scattering by randomly distributed anion potentials. Upon further cooling, superconductivity sets in with $T_c = (1.2 \pm 0.2)$ K. In contrast, for a crystal cooled rapidly, the high-temperature disordered state becomes quenched and the system undergoes a metal-to-insulator transition at $T_{MI} = 6.05$ K. The insulating quenched state has been identified via NMR and ESR measurements [163,164] as a SDW state with an energy gap $2\Delta_0/k_B T_{SDW} = 3.64$ close to the mean-field value of 3.52 [162]. The phase transition at T_{SDW} has been explored recently by specific heat measurements [165]. The right panel of Fig. 18 shows that the low-temperature resistivity may change over several orders of magnitude depending on the thermal history of the sample. Intermediate states with various degrees of frozen anion

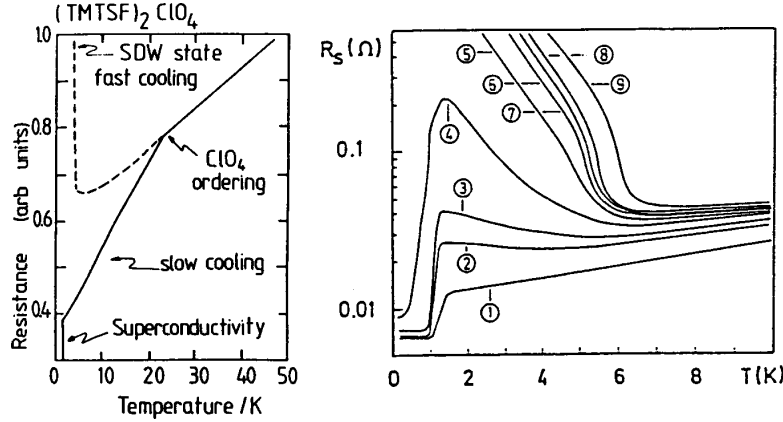


Fig. 18. Left panel: Effects of anion ordering in $(\text{TMTSF})_2\text{ClO}_4$ at $T_{AO} = 24\text{ K}$, on the resistivity, from [161]. Right panel: Semilogarithmic plot of the resistance vs temperature in states with various degrees of disorder characterized by T_Q numbered from 1 to 9 (see text), from [162].

disorder have been produced by rapidly cooling the crystal from different temperatures $T_Q \geq T_{AO}$. Recent specific heat measurements showed that there is no difference between the specific heat anomalies at T_{AO} of slowly cooled and those of quenched-cooled samples, i.e. the structural transition is independent of the kinetic conditions. From these results, the authors concluded that the reordering transition of the anions is of second order and occurs within the experimental timescales [165]. This is contrary to what would be expected for a glass-like transition. Such a glassy behavior, however, has been observed at the ordering temperatures of the compounds with $\text{X} = \text{ReO}_4$ ($T_{AO} = 180\text{ K}$) and FSO_3 ($T_{AO} = 86\text{ K}$). For more details see [33,5] and references therein.

$\kappa\text{-(BEDT-TTF)}_2\text{X}$ salts Indications for frozen-in disorder have been also reported for the quasi-2D salts of the $\kappa\text{-(ET)}_2\text{X}$ family. In an ac-calorimetry study, a glass-like transition has been found for $\kappa\text{-(ET)}_2\text{Cu}[\text{N}(\text{CN})_2]\text{Br}$ and $\kappa\text{-(ET)}_2\text{Cu}[\text{N}(\text{CN})_2]\text{Cl}$ [166–168]. The authors observed step-like anomalies in the heat capacity around 100 K, which have been attributed to a freezing out of the intramolecular motions of the ethylene endgroups at the ET molecules. Clear evidence for a glass-like transition have also been derived from thermal expansion measurements [97] which are extremely sensitive to structural rearrangements such as those involved in the glass-like freezing process. The outcome of this study confirmed, on the one hand, the above-mentioned specific heat results and clarified on the other, the nature of the thermal expansion anomalies previously reported by Kund et al. [88,150]. In addition, this study showed that a glass-like transition also exists for the $\kappa\text{-(ET)}_2\text{Cu}(\text{NCS})_2$ salt. A glass transition is due to a relaxation process where, below a characteristic

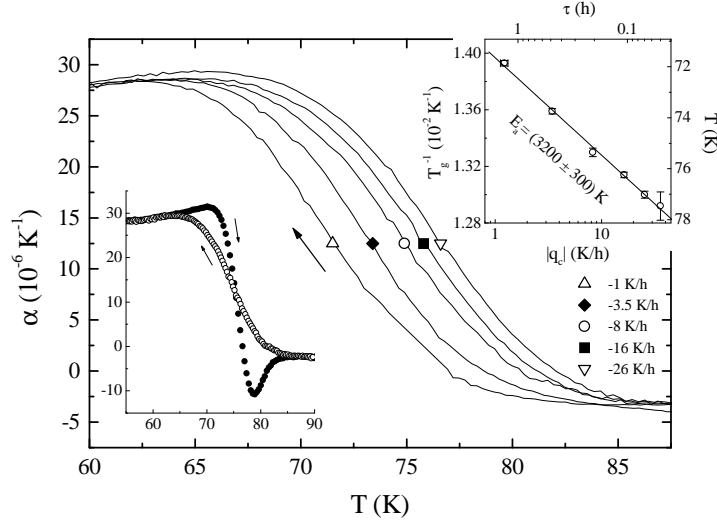


Fig. 19. Linear thermal expansion coefficient, α , vs T measured parallel to the conducting planes of κ -(ET) $_2$ Cu[N(CN) $_2$]Br in the vicinity of the glass transition defined as the midpoint of the step-like change in α for varying cooling rates q_c . Insets: hysteresis between heating and cooling curves around T_g (left side) and Arrhenius plot of T_g^{-1} vs $|q_c|$ and τ (right side), where $|q_c|$ is the cooling rate and τ the relaxation time. Taken from [97].

temperature T_g the relaxation time $\tau(T)$ of certain structural elements or molecules becomes so large that they can no longer reach thermodynamic equilibrium. As a result, a short range order, which is characteristic for this temperature T_g , becomes frozen in. Figure 19 shows exemplarily the linear coefficient of thermal expansion for κ -(ET) $_2$ Cu[N(CN) $_2$]Br measured parallel to the conducting planes at temperatures near T_g . As discussed in [97] the anomaly at $T_g \simeq 75$ K shows all the characteristics expected for a glassy transition [169], i.e. a step in the thermal expansion coefficient, a pronounced hysteresis between heating and cooling (left inset) and a cooling-rate dependent characteristic temperature T_g . The inset on the right side of Fig. 19 shows in an Arrhenius plot the inverse of the glass-transition temperatures, T_g^{-1} , vs the cooling rate $|q_c|$. The data nicely follow a linear behavior as expected for a thermally activated relaxation time [170,171]:

$$\tau(T) = \nu_0^{-1} \cdot \exp\left(\frac{E_a}{k_B T}\right), \quad (7)$$

where E_a denotes the activation energy barrier. The prefactor represents an attempt frequency ν_0 . A linear fit to the data of Fig. 19 yields $E_a = (3200 \pm 300)$ K.

The characteristic activation energy of the $[(\text{CH}_2)_2]$ conformational motion (cf. Fig. 4) was determined to $E_a = 2650$ K by ^1H -NMR measurements [143].

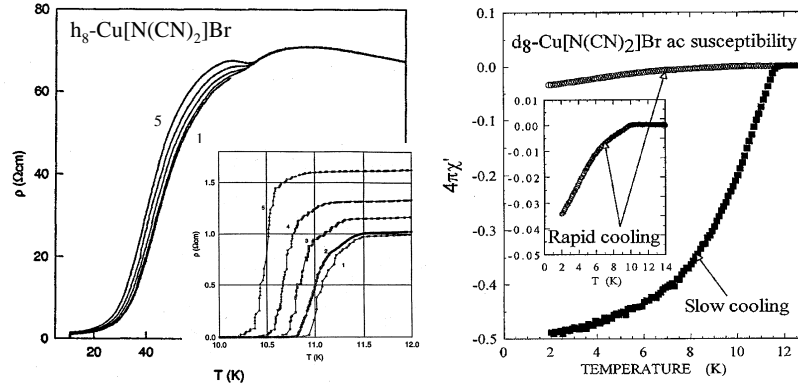


Fig. 20. Left panel: resistivity as a function of temperature for a sample of κ -(H₈-ET)₂Cu[N(CN)₂]Br cooled at different rates ranging from about 0.5 K/min, lower curve (1), to 60 K/min upper curve (5). The inset shows an expansion of the data near the superconducting transition. Reproduced from [173]. Right panel: ac-susceptibility of κ -(D₈-ET)₂Cu[N(CN)₂]Br after slow and rapid cooling. Taken from [177].

The similar size of the activation energy derived from Fig. 19 along with the observation of a mass-isotope shift when replacing the hydrogen atoms in [(CH₂)₂] by deuterium provide clear evidence that the ethylene endgroups are the relevant entities involved in the relaxation process [97].

An influence of the thermal history of the samples around 70 ~ 80 K on the electronic properties had been realized by various authors and interpreted in different ways. Based on resistance measurements of structural relaxation kinetics on κ -(ET)₂Cu[N(CN)₂]Br, Tanatar et al. [89] claimed that the ethylene-endgroup ordering is associated with a sequence of first-order phase transitions around 75 K. A pronounced kink in the resistivity at 75 K accompanied by hysteresis between heating and cooling had been reported early on for κ -(ET)₂Cu[N(CN)₂]Br [172,80]. Similar behavior in the vicinity of T_g was observed also for κ -(ET)₂Cu(NCS)₂ [87]. Besides that, more recent measurements on κ -(ET)₂Cu[N(CN)₂]Br yielded interesting time dependences affecting not only the electronic properties around 70 ~ 80 K but also the properties at lower temperatures: Su et al. reported relaxation effects in $R(T)$ and a separation of the curves below about 80 K as a function of the cooling rate q_c . As shown in the inset of Fig. 20 (left panel) the residual resistivity increases with increasing $|q_c|$ [173,174]. The inset also shows that the way of cooling through 70 ~ 80 K may influence the superconducting properties such that T_c decreases on increasing $|q_c|$. In addition, magnetization measurements revealed that with increasing $|q_c|$, a growing amount of disorder is induced causing an enlarged penetration depth [175]. In reference [176] an ac-susceptibility investigation of the magnetic penetration depths

and their dependence on the cooling-rate-dependent intrinsic disorder have been performed. The authors found that the superconducting-state properties are critically determined by the time scale of the experiment around T_g . For the deuterated κ -(ET)₂Cu[N(CN)₂]Br salt, it has been reported that rapid cooling through 80 K drives the superconducting ground state into an insulating antiferromagnetic state [177,178].⁴ As shown in the right panel of Fig. 20 the ac-susceptibility data reveal a strong suppression of the superconducting volume fraction with increasing cooling rate [177]. It is tempting to assign the apparent deterioration of superconductivity to the frozen disorder at T_g : via the C-H...donor and C-H...anion contact interactions, disorder in the ethylene groups introduces a random potential that may alter the effective transfer integrals t_{eff} and, by this, may destroy superconductivity, see also [37].

3.5 Phase diagrams

(TM)₂X salts Figure 21 comprises in a pressure-temperature plane results of various experiments on the quasi-1D charge-transfer salts (TMTTF)₂X and their sulfur analogues (TMTSF)₂X. The arrows indicate the position of the various salts at ambient pressure (cf. also Fig. 10). The generic character of the phase diagram - first proposed by Jérôme et al. [137] - has been demonstrated recently by pressure studies on the (TMTTF)₂PF₆ salt [67,180,68] for which the ambient-pressure ground state is a dimerized spin-Peierls state. With increasing pressure, the system was found to pass through the whole sequence of ground states as shown in Fig. 22 and eventually becoming superconducting at high pressures above 43.5 kbar [180,68].

On the low-pressure (left) side of the phase diagram in Figs. 21 and 22 the molecular stacks can be considered as only weakly-coupled chains, i.e. the system is close to be truly 1D. In fact upon cooling, the (TMTTF)₂PF₆ compound behaves very much like canonical 1D conductors where spin and charge degrees of freedom are decoupled: below $T_\rho = 250$ K the resistivity increases by several orders of magnitude due to charge localization while the spin susceptibility remains unaffected [6,33,78]. The phase below T_ρ has been interpreted as a Mott insulating state. Upon further cooling to $T_{SP} = 19$ K a spin gap opens and the system enters a distorted spin-Peierls ground state. In (TMTTF)₂Br, position (b) Figs. 21 and 22, a long-range magnetic order is established below the spin-density-wave transition at $T_{SDW} \approx 13$ K. Toward the right side of the phase diagram, which can be carried out either

⁴ The ground state of deuterated κ -(D₈-ET)₂Cu[N(CN)₂]Br is strongly sample dependent; there are both superconducting as well as non-superconducting samples. In [177] it is claimed that the crystals always contain superconducting and non-superconducting components, whereas the latter have a magnetic character, possibly similar to that of κ -(ET)₂Cu[N(CN)₂]Cl. It is thus believed that the system is situated in the critical region of the phase diagram just between the superconducting and antiferromagnetic phases, see section 3.5.

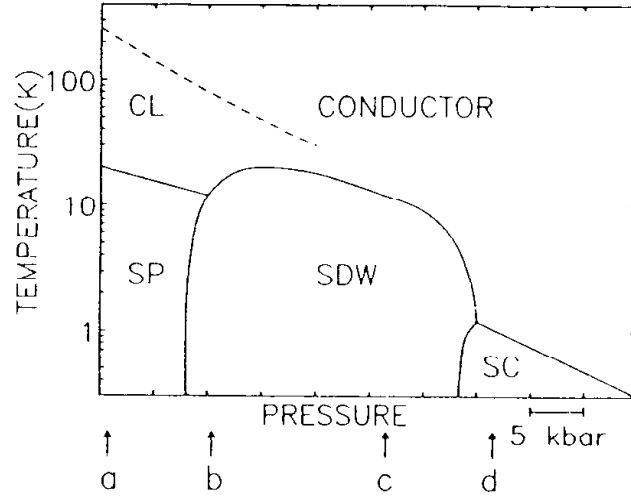


Fig. 21. Generalized phase diagram for the quasi-1D $(\text{TM})_2\text{X}$ salts as proposed first by Jérôme [137]. Arrows indicate the positions of the salts with different anions X at ambient pressure: (a) $(\text{TMTTF})_2\text{PF}_6$, (b) $(\text{TMTTF})_2\text{Br}$, (c) $(\text{TMTSF})_2\text{PF}_6$, (d) $(\text{TMTSF})_2\text{ClO}_4$. The following abbreviations are used: charge-localised insulator (CL), spin Peierls (SP), incommensurate spin-density-wave (SDW) and superconductivity (SC). Taken from [179].

by varying the anion or by the application of hydrostatic pressure, inter-stack interactions become more important. In this region of the phase diagram the electron-phonon interaction is less dominant and electron-electron interactions along with the good nesting properties of the Fermi surface (cf. Fig. 7) lead to a spin-density-wave ground state as observed, e.g. in the Bechgaard salt $(\text{TMTSF})_2\text{PF}_6$ at ambient pressure. After suppression of the SP phase in $(\text{TMTTF})_2\text{PF}_6$ with increasing pressure, a commensurate antiferromagnetic state is adopted before an incommensurate SDW phase is stabilized. With increasing pressure, T_{SDW} becomes progressively reduced until, above some critical pressure, the systems remain metallic and superconductivity replaces the SDW ground state. The effect of pressure is to increase the π -orbital overlap also in the transverse direction, i.e. perpendicular to the stacking axis. As a result the almost perfect nesting properties are destroyed and the systems become more 3D in character.⁵ According to NMR experiments [33,66] and recent transport measurements under hydrostatic pressure [180,68] strong

⁵ Recent measurements under uniaxial strain revealed that the SDW transition is most strongly suppressed and superconductivity can be induced by the strain along the stacking a -axis [181,182]. Considerably smaller effects were observed for strain along the b' - and c' -axes - although the former direction is directly associated with the denesting of the quasi-1D Fermi surface [181]. This has been

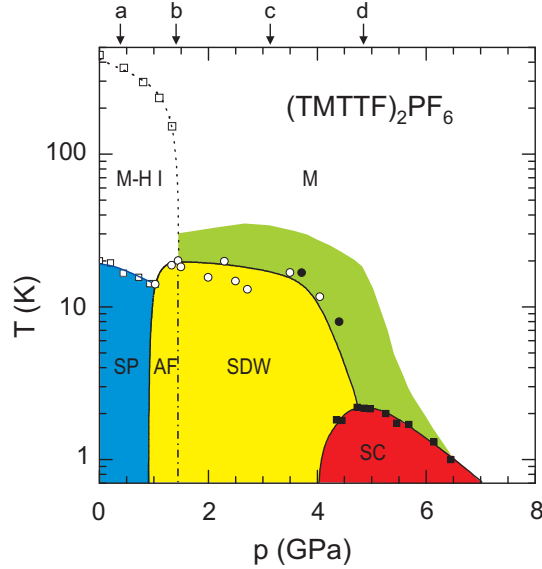


Fig. 22. Temperature-hydrostatic-pressure phase diagram for $(\text{TMTTF})_2\text{PF}_6$. The abbreviations are: Mott-Hubbard insulating state (M-H I), metallic (M) and superconducting (SC) state, spin-Peierls (SP), commensurate (AF) and incommensurate (SDW) antiferromagnetic spin-density-wave state. Arrows: ambient-pressure ground-state location of other salts; (a) $(\text{TMTTF})_2\text{BF}_4$, (b) $(\text{TMTTF})_2\text{Br}$, (c) $(\text{TMTSF})_2\text{PF}_6$, (d) $(\text{TMTSF})_2\text{ClO}_4$. Taken from [68].

SDW correlations are still active in the metallic state even when the SDW instability is replaced by superconductivity in $(\text{TMTSF})_2\text{ClO}_4$. The range of strong SDW correlations for $(\text{TMTTF})_2\text{PF}_6$ derived from these experiments is indicated in Fig. 22 by the shaded region above the SDW and SC phase boundaries.

κ -(BEDT-TTF) $_2\text{X}$ salts Figure 23 shows a conceptual phase diagram proposed by Kanoda for the dimerized κ -type BEDT-TTF salts. Here it has been assumed that it is the effective on-site (dimer) Coulomb interaction U_{eff} normalized to the bandwidth W which is the key factor associated with the various phases and phase transitions [95,96]. The positions of the various salts are determined by their ambient-pressure ground-state properties. The deuterated κ -(D₈-ET) $_2\text{Cu}[\text{N}(\text{CN})_2]\text{Br}$ salt is situated right at the AFI/SC border. The system lies in between the antiferromagnetic insulating $\text{X} = \text{Cu}[\text{N}(\text{CN})_2]\text{Cl}$ and the superconducting hydrogenated κ -(H₈-ET) $_2\text{Cu}[\text{N}(\text{CN})_2]\text{Br}$ salts. It has been proposed that a *partial* substitution of the 2×4 H-atoms by D-atoms allows for fine-tuning the κ -(ET) $_2\text{Cu}[\text{N}(\text{CN})_2]\text{Br}$ system across the AFI/SC border [184–186]. The close proximity of an antiferromagnetic insulating to a superconducting phase has been considered - in analogy to the high- T_c cuprates - as a strong indication that both phenomena are closely connected to each other [4].

interpreted in terms of a pressure-induced decrease in the density of states at the FS [183].

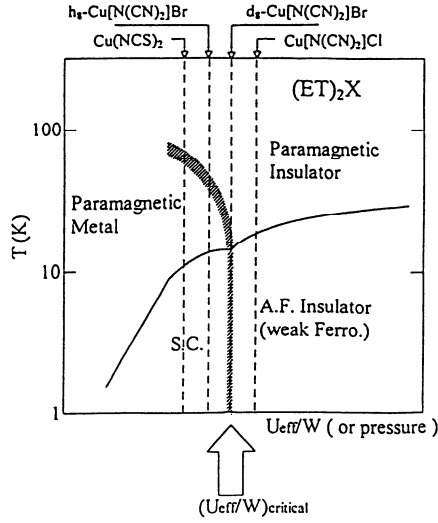


Fig. 23. Conceptual phase diagram for κ -phase $(\text{ET})_2\text{X}$ as proposed by Kanoda [96]. Note that hydrostatic pressure decreases the ratio U_{eff}/W , i.e. the low pressure side is on the right end of the phase diagram. The arrows indicate the ambient-pressure position of the various systems and AF and SC denote an antiferromagnetic insulator and superconductor, respectively.

Figure 24 summarizes experimental data of a detailed thermodynamic study on the various κ -($\text{ET})_2\text{X}$ compounds in a pressure-temperature phase diagram [97,187]. The positions of the various salts at ambient pressure are indicated by the arrows.⁶ The solid lines representing the phase boundaries between the paramagnetic (PM) and the superconducting (SC) or antiferromagnetic insulating (AFI) states refer to the results of hydrostatic-pressure studies of T_c and T_N [188,189,81].

At elevated temperatures, a glass-like transition at a temperature T_g (dotted line) has been identified. It marks the boundary between an ethylene-liquid at $T > T_g$ and a glassy state at $T < T_g$. While at temperatures above T_g , the motional degrees of freedom of the ethylene endgroups are excited with an equal occupancy for the two possible ethylene conformations, a certain disorder becomes frozen in at temperatures below T_g . The glass-like transition which is structural in nature has been shown to cause time dependences in electronic properties and may have severe implications on the ground-state properties of the κ -($\text{ET})_2\text{Cu}[\text{N}(\text{CN})_2]\text{Br}$ salt depending on the cooling rate employed at T_g (see section 3.4).

At intermediate temperatures T^* , anomalies in the coefficient of thermal expansion have been found and assigned to a density-wave transition involving only the quasi-1D parts of the Fermi surface. These anomalies coincide

⁶ Note that hydrostatic pressure has been used as an abscissa for the purpose of compatibility with the conceptual phase diagram in Fig. 23. It has been found, however, that the uniaxial-pressure dependences for the various phase boundaries are strongly anisotropic [151,97,98] with a non-uniform behavior for the uniaxial-pressure coefficients of both the density-wave instability at T^* and those of T_c , cf. Figs. 16 and 31.

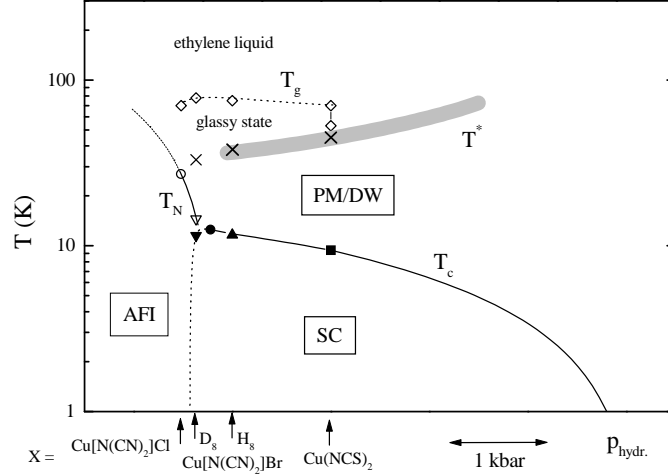


Fig. 24. Temperature-hydrostatic-pressure phase diagram for the κ -(ET) $_2$ X compounds. Arrows indicate the positions of the various compounds at ambient pressure. Circles correspond to results on κ -(ET) $_2$ Cu[N(CN) $_2$]Cl while down and up triangles indicate phase-transition temperatures on deuterated and hydrogenated κ -(ET) $_2$ Cu[N(CN) $_2$]Br, respectively, and squares stand for results on κ -(ET) $_2$ Cu(NCS) $_2$. The transitions into the superconducting and antiferromagnetic states are represented by closed and open symbols, respectively. Diamonds denote the glass-like freezing of ethylene disorder and crosses the density-wave (DW) transition on minor parts of the Fermi surface. These anomalies coincide with various features observed in magnetic, transport and acoustic properties (shaded area, see section 3.3). Taken from [97,187].

with various features observed in magnetic, transport and acoustic properties (thick shaded line in Fig. 24, see also section 3.3). In [97,98] it has been proposed that instead of a pseudogap on the quasi-2D parts of the Fermi surface, a real gap associated with a density wave opens on the minor quasi-1D parts below T^* , see also [99]. This scenario implies that the density wave and superconductivity involve disjunct parts on the Fermi surface and compete for stability.

Details of the pressure-temperature phase diagram of the antiferromagnetic insulating salt κ -(ET) $_2$ Cu[N(CN) $_2$]Cl have been reported by Ito et al. [190] and Lefebvre et al. [191]. In the latter work, it has been shown that the superconducting and antiferromagnetic phases overlap through a first-order boundary that separates two regions of an inhomogeneous phase coexistence [191]. It has been argued that this boundary curve merges with a first-order line of the metal-insulator transition and that this line ends at a critical point at higher temperature, see Fig. 25. The figure also suggests the existence of a point-like region where the metallic, insulating, antiferromagnetic as well as superconducting phases all meet. This would imply the absence of a bound-

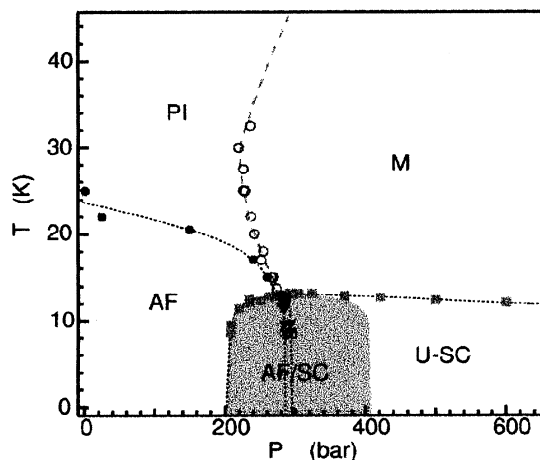


Fig. 25. Pressure-temperature phase diagram for κ -(ET) $_2$ Cu[N(CN) $_2$]Cl. The antiferromagnetic (AF) transition temperature $T_N(p)$ (closed circles) were determined from the NMR relaxation rate while $T_c(p)$ (closed squares) and $T_{MI}(p)$ (open circles) were obtained from ac-susceptibility measurements. U-SC denotes unconventional superconductivity; the AF-SC boundary line separates two regions of inhomogeneous phase coexistence (shaded area). Taken from [191].

ary between metallic and complete antiferromagnetic phases which would be incompatible with an itinerant type of magnetism [191].

(BEDT-TSF) $_2$ X salts Figure 26 shows the phase diagram for the quasi-2D alloy system λ -(BETS) $_2$ Fe $_x$ Ga $_{1-x}$ Cl $_4$ which has recently gained strong interest due to its interesting magnetic and superconducting properties [192]. The system is based on the donor molecule BEDT-TSF or simply BETS which represents the Se analogue to BEDT-TTF, see section 2. λ -(BETS) $_2$ GaCl $_4$ on the left side is a nonmagnetic salt which becomes superconducting at $T_c = 6$ K [31]. A magnetic field of 13 T aligned parallel to the highly conducting planes destroys superconductivity and stabilizes a paramagnetic metallic state. Conversely, λ -(BETS) $_2$ FeCl $_4$ shows a metal-insulator (M-I) transition around 8 K which is accompanied by an antiferromagnetic order of the Fe $^{3+}$ moments in the anion layers [28]. Applying a magnetic field in excess of about 10 T destabilizes the insulating phase and the paramagnetic phase recovers [193,194]. In the mixed series λ -(BETS) $_2$ Fe $_x$ Ga $_{1-x}$ Cl $_4$, the M-I transition becomes suppressed as the concentration x of magnetic Fe ions decreases and a superconducting ground state is formed for $x \leq 0.35$. A striking feature is the metal-superconductor-insulator transition for $0.35 \leq x \leq 0.5$, see Fig. 26. Apparently, the various phases contained in the above phase diagram originate from an intimate coupling between the magnetic moments of the Fe $^{3+}$

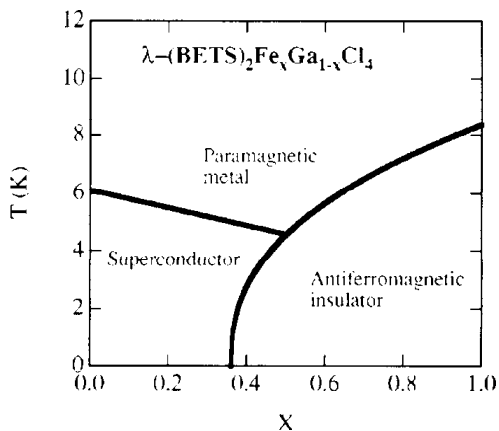


Fig. 26. Phase diagram for $\lambda\text{-(BETS)}_2\text{Fe}_x\text{Ga}_{1-x}\text{Cl}_4$ taken from [32].

3d electrons and the π -conduction-electron spins of the BETS molecule, see e.g. [194,195,32].

4 Superconducting-state properties

Since the discovery of superconductivity in pressurized $(\text{TMTSF})_2\text{PF}_6$ in 1979 [1], continuing efforts to design new potential donor and acceptor molecules have led to more than about 80 organic superconductors.⁷ In the vast majority of cases, the donor molecules are derivatives of the prototype TMTSF molecule including BEDT-TTF as well as the selenium and oxygen substituted variants BEDT-TSF and BEDO-TTF, respectively. In addition, superconductors have been derived using asymmetric hybrids such as DMET and MDT-TTF. For a comprehensive list of organic superconductors the reader is referred to [5].

In the following discussion of superconducting properties we will confine ourselves to a few selected examples. These are the $(\text{TMTSF})_2\text{X}$ and the quasi-2D $(\text{BEDT-TTF})_2\text{X}$ and $(\text{BEDT-TSF})_2\text{X}$ salts which are representative for a wide class of materials.

4.1 The superconducting phase transition

Organic superconductors are characterized by a highly anisotropic electronic structure, a low charge carrier concentration and unusual lattice properties. As will be discussed below, the combination of these unique material parameters lead to a variety of remarkable phenomena of the superconducting state

⁷ The materials discussed in this article have to be distinguished from another class of molecular superconductors - the alkali-metal-doped fullerenes discovered in 1991 [196] - which are usually not referred to as organic materials as they contain only carbon atoms.

such as pronounced thermal fluctuations, an extraordinarily high sensitivity to external pressure and anomalous mixed-state properties.

Superconducting anisotropy The abrupt disappearance of the electrical resistance is one of the hallmarks that manifests the transition from the normal into the superconducting state for usual 3D superconductors. For the present low-dimensional organic superconductors - as in the layered high- T_c cuprates - however, strong fluctuations of both the amplitude and phase of the superconducting order parameter may cause a substantial broadening of the superconducting transition. This becomes particularly clear when a strong magnetic field is applied. As a consequence, for these materials zero-resistance is no longer a good measure of the superconducting transition temperature in a finite magnetic field. Therefore, for a precise determination of the upper critical fields, thermodynamic investigations such as magnetization, specific heat or thermal expansion measurements are necessary.

For materials with strongly directional-dependent electronic properties, a highly anisotropic superconducting state is expected as well. In an attempt to account for these anisotropies, the phenomenological Ginzburg-Landau and London models have been extended by employing an effective-mass tensor [197]. In the extreme case of a quasi-2D superconductor characterized by a superconducting coherence length perpendicular to the planes, ξ_\perp , being even smaller than the spacing between the conducting layers, s , these anisotropic 3D models are no longer valid. Instead, the superconductor has to be described by a model that takes the discreteness of the structure into account. Such a description is provided by the phenomenological Lawrence-Doniach model [198] which encloses the above anisotropic Ginzburg-Landau and London theories as limiting cases for $\xi_\perp > s$. This model considers a set of superconducting layers separated by thin insulating sheets implying that the 3D phase coherence is maintained by Josephson currents running across the insulating layers. In fact, the presence of an intrinsic Josephson effect has been demonstrated for several layered superconductors including some of the high- T_c cuprates and the present κ -(ET) $_2$ Cu(NCS) $_2$ salt [199,200].

To quantify the degree of anisotropy, it is convenient to compare the results of orientational-dependent measurements with the above anisotropic models. For layered systems such as the present (BEDT-TTF) $_2X$ compounds, it is customary to use the effective-mass ratio $\Gamma = m_\perp^*/m_\parallel^*$, where m_\perp^* and m_\parallel^* denote the effective masses for the superconducting carriers moving perpendicular and parallel to the conducting planes, respectively. In the London and Ginzburg-Landau theories, Γ is directly related to the anisotropies in the magnetic penetration depths λ and coherence lengths ξ by

$$\sqrt{\Gamma} = \frac{\lambda_\perp}{\lambda_\parallel} = \frac{\xi_\parallel}{\xi_\perp}. \quad (8)$$

As an example for the highly anisotropic response of the superconducting transition to a magnetic field, we show in Fig. 27 results of the coefficient

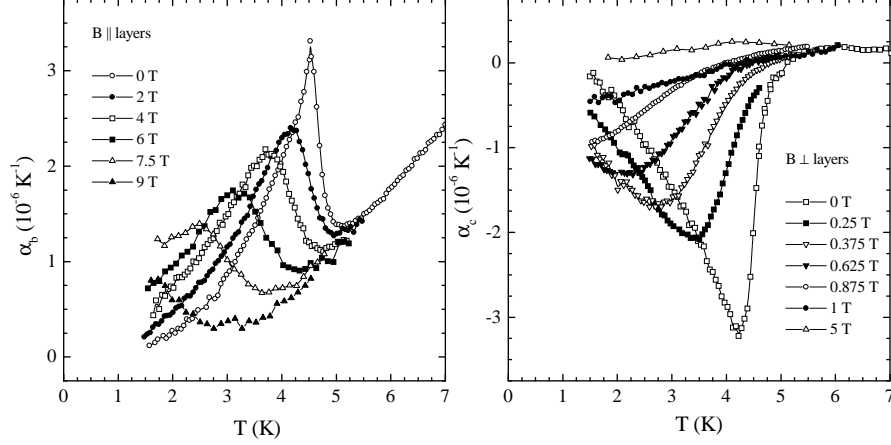


Fig. 27. Coefficient of thermal expansion of β'' -(ET) $_2$ SF $_5$ CH $_2$ CF $_2$ SO $_3$ measured parallel (left panel) and perpendicular (right panel) to the conducting planes in varying fields applied along the measuring directions. Taken from [151].

of thermal expansion $\alpha(T)$ near T_c for β'' -(ET) $_2$ SF $_5$ CH $_2$ CF $_2$ SO $_3$.⁸ While for fields parallel to the planes (left panel) the phase transition in $\alpha(T)$ is still visible even in $B = 9$ T, a field of 1 T applied perpendicular to the conducting planes is sufficient to suppress almost completely superconductivity (right panel of Fig. 27). In addition, for this field orientation, a pronounced rounding of the phase-transition anomaly even for very small fields can be observed. From these measurements the upper critical fields, B_{c2} , can be determined permitting an estimate of the anisotropy parameter Γ :

$$B_{c2}^{\perp'} = \left| \frac{dB_{c2}^{\perp}}{dT} \right| = \frac{\phi_0}{2\pi\xi_{\parallel}^2 T_c} \quad \text{and} \quad \frac{B_{c2}^{\perp'}}{B_{c2}^{\parallel'}} = \frac{\xi_{\perp}}{\xi_{\parallel}} = \frac{1}{\sqrt{\Gamma}}, \quad (9)$$

where $B_{c2}^{\perp'}$ and $B_{c2}^{\parallel'}$ are the initial slopes of the upper critical fields for B perpendicular and parallel to the conducting planes, respectively [203,204] and ϕ_0 is the flux quantum. For β'' -(ET) $_2$ SF $_5$ CH $_2$ CF $_2$ SO $_3$ one finds $\xi_{\parallel} = (144 \pm 9)$ Å, $\xi_{\perp} = (7.9 \pm 1.5)$ Å and $\Gamma \approx 330$ [151] (cf. Table 1 in section 2.2 and Table 2 in section 4.2), which underlines the quasi-2D character of the superconducting state in this material. The large anisotropy parameter $\Gamma \approx 330$ exceeds the value of $\Gamma \approx 100$ found for the κ -(ET) $_2$ Cu(NCS) $_2$ salt in dc-magnetization experiments [205].

The so-derived Γ values, however, may serve only as a rough estimate of the actual anisotropy parameters. The latter can be probed most sensitively by employing torque-magnetometry. For κ -(ET) $_2$ Cu(NCS) $_2$ for example, Γ

⁸ This salt of the β'' -type structure contains large discrete anions and is unique in being the first superconductor free of any metal atoms [201,202].

values ranging from 200 to 350 have been reported [206,207] which place this material in the same class of quasi-2D superconductors as the most anisotropic high- T_c cuprates with $\Gamma = 150 \sim 420$ for $\text{Bi}_2\text{Sr}_2\text{CaCu}_2\text{O}_{8+x}$ [208,209].

Fluctuation effects The highly anisotropic response of the present quasi-2D superconductors to a magnetic field is also demonstrated in Fig. 28 where the temperature dependence of the magnetization around the superconducting transition is shown for $\kappa\text{-(ET)}_2\text{Cu(NCS)}_2$. While for fields aligned perpendicular to the planes (left panel) the transition considerably broadens with increasing field strength, there is only a little effect on the transition for fields parallel to the layers (right panel) [205], cf. also Fig. 27. This behavior is quite different from that which is found in a usual 3D superconductor and indicates the presence of strong superconducting fluctuations which are strongly enhanced in systems with reduced dimensionality [210].

A measure of the strength of thermal order-parameter fluctuations is provided by the so-called Ginzburg number

$$G = \frac{|T - T_c|}{T_c} = \frac{1}{2} \left(\frac{k_B T}{B_{cth}^2(0) \xi_{\parallel}^2 \xi_{\perp}} \right)^2, \quad (10)$$

where $B_{cth}(0)$ is the thermodynamic critical field. G measures the ratio of thermal energy to the condensation energy per coherence volume. For classical 3D superconductors like niobium G amounts to about $G \sim 10^{-11}$. In contrast, for the present compounds and some of the high- T_c cuprates one finds $G \sim 10^{-2} - 10^{-3}$ [205,211,212]. Here, the relatively high transition temperatures together with a low charge-carrier concentration - the latter results in a

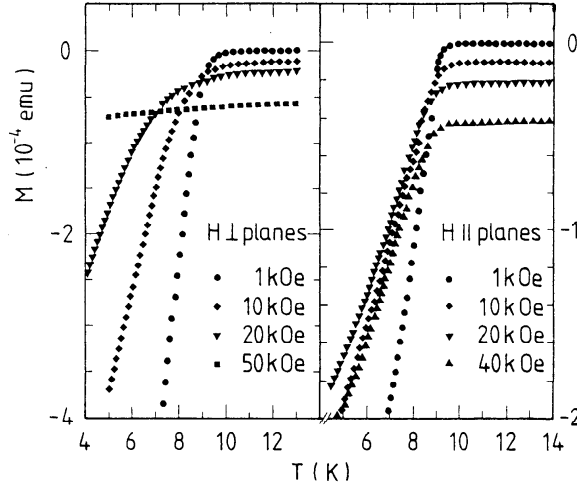


Fig. 28. Raw data of the dc-magnetization of single crystalline $\kappa\text{-(ET)}_2\text{Cu(NCS)}_2$ in various fields perpendicular (left panel) and parallel (right panel) to the conducting planes. The offset of each curve is due to contributions from the core electrons, the spin susceptibility as well as a small background signal. Taken from [205].

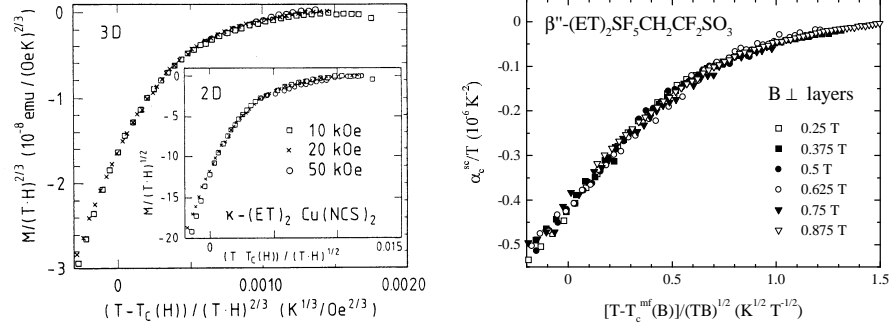


Fig. 29. Scaling behavior of the superconducting contribution to the magnetization of $\kappa-(\text{ET})_2\text{Cu}(\text{NCS})_2$ (left panel) [205] and the linear coefficient of thermal expansion of $\beta''-(\text{ET})_2\text{SF}_5\text{CH}_2\text{CF}_2\text{SO}_3$ (right panel) [151] in magnetic fields applied perpendicular to the planes.

small Fermi velocity, v_F , and thus a short coherence length $\xi \propto \hbar v_F / (k_B T_c)$ - enhance the effect of superconducting fluctuations. The strong rounding of the phase-transition anomaly with increasing magnetic fields aligned perpendicular to the conducting planes is then understood to be a result of a field-induced dimensional crossover: while the electronic state in small fields is quasi-2D, the confinement of the quasiparticles to their lower Landau levels in high fields leads to a quasi-zerodimensional situation [213,214]. As a result, the relatively sharp phase-transition anomaly in zero field becomes progressively rounded and smeared out with increasing field. Instead of a well defined phase boundary between normal and superconducting states, the high-field range of the B - T phase diagram is characterized by a crossover behavior with extended critical fluctuations. Here, the assertion of a mean-field transition temperature, $T_c^{\text{mf}}(B)$, from the raw data is difficult and a fluctuation analysis has to be invoked.

The effect of fluctuations on transport and thermodynamic properties has been studied by several authors [215,216]. Assuming the lowest-Landau-level approximation and taking into account only non-interacting Gaussian fluctuations, Ullah and Dorsey obtained an expression for a scaling function of various thermodynamic quantities as the magnetization M or the specific heat C :

$$\Xi_i = F_i \left(A \frac{T - T_c^{\text{mf}}(B)}{(TB)^n} \right), \quad (11)$$

with $\Xi_i = M/(TB)^n$ or C/T [211]. F_i is an unknown scaling function, A a temperature- and field-independent coefficient characterizing the transition width and $n = 2/3$ for anisotropic 3D materials and $n = 1/2$ for a 2D system. Thus from a scaling analysis both the actual dimensionality as well as the mean-field-transition temperature $T_c^{\text{mf}}(B)$ can be determined.

Figure 29 shows the data of the dc-magnetization of κ -(ET)₂Cu(NCS)₂ (Fig. 28) and thermal expansion of β'' -(ET)₂SF₅CH₂CF₂SO₃ (Fig. 27) taken in varying fields in the proper scaling forms $M/(TH)^{(n)}$ vs $(T - T_c^{mf}(B))/(TB)^n$ and α_c^{sc}/T vs $(T - T_c^{mf}(B))/(TB)^{1/2}$, respectively, where α_c^{sc} denotes the superconducting contribution to the coefficient of thermal expansion.⁹ As shown in Fig. 29 the various field curves $\alpha_c^{sc}(T, B)$ show the 2D scaling over a rather wide temperature and field range, see also [211,217]. According to the scaling analysis of the high-field magnetization in Fig. 29 as well as the high-field conductivity in [218], κ -(ET)₂Cu(NCS)₂ is at the threshold from being a strongly anisotropic 3D to a 2D superconductor. On the other hand, a distinct 2D behavior has been claimed from a scaling analysis of low-field magnetization data by Ito et al. [219].

Pressure dependence of T_c By applying pressure to a superconductor, one can study the volume dependence of the pairing interaction through changes of T_c . For the (TMTSF)₂X and (ET)₂X superconductors, one generally finds an extraordinarily high sensitivity to external pressure and, in the vast majority of cases, a rapid decrease of T_c with pressure.

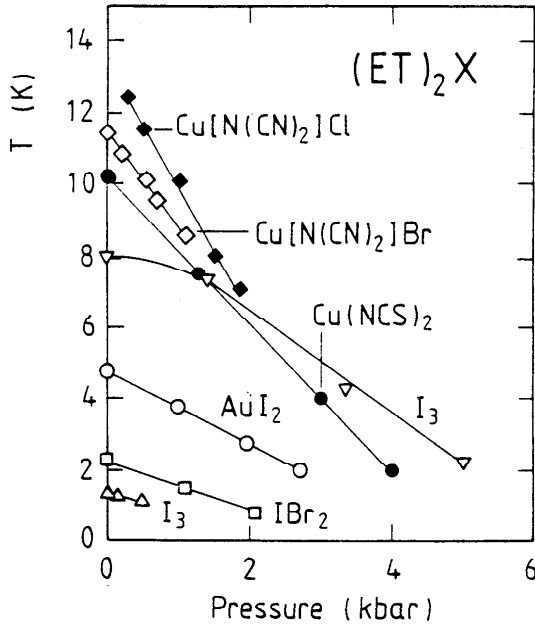


Fig. 30. Hydrostatic-pressure dependence of T_c for various β - and κ -type (ET)₂X superconductors. Reproduced from [5].

⁹ Since the volume coefficient of thermal expansion, $\beta(T)$, is related to the specific heat via the Grüneisen relation $\beta(T) = \gamma \cdot \frac{\kappa_T}{V_{mol}} \cdot C_V(T)$, where κ_T denotes the isothermal compressibility, V_{mol} the molar volume and γ a field- and temperature-independent Grüneisen parameter, the scaling form holds also for α/T .

Figure 30 shows the variation of T_c for a selection of β - and κ -type $(\text{ET})_2\text{X}$ salts under hydrostatic-pressure conditions. The initial slope of the pressure dependence of T_c , $(\partial T_c/\partial p)_{p \rightarrow 0}$, determined via resistivity measurements ranges from -0.25 K/kbar for α -($\text{ET})_2\text{NH}_4\text{Hg}(\text{SCN})_4$ ($T_c = 1 \text{ K}$) [220] to -3.2 K/kbar for κ -($\text{ET})_2\text{Cu}[\text{N}(\text{CN})_2]\text{Cl}$ ($T_c = 12.8 \text{ K}$ at 0.3 kbar) [81]. For $(\text{TMTSF})_2\text{PF}_6$, one finds $-(8 \pm 1) \cdot 10^{-2} \text{ K/kbar}$ ($T_c = 1.1 \text{ K}$ at 6.5 kbar) [136]. At first glance a strong pressure dependence of T_c appears not surprising in view of the weak van der Waals bonds between the organic molecules, giving rise to a highly compressible crystal lattice. In fact, the isothermal compressibility $\kappa_T = -\partial \ln V/\partial p$ for κ -($\text{ET})_2\text{Cu}(\text{NCS})_2$ of $\kappa_T = (122 \text{ kbar})^{-1}$ [221,222] exceeds the values found for ordinary metals by about a factor of five. To account for this "lattice effect" one should, therefore, consider the physically more meaningful volume dependence of T_c :

$$\frac{\partial \ln T_c}{\partial \ln V} = \frac{V}{T_c} \cdot \frac{\partial T_c}{\partial V} = -\frac{1}{\kappa_T \cdot T_c} \cdot \frac{\partial T_c}{\partial p}. \quad (12)$$

Using the above isothermal compressibility, one finds $\partial \ln T_c/\partial \ln V \approx 40$ for κ -($\text{ET})_2\text{Cu}(\text{NCS})_2$ [151] which exceeds the values found for ordinary metallic superconductors, as e.g. for Pb with $\partial \ln T_c/\partial \ln V = 2.4$ [223], or the layered copper-oxides with $-(0.36 \sim 0.6)$ reported for $\text{YBa}_2\text{Cu}_3\text{O}_7$ [224] by $1 \sim 2$ orders of magnitude.

For strongly anisotropic superconductors like those discussed here, even more information on the relevant microscopic couplings can be obtained by studying the effect of uniaxial pressure on T_c . Different techniques have been employed to determine the uniaxial-pressure coefficients of T_c for the $(\text{TMTSF})_2\text{X}$ and $(\text{ET})_2\text{X}$ salts including measurements under uniaxial strain or stress [225–228] or by using a thermodynamic analysis of ambient-pressure thermal expansion and specific heat data [229,230,151,97]. The latter approach is based on the Ehrenfest relation which connects the pressure coefficients of T_c for uniaxial pressure along the i -axis (in the limit of vanishing pressure) to the phase-transition anomalies at T_c in the coefficient of thermal expansion, $\Delta\alpha_i$, and specific heat, ΔC :

$$\left(\frac{\partial T_c}{\partial p_i}\right)_{p_i \rightarrow 0} = V_{mol} \cdot T_c \cdot \frac{\Delta\alpha_i}{\Delta C}, \quad (13)$$

with V_{mol} being the molar volume. Figure 31 shows results of the linear thermal expansion coefficients along the three principal crystal axes of the superconductors β'' -($\text{ET})_2\text{SF}_5\text{CH}_2\text{CF}_2\text{SO}_3$, κ -(D_8 - $\text{ET})_2\text{Cu}(\text{NCS})_2$ and κ -($\text{ET})_2\text{Cu}[\text{N}(\text{CN})_2]\text{Br}$. In all three cases, the uniaxial expansion coefficients are strongly anisotropic with striking similarities in the α_i 's for the β'' and κ -($\text{ET})_2\text{Cu}(\text{NCS})_2$ salts. Using equation (13), the uniaxial-pressure coefficients can be derived [151,97]. For κ -($\text{ET})_2\text{Cu}[\text{N}(\text{CN})_2]\text{Br}$ one finds $\partial T_c/\partial p_b = -(1.26 \pm 0.25) \text{ K/kbar}$ for the out-of-plane coefficient and $\partial T_c/\partial p_a = -(1.16 \pm 0.2) \text{ K/kbar}$ and $\partial T_c/\partial p_c =$

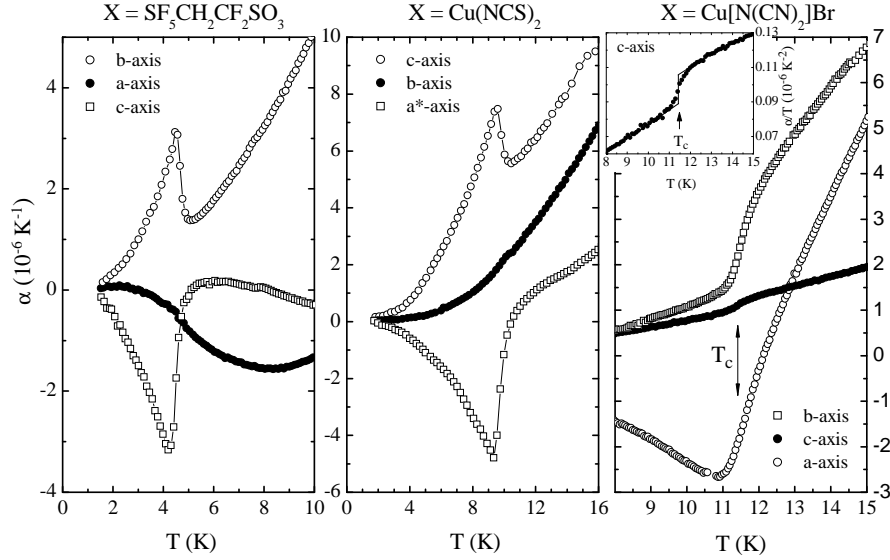


Fig. 31. Uniaxial coefficients of thermal expansion, α_i , vs temperature around the superconducting transition for $(\text{ET})_2\text{X}$ with $\text{X} = \text{SF}_5\text{CH}_2\text{CF}_2\text{SO}_3$ (left), $\text{Cu}(\text{NCS})_2$ (middle) and $\text{Cu}[\text{N}(\text{CN})_2]\text{Br}$ (right panel), taken from [151,97,187]. Open squares indicate α data perpendicular to the planes; open and closed circles correspond to the in-plane expansion coefficients.

$-(0.12 \pm 0.05) \text{ K/kbar}$ for the in-plane coefficients, employing a jump height in the specific heat ΔC as reported by [267]. In the same way, one obtains for $\beta''\text{-(ET)}_2\text{SF}_5\text{CH}_2\text{CF}_2\text{SO}_3$ $-(5.9 \pm 0.25) \text{ K/kbar}$ along the out-of-plane c -axis and $+(3.9 \pm 0.15) \text{ K/kbar}$ and $+(0.39 \pm 0.1) \text{ K/kbar}$ for the in-plane coefficients along the b - and a -axis, respectively, using the ΔC value given in [231]. To check for consistency, the hydrostatic-pressure dependences can be calculated by summing over the uniaxial-pressure coefficients yielding $\partial T_c / \partial p_{\text{hydr}} = \sum_i (\partial T_c / \partial p_i) = -(2.54 \pm 0.5) \text{ K/kbar}$ and $-(1.6 \pm 0.5) \text{ K/kbar}$ for the κ and the β'' salt, respectively. These values are found to be in good agreement with the results obtained by hydrostatic-pressure experiments, i.e. $-(2.4 \sim 2.8) \text{ K/kbar}$ for $\kappa\text{-(ET)}_2\text{Cu}[\text{N}(\text{CN})_2]\text{Br}$ [189,94] and -1.43 K/kbar for $\beta''\text{-(ET)}_2\text{SF}_5\text{CH}_2\text{CF}_2\text{SO}_3$ [231].¹⁰

An obvious step towards a microscopic understanding of this class of super-

¹⁰ Figure 31 shows that there is a strikingly similar behavior for the uniaxial thermal expansion coefficients and thus the uniaxial-pressure coefficients of T_c of $\beta''\text{-(ET)}_2\text{SF}_5\text{CH}_2\text{CF}_2\text{SO}_3$ and $\kappa\text{-(D}_8\text{-ET)}_2\text{Cu}(\text{NCS})_2$. The same observation was made also for the hydrogenated $\kappa\text{-(H}_8\text{-ET)}_2\text{Cu}(\text{NCS})_2$ compound [230,187]. Due to the lack of specific heat data for the deuterated salt, the uniaxial-pressure coefficients of $\kappa\text{-(ET)}_2\text{Cu}(\text{NCS})_2$ can only be discussed qualitatively. According to a recent comparative study on the pressure dependences of the normal- and superconducting-state properties of hydrogenated and deuterated

conductors is to trace out those uniaxial-pressure effects which are common to all systems and thus reflect a generic property. Such information would provide a most useful check of theoretical models attempting to explain superconductivity and its interrelation with the various other instabilities in the pressure-temperature plane. As Fig. 31 demonstrates, an extraordinarily large negative uniaxial-pressure coefficient of T_c for uniaxial pressure perpendicular to the conducting planes is common to all three superconductors shown there. Apparently, it is this huge component which predominates the large response of T_c under hydrostatic pressure. On the other hand, and in contrast to what has been frequently assumed, the systems behave quite non-uniformly concerning the in-plane pressure effects. While for κ -(ET)₂Cu(NCS)₂ the in-plane pressure coefficients of T_c are either vanishingly small or positive, they are both negative for the related κ -(ET)₂Cu[N(CN)₂]Br system [97].

The above finding of a large negative uniaxial-pressure coefficient of T_c for pressure perpendicular to the planes as the only universal feature common to the κ -(ET)₂X family is supported by results on the related κ -(ET)₂I₃ salt, see [233].¹¹

As has been discussed in [9], a large cross-plane pressure effect on T_c may arise from several factors: (i) Pressure-induced changes in the interlayer interaction. This effect includes changes of both the interlayer coupling, i.e. the degree of two-dimensionality, as well as changes in the electron-electron and electron-phonon coupling constants and (ii) changes in the phonon frequencies. Likewise, changes in the vibrational properties could be of relevance for the intraplane-pressure effects on T_c . In addition, in-plane stress effectively modifies the electronic degrees of freedom by changing the transfer integrals between the HOMO's of the nearest-neighbour ET molecules. Most remarkably, for some compounds like κ -(ET)₂Cu(NCS)₂ the in-plane-stress effect is either positive or zero. This makes a purely density-of-states effect account for the pressure-induced T_c shifts very unlikely: pressure-induced changes in the density-of-states should be strongest for in-plane stress owing to the quasi-2D electronic band structure. According to the simple BCS relation [234]

$$T_c = 1.13 \Theta_D \exp\left(-\frac{1}{\lambda}\right) \quad \text{with} \quad \lambda = \frac{N(E_F)\langle I^2 \rangle}{M\bar{\omega}^2}, \quad (14)$$

where Θ_D denotes the Debye temperature, $\langle I^2 \rangle$ the electron-phonon matrix element averaged over the Fermi surface, M the ionic mass and $\bar{\omega}$ an average phonon energy, an in-plane-stress-induced increase in the π -orbital overlap,

κ -(ET)₂Cu(NCS)₂, the latter compound reveals an even stronger pressure dependence of T_c [232].

¹¹ A different situation is encountered for the α -(ET)₂MHg(SCN)₄ salt, where uniaxial pressure perpendicular to the planes is found to either induce superconductivity by suppressing an ambient-pressure density-wave ground state for $M = \text{K}$, or enhance T_c for $M = \text{NH}_4$ [226,187]. This behavior is most likely related to the exceptionally thick anion layers specific to this compound resulting in a strong decoupling of the conducting layers.

i.e. a reduced density-of-states at the Fermi level $N(E_F)$ is expected to cause a reduction of T_c . This is in contrast to the experimental observations. An important piece of information contained in the above uniaxial-pressure results is that there is *no* uniform behavior in the intralayer-pressure effects on T_c for the various $(\text{ET})_2\text{X}$ superconductors. It is especially the results on κ -(ET)₂Cu(NCS)₂ which show that in-plane pressure can even cause an increase of T_c [151,228]. This is in contrast to what has been assumed in the 2D electronic models discussed in [235,236]. In addition, the studies revealed a predominant effect of uniaxial pressure perpendicular to the planes clearly demonstrating that attempts to model the pressure-temperature phase diagrams by solely considering *in-plane* electronic degrees of freedom are inappropriate, see also [237].

Isotope substitution Studying the effect of isotope substitutions on the superconducting transition temperature is one of the key experiments to illuminate the role of phonons in the pairing mechanism. For elementary superconductors, the observation of a $M^{-1/2}$ dependence of T_c where M is the isotopic mass, provided convincing evidence that the attractive interaction between the electrons of a Cooper pair is mediated by the exchange of lattice deformations, i.e. by phonons.

For the κ -phase $(\text{ET})_2\text{X}$ compounds, the mass-isotope effect on T_c has been intensively studied, see [5], including isotope substitutions in both the ET donor molecule as well as the charge compensating anions. A most comprehensive study has been performed by the Argonne group on κ -(ET)₂Cu(NCS)₂ where overall seven isotopically labelled BEDT-TTF derivatives - with partial substitutions of ¹³S, ³⁴C and ²D - as well as isotopically labelled anions [$\text{Cu}^{15}\text{N}^{13}\text{CS}_2$]⁻ have been used [127]. As will be discussed below in section 4.5, these studies revealed a genuine mass-isotope effect on T_c .

An "inverse" isotope effect on T_c has been observed for κ -(ET)₂Cu(NCS)₂ where T_c of deuterated samples κ -(D₈-ET)₂Cu(NCS)₂ was found to be higher than that of hydrogenated salts, see [5]. This effect has been confirmed and quantified by the above mentioned study where particular care has been taken to guarantee otherwise comparable quality of both the labelled and unlabelled crystals [127]. The physical reason for the inverse isotope effect is still unclear. A geometric H-D isotope effect has also been found for two other $(\text{ET})_2\text{X}$ compounds κ_L -(ET)₂Ag(CF₃)₄(solvent) and β'' -(ET)₂SF₅CH₂CF₂SO₃ having different packing motifs and anion structures. Although the T_c values vary considerably among these salts ranging from 2.9 K to 9.2 K the investigations reveal an almost identical "universal" shift of T_c of $\Delta T_c = +(0.26 \pm 0.06)$ K [238,239]. Taking into account the results of thermal expansion and X-ray studies of the lattice parameters [151,240], it has been proposed that the inverse isotope effect is not directly related to the pairing mechanism. Instead it has been attributed to a geometrical isotope effect, i.e. changes in the internal chemical pressure: provided that the interlayer lattice parameter is identical

for both compounds, the effectively shorter C–D bond of the deuterated salt [241] corresponds to a higher chemical pressure perpendicular to the planes for the hydrogenated salt. The negative values of $\partial T_c / \partial p_\perp$ then result in a higher T_c for the deuterated compound [238,239], see also [187].

An alternative explanation has been proposed recently by Biggs et al. based on their measurements of the Shubnikov-de Haas effect focusing on pressure-induced changes of the Fermi-surface topology of deuterated and protonated κ -(ET)₂Cu(NCS)₂ [232]. It has been suggested that the superconducting mechanism is most sensitively influenced by the exact topology of the Fermi surface. Since the latter has been found to change more drastically with pressure in the deuterated salt, this effect might also be responsible for the inverse isotope effect [232]. In addition from recent millimeter-wave magnetoconductivity experiments it has been inferred that the quasi-one-dimensional FS sheets (see Fig. 7) are more corrugated in the deuterated salt (higher T_c) suggesting that the "nestability" of the FS may be important for T_c [242].

4.2 Superconducting parameters

(TMTSF)₂X salts As a consequence of the highly anisotropic electronic structure, strong directional dependences are also expected for the superconducting-state properties such as the lower and upper critical fields. Among the (TMTSF)₂X salts, the latter have been extensively studied for the ambient-pressure superconductor X = ClO₄, see [33,5] and, more recently, also for pressurised (TMTSF)₂PF₆, see also section 4.5 below. For (TMTSF)₂ClO₄ the Meissner and diamagnetic shielding effects have been examined for magnetic fields aligned along the three principal axes [243]. From these experiments the lower critical field values B_{c1} (at 50 mK) have been determined to 0.2, 1 and 10 (in units of 10⁻⁴ T) along the *a*-, *b*- and *c*-axis, respectively. The thermodynamic critical field, as estimated from the condensation energy, amounts to $B_{cth} = (44 \pm 2) \cdot 10^{-4}$ T [244]. Figure 32 shows the temperature dependence of the upper critical fields, $B_{c2}(T)$, for (TMTSF)₂ClO₄ as determined by early resistivity measurements [245]. The $B_{c2}(0)$ values of 2.8 T, 2.1 T and 0.16 T for the *a*-, *b*- and *c*-axis, respectively, have been obtained from the data of Fig. 32 by an extrapolation to zero temperature. The so-derived value for fields aligned parallel to the *a*-axis, where B_{c2} is the largest, is close to the Pauli-limiting field B_P which is the critical value required to break spin-singlet ($S = 0$) Cooper pairs. For a non-interacting electron gas this is the case when the Zeeman energy just equals the condensation energy, i.e.

$$B_P = \Delta_0 \frac{1}{\sqrt{2}\mu_B}, \quad (15)$$

where μ_B denotes the Bohr magneton [246,247]. Assuming a BCS ratio for the energy gap $\Delta_0 = 1.76 k_B T_c$ yields B_P (in Tesla) = $1.84 \times T_c$ (in K) = 2.3 T for (TMTSF)₂ClO₄. The fairly good coincidence with the experimentally derived critical field has been taken as an indication for a spin-singlet pairing

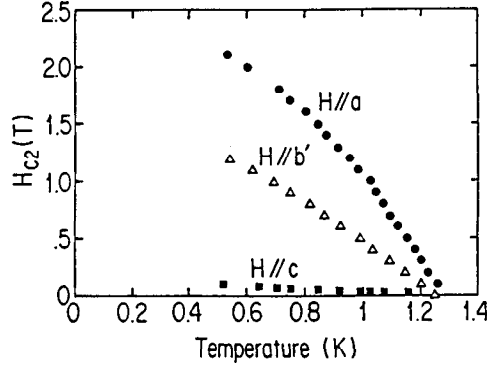


Fig. 32. Upper critical fields B_{c2} determined from resistivity measurements as a function of temperature for $(\text{TMTSF})_2\text{ClO}_4$ for the three principal crystal axes [245].

state [245,248,249]. As will be discussed in more detail in section 4.5, more recent resistivity measurements on the pressurized $\text{X} = \text{PF}_6$ salt down to lower temperatures revealed upper critical field curves which show an upward curvature for $T \rightarrow 0$ with no sign of saturation down to 0.1 K [250]. It has been argued in [250] that this unusual enhancement of B_{c2} which exceeds the Pauli paramagnetic limit by a factor of 4 is strongly suggestive of a spin-triplet ($S=1$) pairing state.

Yet from the initial slopes of the upper critical field curves in Fig. 32, $B_{c2}^{i'}$, the Ginzburg-Landau coherence lengths $\xi_i(0)$ can be derived using the following relation: $B_{c2}^{i'} = \phi_0 / (2\pi\xi_j\xi_kT_c)$, where i, j and k can be a, b and c [203,204]. The so-derived ξ_c value of about 20 Å being much smaller than the numbers for the a - and b -axis coherence lengths of 700 Å and 335 Å respectively, but comparable to the lattice parameter $c = 13.5$ Å indicates that superconductivity has, in fact, a more quasi-2D character. For the London penetration depth for B parallel to the a -axis, the axis of highest conductivity, a value of $\lambda = 40 \mu\text{m}$ has been reported [251]. This number exceeds the GL coherence lengths by orders of magnitude indicating that the present system is an extreme type-II superconductor.

$(\text{BEDT-TTF})_2\text{X}$ and $(\text{BEDT-TSF})_2\text{X}$ salts Due to the strong effects of fluctuations in these superconductors of reduced dimensionality, an accurate determination of the upper critical fields is difficult and in many cases not free of ambiguities. This holds true in particular for resistivity measurements in finite fields aligned perpendicular to the highly conducting planes as phase fluctuations of the order parameter give rise to a resistive state which tends to descend far below the mean-field transition temperature. A more reliable way to determine the upper critical fields is provided by measuring thermodynamic properties and employing a fluctuation analysis as described in section 4.1. The left panel of Fig. 33 shows B_{c2} curves for $\kappa\text{-(ET)}_2\text{Cu}[\text{N}(\text{CN})_2]\text{Br}$ as determined from dc-magnetization measurements [205,9] using equation

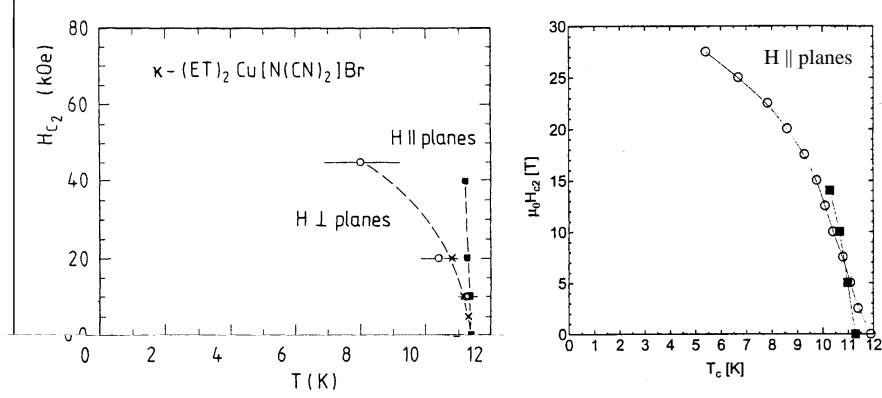


Fig. 33. Upper critical fields of κ -(ET) $_2$ Cu[N(CN) $_2$]Br. Left panel: anisotropy of B_{c2} as a function of temperature as determined from dc-magnetization measurements, taken from [205]. Right panel: $B_{c2}(T)$ for fields aligned parallel to the conducting planes as determined from resistivity measurements using different criteria (closed and open symbols), reproduced from [252].

(11), cf. Figs. 28 and 29. The $B_{c2}(T)$ curve for B aligned parallel to the highly conducting planes as determined from resistivity measurements are shown in the right panel of Fig. 33 over an extended field range. For the layered superconductors with negligible in-plane anisotropy, the expression (9) can be used to determine the GL coherence lengths perpendicular and parallel to the conducting planes.

Table 2 compiles the B_{c2} values together with other superconducting parameters for the above BEDT-TTF compounds. For comparison, the table also contains data for the BETS-based system λ -(BETS)GaCl $_4$. As indicated in the table, the transition temperatures reported in the literature show a considerably large variation depending on the method and criterion used to determine T_c . This may partly be related to the fact that the superconducting transition is usually found to be relatively broad. Even for high quality single crystals with an in-plane mean free path of typically ~ 2000 Å [106], the transition can be broadened due to internal strain fields as a consequence of the extraordinarily large pressure dependence of T_c . In addition, the quasi-2D nature of the electronic structure gives rise to pronounced fluctuations which cause a rounding of the transition [10].

According to recent magnetoresistivity studies, the in-plane Fermi surface of λ -(BETS)GaCl $_4$ strongly resembles that of κ -(ET) $_2$ Cu(NCS) $_2$ with the effective masses being almost identical for both compounds [254]. However, the interplane transfer integral of $t_{\perp} \approx 0.21$ meV for the BETS salt is about a factor of 5 larger [254], indicating that λ -(BETS)GaCl $_4$ is more three-dimensional. Figure 34 compares the magnetic field-temperature phase diagrams of the above compounds for fields aligned perpendicular to the planes. A dimensional crossover has been suggested to account for the unusual temperature

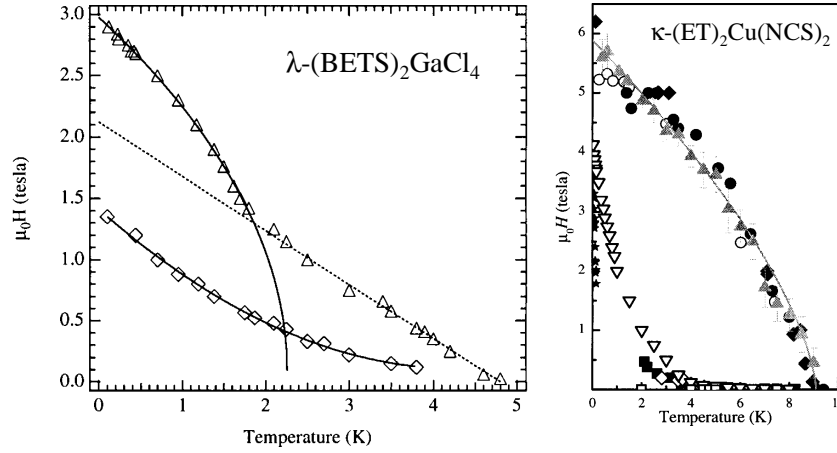


Fig. 34. Left panel: Upper critical field for $B \perp$ to the planes (triangles) of λ -(BETS) $_2$ GaCl $_4$. Upper solid curve is $B_{c2} \propto (T^* - T)^{1/2}$; the dashed curve $B_{c2} \propto (T_c - T)$ (see text). Diamonds and the lower solid curve indicate the flux-lattice melting line (see also section 4.3). Right panel: $B_{c2}(T)$ for $B \perp$ to the planes of κ -(ET) $_2$ Cu(NCS) $_2$ as determined from different experimental techniques, see [254]. The solid curve is $B_{c2} \propto (T_c - T)^{2/3}$ (see text). Also shown are transition and crossover lines in the mixed state, cf. Figs. 35 and 36 in section 4.3 below. Reproduced from [254].

dependence of $B_{c2}^\perp(T)$ observed for the BETS-based compound (left panel): $B_{c2}(T)$ shows a 3D-like linear behavior close to T_c which turns into a power-law dependence characteristic for a 2D superconductor with weakly coupled layers below some crossover temperature labelled as T^* [254,10]. In contrast, $B_{c2}(T)$ for the κ -(ET) $_2$ Cu(NCS) $_2$ salt follows a $B_{c2}(T) \propto (T - T_c)^{2/3}$ over the whole temperature range. The additional crossover and transition lines in the mixed state below the $B_{c2}(T)$ curves indicated in Fig. 34 will be discussed in section 4.3.

Important information on the spin state of the Cooper pairs can be gained by comparing the experimentally determined $B_{c2}(T)$ for $T \rightarrow 0$ with the Pauli-limiting field, B_P , as defined in equation (15). Using this formula, which neglects any orbital effects, and assuming a weak-coupling BCS ratio for the gap, i.e. $\Delta_0 = 1.76 k_B T_c$, B_P amounts to ~ 18 T and ~ 21 T for κ -(ET) $_2$ Cu(NCS) $_2$ and κ -(ET) $_2$ Cu[N(CN) $_2$]Br, respectively. Apparently, these numbers are significantly smaller than the $B_{c2}^\parallel(0)$ values found experimentally and listed in Table 2. On the other hand, clear evidence for a spin-singlet pairing state has been inferred from Knight shift measurements on κ -(ET) $_2$ Cu[N(CN) $_2$]Br yielding a vanishingly small spin susceptibility at low temperatures [253]. These deviations might find a natural

Table 2. Superconducting-state parameters of two representative κ -phase (ET)₂X salts X = Cu(NCS)₂ and Cu[N(CN)₂]Br as well as λ -(BETS)GaCl₄.

	κ -(ET) ₂ Cu(NCS) ₂	κ -(ET) ₂ Cu[N(CN) ₂]Br	λ -(ET) ₂ GaCl ₄
T_c	8.7 ~ 10.4	11.0 ~ 11.8	5 ~ 6
$B_{c_2}^\perp(0)$ (T) ¹²	6	8 ~ 10	3
$B_{c_2}^\parallel(0)$ (T) ¹³	30 ~ 35	> 30	12
$B_{c_1}^\perp(0)$ (mT) ¹⁴	6.5	3	
$B_{c_1}^\parallel(0)$ (mT) ¹⁵	0.2		
$B_{cth}(0)$ (mT) ¹⁶	54	65	
$\xi_\perp(0)$ (Å) ¹⁷	5 ~ 9	5 ~ 12	9 ~ 14
$\xi_\parallel(0)$ (Å) ¹⁸	53 ~ 74	28 ~ 64	143
$\xi_\parallel(0)$ (Å) ¹⁹	74	60	105
$\lambda_\perp(0)$ (μm) ^{20,21}	40 ~ 200	38 ~ 133	
$\lambda_\parallel(0)$ (Å) ²²	5100 ~ 20000	6500 ~ 15000	1500
κ_\parallel ²³	100 ~ 200	200 ~ 300	107

explanation by recalling that equation (15) is valid only in the weak-coupling limit. For a strong-coupling superconductor, on the other hand, the density of states is renormalized leading to a Pauli field which is enhanced by a factor of $(1 + \lambda)^{1/2}$ [246,203], where λ denotes the interaction parameter, see equation (14). Clear evidence for a strong-coupling type of superconductivity has been found in specific heat experiments on the κ -(ET)₂Cu[N(CN)₂]Br and κ -(ET)₂Cu(NCS)₂ salts [267,268,50,51], see section 4.5. As an alternative mechanism to account for a $B_{c_2}^\parallel(0)$ value in excess of the Pauli field,

¹² [9,253–255]

¹³ [252,255–258]

¹⁴ [40,259]

¹⁵ [40]

¹⁶ $B_{cth}(0) = T_c \cdot \sqrt{\frac{\mu_0 \gamma}{2 V_{\text{mol}}}}$

¹⁷ [205,260,9,40,187,254,255]

¹⁸ [205,260,9,40,255]

¹⁹ $\xi_\parallel(0) = \sqrt{\frac{\phi_0}{2 \pi B_{c_2}^\perp}}$

²⁰ λ_\perp and λ_\parallel denote the screening of supercurrents flowing perpendicular and parallel to the conducting planes, respectively, and *not* the direction of the magnetic field.

²¹ [260–262]

²² [262–266,260,254]

²³ [9,254]

a transition into a Fulde-Ferrell-Larkin-Ovchinnikov (FFLO) state [269,270] has been proposed [257,271] and discussed controversially, see e.g. [272,10]. In such a scenario, a superconductor with suitable materials parameter adopts a new state at sufficiently high fields where the order parameter is spatially modulated. A more detailed discussion on this issue will be given in section 4.3 below.

Besides T_c and the upper critical fields, Table 2 contains further superconducting-state parameters such as the lower and the thermodynamic critical fields B_{c1} and B_{cth} , respectively, as well as the GL coherence lengths $\xi_{\parallel,\perp}$ and the London penetration depths $\lambda_{\parallel,\perp}$. B_{c1} is usually determined by measuring the magnetization as a function of field under isothermal conditions where B_{c1} corresponds to the field above which flux starts to penetrate the sample. Due to the smallness of B_{c1} , the plate-like shapes of the crystals and the peculiar pinning properties of these layered superconductors, an accurate determination of B_{c1} is difficult. A more reliable way to determine $B_{c1}^\perp(0)$ has been proposed by Hagel et al. based on a model for thermally activated flux creep yielding $B_{c1}^\perp(0) = (3 \pm 0.5) \text{ mT}$ for $\kappa\text{-(ET)}_2\text{Cu[N(CN)}_2\text{]Br}$ [259]. The values for the thermodynamic critical fields, B_{cth} , in Table 2 are estimated from specific heat results using $B_{cth}(0) = T_c \cdot \sqrt{\mu_0 \gamma / (2 V_{\text{mol}})}$ where γ is the Sommerfeld coefficient. These values roughly agree with those calculated from $B_{cth} = B_{c2}/(\kappa\sqrt{2}) = B_{c1}\sqrt{2}\kappa/\ln\kappa$, where $\kappa = \lambda/\xi$ is the GL parameter. The large numbers of κ reflect the extreme type-II character of these superconductors.

Also listed in Table 2 are values of the magnetic penetration depth λ , the characteristic length over which magnetic fields are attenuated in the superconductor. While the absolute values for λ derived from various experimental techniques are in fair agreement within a factor $4 \sim 5$, no consensus has yet been achieved concerning its temperature dependence, see section 4.5 below.

4.3 Mixed state

The peculiar material parameters of the present organic superconductors such as the pronounced anisotropy of the electronic states, the small coherence lengths and large magnetic penetration depths give rise to highly anomalous mixed-state properties and a rich B - T phase diagram in the superconducting state. Exploring the unusual features of extreme type-II layered superconductors continues to be a subject of considerable interest owing to the variety of exciting phenomena that has been found in these materials, see e.g. [273]. Among them is a first-order melting transition of the Abrikosov vortex lattice into a vortex-liquid phase [274,275] not known for usual 3D superconductors. One of the striking early observations related to the anomalous mixed-state properties was the appearance of a so-called irreversibility line, B_{irr} , which separates the B - T plane into an extended range $B_{\text{irr}} < B < B_{c2}$ where the magnetization is entirely reversible from a magnetically irreversible state at $B < B_{\text{irr}}$.

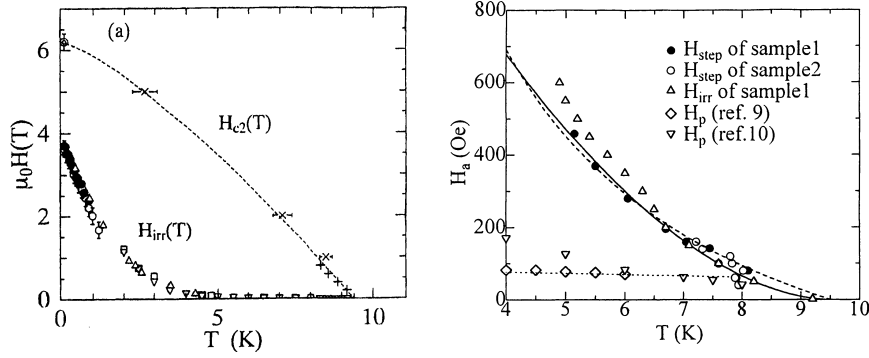


Fig. 35. Details of the B - T phase diagram for fields perpendicular to the conducting planes of κ -(ET) $_2$ Cu(NCS) $_2$. Left panel: temperature dependence of the irreversibility field and the upper critical field taken from [277]. Right panel: first-order transition line (open and closed circles) determined by a step in the local induction. Solid and dashed curves represent theoretical predictions for the melting and decoupling transitions, respectively, see text. Open diamonds and down triangles indicate an anomalous second peak in magnetization associated with the dimensional-crossover field B_{2D} of the vortex system, taken from [278].

When a layered superconductor is exposed to a magnetic field $B > B_{c1}$ aligned perpendicular to the planes, the confinement of the screening currents to the superconducting layers results in a segmentation of the flux lines into two-dimensional objects, the so-called vortex pancakes [276]. The coupling between vortex segments of adjacent layers is provided by their magnetic interaction and the Josephson coupling. The latter interaction drives tunnelling currents when two vortex segments are displaced relative to each other. As a result of both effects, the vortex pancakes tend to align thereby forming extended stacks.

A quite different situation arises for fields aligned parallel to the layers. In the limiting case of a quasi-2D superconductor characterized by a cross-plane coherence length ξ_{\perp} being smaller than the interlayer distance s , the vortex cores slip into the insulating layers where the superconducting order parameter is small. Such a Josephson vortex has an elliptically deformed cross section and lacks a normal core. Since the Josephson screening currents across the insulating layers are very weak, the material is almost transparent for fields parallel to the planes corresponding to a large value for the upper critical field B_{c2}^{\parallel} , cf. Table 2. Below we will discuss some of the anomalous mixed-state properties such as the vortex-lattice melting transition, the irreversibility line, the lock-in transition as well as the possible realization of an anomalous high-field state.

Muon spin rotation measurements on the κ -(ET) $_2$ Cu(NCS) $_2$ salt have shown that a 3D flux-line lattice exists only at very low fields $B < 7$ mT

[279].²⁴ Using a decoration technique, Vinnikov et al. succeeded in imaging the vortex lattice in the low-field range [280]. Upon increasing the field to above some dimensional crossover field, B_{2D} , the vortex lattices of adjacent layers become effectively decoupled. Theory predicts that the crossover field is related to the anisotropy parameter Γ and the interlayer distance s by $B_{2D} = \phi_0/(\Gamma^2 s^2)$ [273], which for the κ -(ET)₂Cu(NCS)₂ salt results in $B_{2D} = 7.3 \sim 30$ mT [279,281]. An anomalous second peak in magnetization curves indicating a redistribution of pancake vortices at more suitable pinning centers, has been associated with B_{2D} [281,278]. According to measurements of the interlayer Josephson-plasma resonance [282], a long-range quasi-2D order among vortices within the individual layers characterizes the state above B_{2D} and persists up to the irreversibility line. In this region of the B - T plane the pancake vortices of adjacent layers become effectively decoupled leading to a pinned quasi-2D vortex solid in each layer with no correlations between the locations of vortices among the layers [283]. A somewhat different point of view is taken in [278,284], where B_{2D} marks the crossover from a 3D flux line lattice below B_{2D} to a state with less strong interlayer coupling on a long range scale above, where a coupling between the layers is, to some extent, still present.

Another striking property common to the present quasi-2D superconductors is an extended vortex-liquid phase above B_{irr} . Here the magnetization behaves entirely reversible upon increasing and decreasing the magnetic field, indicating that in this range flux pinning is ineffective. The abrupt onset of magnetic hysteresis at $B \leq B_{irr}$ indicates a drastic increase in the pinning capability. The temperature dependence of the irreversibility field has been studied in detail for κ -(ET)₂Cu(NCS)₂ and κ -(ET)₂Cu[N(CN)₂]Br using a variety of techniques including ac-susceptibility [259], dc-magnetization [205], magnetic torque [281,277] or Josephson-plasma-resonance experiments [282]. Figure 35 shows on a linear phase scale the irreversibility line in the B - T phase diagram of κ -(ET)₂Cu(NCS)₂ deduced from torque-magnetometry measurements in fields perpendicular to the planes [277]. As demonstrated in the left panel of Fig. 35, the irreversibility field at the lowest temperatures lies well below the upper critical field. Thus quantum fluctuations of the vortices as opposed to thermally driven motions are responsible for the vortex liquid state in this region of the phase diagram [277]. The crossover from quantum to thermal fluctuations manifests itself in the temperature dependence of $B_{irr}(T)$. Below ~ 1 K where quantum fluctuations are predominant, $B_{irr}(T)$ varies linearly with temperature [277], whereas in the thermal fluctuation regime an exponential behavior $B_{irr} = B_0 \exp(-AT/T_c)$ has been observed above the dimensional crossover field B_{2D} in contrast to a power-law behavior in the 3D vortex line lattice region below B_{2D} [205,281]. A similar behavior has been observed also for κ -(ET)₂Cu[N(CN)₂]Br where the crossover in the

²⁴ Here the sample was arranged so that the superconducting planes enclose an angle of 45° in respect to the magnetic field.

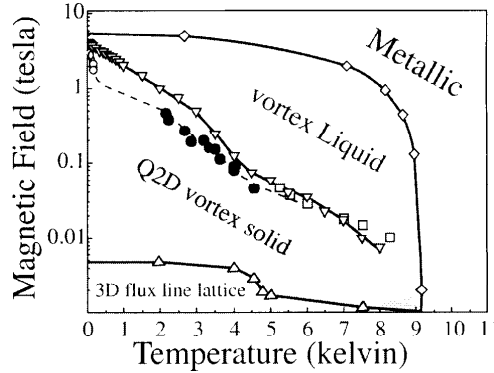


Fig. 36. Mixed-state B - T phase diagram for κ -(ET) $_2$ Cu(NCS) $_2$ for $B \perp$ planes in a semi-logarithmic representation. B_{irr} is indicated by down triangles, the dimensional-crossover field by up triangles. Open squares denote a first order decoupling and/or melting transition. Closed and open circles refer to thermal melting or depinning and quantum melting transition from a quasi-2D vortex lattice to a liquid phase, respectively. Taken from [283].

temperature dependence of the irreversibility line has been interpreted as a crossover from 2D to 3D pinning [259].

Indications for a first-order phase transition associated with a melting and/or a decoupling of the quasi-2D vortex lattice near the irreversibility line - similar to what has been found in some high- T_c cuprates [274,275] - have been reported for κ -(ET) $_2$ Cu(NCS) $_2$ [278,285]. This refers to results from micro Hall-probe experiments where the local induction as a function of temperature at constant fields shows step-like changes. As shown in the right panel of Fig. 35 the first-order transition line can be fitted equally well by a melting or a decoupling transition. Steps in the equilibrium and local magnetization have been observed also in SQUID and micro-hall-probe measurements, respectively, for κ -(ET) $_2$ Cu[N(CN) $_2$]Br [286,284]. In addition, Josephson-plasma-resonance experiments revealed evidence that at the first-order transition, the interlayer coherence becomes lost indicating that the melting and the decoupling occur simultaneously [284].

Figure 36 shows in a semi-logarithmic plot the B - T phase diagram for κ -(ET) $_2$ Cu(NCS) $_2$ as proposed by [283]. Note that here the crossover field B_{2D} separating the 3D flux-line lattice from the quasi-2D vortex solid is temperature dependent in contrast to the results shown in Fig. 35. A first-order melting transition driven by quantum fluctuations has been inferred from torque-magnetization measurements at very low temperatures [283].

An interesting situation arises when the magnetic field is aligned parallel to the planes enabling the vortices to slip in between the superconducting layers where the order parameter is small. For small tilt angles of the field in respect to the exact alignment, the vortex lattice can gain energy by remaining in this parallel "lock-in" configuration. This new state remains stable until the perpendicular field component, B_{\perp} , exceeds a threshold field at which the energy required to expel B_{\perp} exceeds that associated with the creation of normal cores in the layers. Evidence for coreless Josephson vortices parallel

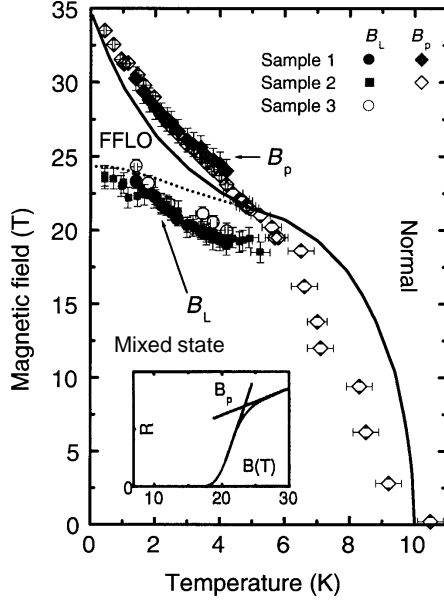


Fig. 37. Magnetic field-temperature phase diagram of κ -(ET) $_2$ Cu(NCS) $_2$ for B aligned parallel to the planes compared with the theoretical FFLO phase diagram discussed in [290]. B_P as defined in the inset serves as a rough estimate for B_{c2} . B_L indicates changes in the rigidity of the vortex arrangement within the superconducting state. Reproduced from [257,10].

to the superconducting layers and a lock-in state has been reported from ac-susceptibility measurements for κ -(ET) $_2$ Cu(NCS) $_2$ [261] and from torque magnetometry on κ -(ET) $_2$ Cu(NCS) $_2$ and κ -(ET) $_2$ Cu[N(CN) $_2$]Br [207,287], see also [9].

Further interest in the behavior of the present quasi-2D organic superconductors in fields precisely aligned parallel to the planes arose from the proposal that these systems are possible candidates for a Fulde-Ferrell-Larkin-Ovchinnikov (FFLO) state [288]. Under suitable conditions, a spin-singlet superconductor can reduce the pair-breaking effect of a magnetic field by adopting a spatially modulated order-parameter along the field direction [269,270]. The wavelength of the modulation is of the order of the coherence length which results in a periodic array of nodal planes perpendicular to the vortices [269,270]. In the case of an anisotropic superconductor, calculations show that the FFLO state might lead to an enhancement of the upper critical field to between 1.5 and 2.5 times the Pauli paramagnetic limit [288,289].

By studying the magnetic behavior and the resistivity of κ -(ET) $_2$ Cu(NCS) $_2$ in high magnetic fields employing a tuned circuit differential susceptometer, changes in the rigidity of the vortex arrangement at certain fields B_L within the superconducting state have been found for fields precisely aligned parallel to the planes [257,271]. These effects have been interpreted as the manifestation of a phase transition from the superconducting mixed state into an FFLO

state.²⁵ Figure 37 shows the temperature dependence of B_L and B_P , the latter serves as a rough estimate of B_{c2} [257,271], see inset of Fig. 37. Comparing the results with theoretical calculations derived for a generic quasi-2D metal [290] (solid and dotted lines in Fig. 37) using the parameter $B_{c2}(0) = 35$ T yielded a fairly good agreement with the predictions of the FFLO model. In particular, the temperature T^* below which the new state is stabilized was found to meet the theoretical predictions of $T^* = 0.56 T_c$. However, recent magnetic torque measurements failed to detect any indication for such a transition [283].

4.4 Magnetic-field-induced superconductivity

The λ -(BETS)₂FeCl₄ systems has attracted strong interest recently owing to the intriguing behavior found when the system is exposed to a magnetic field [293]. With increasing field aligned parallel to the planes, the low-temperature antiferromagnetic insulating state becomes suppressed and vanishes above about 10 T. At higher fields the paramagnetic metallic state which governs the $B = 0$ T behavior above the Néel temperature of about 10 K is restored. For fields aligned exactly parallel to the highly conducting planes, a further increase to above 17 T has been found to induce a superconducting state at low temperatures, see Fig. 38. For this field configuration, the orbital effect is strongly suppressed so that superconductivity is limited only by the Zeeman effect, i.e. the Pauli limit, resulting in a high upper critical field. The field-induced superconducting state which is stable up to 41 T has been attributed to the Jaccarino-Peter effect, where the external magnetic field compensates the exchange field of the aligned Fe³⁺ moments [294]. The field-induced superconductivity is suppressed if the magnetic field is tilted from the conducting plane.

In the concentration range $0.35 \leq x \leq 0.5$ of the series λ -(BETS)₂Fe_{*x*}Ga_{1-*x*}Cl₄ (cf. Fig. 26 in section 3.5), where superconductivity shares a common phase

²⁵ According to [269,270], see also [291,292], the stabilization of a FFLO state requires: (i) a large electronic mean free path $l > \xi_0$, i.e. clean limit, (ii) a Pauli limiting that predominates the orbital pair-breaking effect, (iii) a Zeeman energy that overcompensates the loss of superconducting condensation energy and (iv) a short coherence length (or a large GL parameter $\kappa = \lambda/\xi$). As already discussed in section 4.2, the criteria (i) and (iv) are met for the present κ -(ET)₂X salts. Condition (ii) is fulfilled since $H_P = \frac{1}{2}H_c(\pi\chi_{\text{Spin}})^{-1/2} \approx 17$ T is considerably smaller than the orbital critical field as derived from equation (9) taking the values from Table 2. To check for condition (iii) one has to compare the Zeeman energy with the condensation energy. Using $\chi_{\text{Spin}} = 4 \cdot 10^{-4}$ emu/mol for κ -(ET)₂Cu(NCS)₂ [86] and the upper critical field of 35 T yields a Zeeman-energy density of $E_Z = \frac{1}{2}\chi_{\text{Spin}}H_{c2}^2 = 5$ mJ/cm³ ($= 5 \cdot 10^4$ erg/cm³), which exceeds the condensation-energy density of $E_c = H_c^2/(8\pi) = \frac{1}{4} \cdot \gamma/V_{\text{mol}} \cdot T_c^2 = 1$ mJ/cm³ ($= 10^4$ erg/cm³) calculated by employing the experimentally determined Sommerfeld coefficient $\gamma = (23 \pm 1)$ mJ/mol K² for κ -(ET)₂Cu(NCS)₂ [50,51].

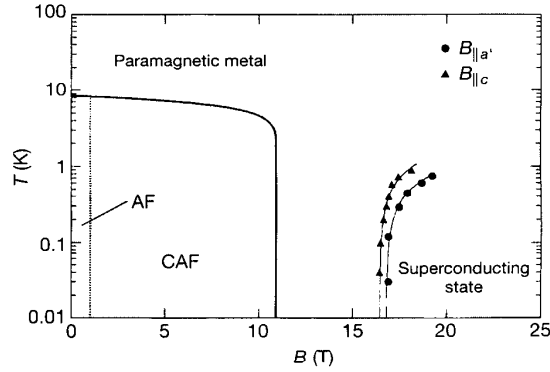


Fig. 38. Temperature vs magnetic field phase diagram for λ -(BETS) $_2$ FeCl $_4$ with the magnetic field aligned parallel to the conducting planes. AF and CAF indicate the antiferromagnetic and canted antiferromagnetic phase, respectively. Taken from [293].

boundary with an antiferromagnetically ordered insulating state, a field-induced afm insulator-to-superconductor transition has been observed [295]. It has been suggested that the pairing interaction arises from the magnetic fluctuations through the paramagnetic Fe moments [293].

4.5 The superconducting state - pairing mechanism and order-parameter symmetry

Understanding the nature of superconductivity in all its variants continues to pose a challenging problem of enormous complexity. Elementary superconductors like Al or Zn are well described by the BCS model [296] which envisages pairing between quasiparticles in a relative zero angular momentum ($L=0$) and spin-singlet ($S=0$) state, with an attractive pairing interaction mediated by the exchange of virtual phonons. In the ground state, all electron pairs (Cooper pairs) are in the same quantum-mechanical state described by a single macroscopic wavefunction. Excitations, i.e. the creation of unpaired quasiparticles, require an energy in excess of 2Δ , where Δ is the energy gap, known as the order parameter. In the BCS model the gap amplitude $\Delta(\mathbf{k})$ is uniform over the whole Fermi surface. In addition, the following quantitative relations are implied in the BCS model: a universal ratio $\Delta_0/k_B T_c = 1.76$, where Δ_0 is the energy gap at zero temperature, and $\Delta C/\gamma T_c = 1.43$ with ΔC being the jump height in the specific heat at T_c and γ the Sommerfeld coefficient.

In recent decades, novel classes of superconductors have been discovered in complex materials such as heavy-fermion metals [297], cuprates [298], ruthenates [299] and the present organic materials [1]. These systems have properties which are markedly different from those of the simple elements Al or Zn. The differences manifest themselves particularly clearly in the role of electron-electron interactions, which are strong in the new superconductors but of no relevance in the simple metals. The question at hand is whether superconductivity in the new materials is of a fundamentally different type to what

is described in the BCS model and proved valid to a good approximation in so many superconductors. As for the present organic materials this question covers the following aspects:

- (i) Are the superconducting carriers "BCS-type" pairs of electrons that form below T_c (Cooper-pairs)? Or do tightly bound electron pairs preexist already at higher temperatures $T > T_c$ which undergo a Bose-Einstein condensation?
- (ii) Is the relevant pairing mechanism different from a conventional phononic mechanism? The exchange of antiferromagnetic spin fluctuations as one of the models discussed for the high- T_c cuprates and also for the present organic materials is an example for an unconventional pairing interaction.
- (iii) Is the symmetry of the order parameter lower than that of the Fermi surface? It is customary to refer to an unconventional superconducting state as one where the order parameter breaks at least one of the crystal symmetries.
- (iv) Is the spin part of the superconducting pair wavefunction an antisymmetric singlet or a symmetric triplet state?

Although a local pairing scheme as distinguished from the BCS-type pairing has been discussed also for the present organic systems [300,301], the bulk of experimental observations do not support such a scenario. Rather the formation of Cooper-pairs below T_c implying an energy gap Δ with a maximum at $T = 0$ that vanishes for $T \geq T_c$ has been widely established, see e.g. [9].

The discussion of the above issues (ii)–(iv) in the context of the organic superconductors is complicated by the fact that even for the most fundamental properties contradictory experimental evidences exist. Since some of these discrepancies might simply reflect extrinsic effects as a consequence of an incomplete sample characterization, we shall therefore concentrate the discussion on those materials which are best characterized and where most data are available. These are the κ -phase $(\text{ET})_2\text{X}$ and the $(\text{TMTSF})_2\text{X}$ salts.

On the nature of the superconducting state The central question for the present organic superconductors concerns the nature of the pairing interaction. The excitonic mechanism proposed by Little [3,302] for certain quasi-1D organic polymers was of great importance historically in giving the initial impetus to the development of the field. From today's perspective, however, it is fair to say that the search for materials with suitable chemical and physical properties for such a mechanism to work has been unsuccessful so far.

In the discussion of the transport and optical properties in section 3.2 it became clear that there is a substantial coupling of the charge carriers to both intra- as well as intermolecular phonons. Consequently, some researchers in the field believe in a conventional electron-phonon coupling mechanism. On the other hand, the fact that for the present materials - as for the cuprates

and heavy-fermion systems - the superconducting region in the phase diagram lies next to a magnetically ordered state suggests that magnetic interactions are involved in the pairing mechanism.

Models considering the role of phonons in the pairing mechanism One example for a conventional electron-phonon pairing scenario has been discussed by Yamaji [303]. In this model he considers an attractive interaction mediated by several high-frequency internal molecular vibrations in addition to one low-frequency intermolecular phonon.

A more general account for the complex role of phonons for superconductivity has been given by Girlando et al. [304,305,60]. By calculating the lattice phonons for the κ -(ET)₂I₃ and β -(ET)₂I₃ superconductors using the quasi-harmonic-lattice-dynamics method and evaluating the coupling to the electrons, λ , they succeeded in reproducing all available experimental data related to the phonon dynamics, for example the lattice specific heat. They showed that a lattice mode that couples particularly strongly to the electrons is one in which the relative displacement of the ET molecule is along the long axis of the molecule, i.e. perpendicular to the conducting planes. As an interesting side result of their study on κ -(ET)₂I₃, it is mentioned, that the coupling of acoustic phonons is very anisotropic and likely to cause gap anisotropies, though of a conventional type. In addition, it has been shown that the lattice phonons alone cannot account for the T_c values in these compounds. High-frequency intramolecular phonons modulating the on-site electronic energies have to be taken into account to reproduce the critical temperatures [304]. Recently, a distinct kind of phonon-mediated pairing has been suggested for the (ET)₂X salts [306]. It is based on the idea that in a system in which Coulomb correlations are screened to be short range, i.e. Hubbard type, the electron-phonon scattering is dominated by forward processes. This results in an effective small-q pairing potential. Subsequent self-consistent solutions of the BCS gap equation using a band structure based on the effective-dimer approximation, lead to a gap structure where d - and anisotropic s -wave states are nearly degenerate. Furthermore it has been argued that the conflicting experimental results about the gap symmetry may originate in the decorrelation of superconductivity on various parts of the Fermi surface - a consequence of small-q dominated pairing - and the near degeneracy of s - and d -wave superconducting gap states [306].

Models which consider a magnetic interaction On the other hand, the rich phase diagram and the anomalous properties of the metallic state of these materials may suggest that the key elements dominating the physical behavior are the layered structure and the strong interactions between the electrons [4]. As a consequence, some researchers even resign from considering any coupling to the phonons and instead consider mechanisms which are solely based on two-dimensional electronic interactions. Most of these proposals deal with a spin-fluctuation-mediated pairing mechanism. The latter is motivated

by the close proximity of the superconducting region in the phase diagram to an antiferromagnetic insulating state which - in analogy to the high- T_c cuprates - suggests that both phenomena are closely connected to each other [235,4,307].

An approach in this direction has been proposed by Kino and Fukuyama [235] who studied the effects of on-site Coulomb interaction and dimer structure in a strictly two-dimensional system within the Hartree-Fock approximation, see also [308]. In their picture, the antiferromagnetic insulating state of κ -(ET)₂X is a Mott insulator. The Mott-Hubbard scenario for the present organic superconductors implies a half-filled conduction band, together with strong electron correlations. Because of the approximate square-lattice configuration of the dimers the authors expect a similar spin-fluctuation mediated superconductivity with probably $d_{x^2-y^2}$ symmetry as in the cuprates [235]. Such a possibility has been studied in detail by Schmalian [307]. Using a two-band Hubbard model to describe the antibonding orbitals on the ET dimer he succeeded in creating a superconducting state with $T_c \simeq 10$ K mediated by short-ranged antiferromagnetic spin fluctuations. It has been argued that despite the frustrating interactions and in-plane anisotropies which distinguish the organic materials from the high- T_c cuprates, the origin of superconductivity is very similar for both material classes [307].

A spin-fluctuation-based superconductivity similar to that of the cuprates has been claimed also by Kondo and Moriya [309–311]. They investigated the properties of a half-filled Hubbard model in a fluctuation exchange approximation (FLEX) with a right-angle isosceles triangular lattice with transfer matrices $-\tau'$ and $-\tau$. They revealed an energy gap of $d_{x^2-y^2}$ symmetry which upon cooling grows much faster compared to that expected in the BCS model. In addition they showed, that the appearance of d -wave superconductivity near an antiferromagnetic instability requires a suitable electronic structure, i.e. $\tau'/\tau > 0.3$ [309,310,236].

A spin-fluctuation mediated d -wave superconducting state has been found also by several other approaches including FLEX, perturbation theory or quantum Monte Carlo simulation applied to κ -(ET)₂X [312–315] or the quasi-one-dimensional (TM)₂X salts [314,316]. In [317] and [316] an explanation for the pseudogap behavior at elevated temperatures T^* has been proposed in terms of strong antiferromagnetic spin-fluctuations.

While the starting point of the above models is in the limit of strong correlations, i.e. near the Mott-insulating state, a somewhat different viewpoint is taken in the work by Louati et al. [318]. These authors studied the effect of spin fluctuations in a two-dimensional model in the weak correlation regime by varying the bandwidth and the nesting properties of the Fermi surface. They argued that spin fluctuations are enhanced by the good nesting properties which may account for the anomalous NMR relaxation rate observed at temperatures T^* above T_c in the κ -(ET)₂Cu[N(CN)₂]Br salt. Furthermore

they found that spin fluctuations can induce a superconducting coupling with d -wave symmetry that lies next to a spin-density-wave instability [318].

The above models address systems at half filling, which is realized in the dimerized κ -phase (ET)₂X and (TMTSF)₂X salts, suggesting spin-fluctuation-mediated superconductivity with a $d_{x^2-y^2}$ symmetry. A different scenario has been proposed for the θ and β'' structures [319]. Here the ET molecules are not dimerized which results in a quarter-filled hole band. In this case, a nearby insulating phase is believed to be due to a charge ordering, driven by strong inter-site Coulomb correlations. Applying slave-boson theory to an extended Hubbard model at quarter filling, superconductivity mediated by charge fluctuations has been found. This results in a d_{xy} symmetry of the superconducting state [319] as opposed to the $d_{x^2-y^2}$ symmetry for the above spin-fluctuation mechanism.

Experiments probing the superconducting state On the experimental side, the determination of the actual pairing mechanism is a most difficult task as there is no decisive probe to pin down the relevant pairing interaction. There are, however, some crucial experiments which may help to delineate the various possibilities. Investigating the mass-isotope effect on T_c is such a key experiment. Another one is to study the phonon system to probe the role of electron-phonon interactions. If phonons are involved in the pairing interaction this would result in renormalization effects in the temperature dependences of the phonon frequencies and linewidths upon cooling through T_c . Likewise, if a non-phononic mechanism is at work leading to an anisotropic gap with nodes along certain directions on the Fermi surface, a determination of the orientation of the gap zeroes by angular-dependent measurements can provide important information on the pairing mechanism.

For classical phonon-mediated superconductors the gap amplitude $\Delta(\mathbf{k})$ is assumed to be isotropic or at least to have an isotropic component combined with a \mathbf{k} -dependent part which obeys all symmetries of the crystal lattice. In contrast to such a conventional "finite-gap" state, the above mentioned electronic coupling schemes lead to a pairing state with higher angular momentum where $L = 2$ (d -wave) being the most favored one. In this case the amplitude of the Cooper-pair wave function vanishes at the origin of the relative coordinate which keeps the constituent quasiparticles of the Cooper pair apart. Therefore, $L \neq 0$ pairing states are good candidates for materials with strong on-site Coulomb repulsion. The gap-function of such an $L \neq 0$ state has a \mathbf{k} -dependence which is given by the spherical harmonics of the same angular momentum. For those states where the $\Delta(\mathbf{k})$ functions vanish at certain \mathbf{k} -vectors at the Fermi surface, the quasiparticle excitation spectrum at low energies is markedly different from that of an isotropic finite gap state. For the above d -wave order parameter $\Delta(\mathbf{k}) = \Delta_0 (\cos(k_x a) - \cos(k_y b))$ the zero crossings along the diagonals correspond to line nodes at the Fermi surface. This should be reflected in all quantities that depend on the num-

ber of thermally excited quasiparticles such as specific heat, NMR relaxation rate, magnetic penetration depth, etc. in the form of simple power-law dependences at sufficiently low temperatures. In contrast, an exponentially weak T -dependence in these quantities characterizes an isotropic non-vanishing order parameter. Thus, careful measurements of the above thermal properties should, in principle, provide a handle on the order-parameter symmetry, or at least permit to discriminate whether gap zeroes exist or not. In this context, it should be noted, however, that the observation of a non-exponential or power-law T -dependence in one of these quantities does not necessarily imply a gap structure with nodes. As an example, we mention gapless superconductivity via pair breaking which destroys an exponential behavior [320,321]. Likewise, a power-law T -dependence could be of conventional origin, as e.g. a T^3 dependence in the specific heat for $0.2T_c < T < T_c$ which has been attributed to strong-coupling effects [322,323].

To our knowledge, the only example where a non-phononic mechanism has been clearly identified is the heavy-fermion superconductor UPd_2Al_3 . Here, the combination of tunnel spectroscopy [324] and neutron scattering experiments [325] has provided sound evidence for a magnetic pairing interaction, i.e. the exchange of magnetic excitons.

Although numerous experiments have been devoted to the issue of the order parameter symmetry for the organic materials, no consensus has yet been achieved. It is fair to say that for the present systems direct evidence for a non-phononic mechanism such as the one mentioned above does not exist. Also phase-sensitive experiments as those applied successfully to the high- T_c cuprates [326,327] have not been performed so far for the organic materials. In what follows we shall give a discussion of a selection of experimental results on the pairing mechanism and the symmetry of the order parameter. To begin with we shall focus on the $(\text{ET})_2\text{X}$ salts.

Experiments on the pairing mechanism

Isotope effect and electron-phonon coupling The effect of isotope substitution has been studied for various members of the $(\text{ET})_2\text{X}$ superconductors. Isotopes have been substituted in the ET molecule by replacing ^1H by ^2D in the ethylene endgroups, by a partial exchange of ^{12}C by ^{13}C or ^{32}S by ^{34}S atoms in the inner skeleton of the molecule. In addition, systems have been studied where the acceptor molecule has been isotopically labelled. First experiments focused on the role of the electron-molecular-vibration (EMV) coupling by substituting ^{13}C for ^{12}C in the central double bond of the ET molecule. The large decrease of T_c of $\Delta T_c/T_c = -2.5\%$ found for the high-temperature variant (β_H) of β -($\text{ET})_2\text{I}_3$ by the Orsay group [328] could not be reproduced by a subsequent study where no systematic decrease of T_c could be detected [329]. Most intensive studies on the isotope effect have been carried out on the κ -($\text{ET})_2\text{Cu}(\text{NCS})_2$ salt by the Argonne group [127].

Their investigations include isotope substitutions on both the BEDT-TTF molecules (all together seven differently labelled BEDT-TTF derivatives) as well as the anions. In each case, a batch of unlabelled samples has been synthesized under strictly parallel experimental conditions. These crystals serve as a reference for comparison. By sampling a large number of crystals, typically eight or more of both labelled and unlabelled material, a genuine mass-isotope effect on T_c has been found: upon replacing all eight sulfur atoms by ^{34}S and the outer-ring-carbon atoms of the $[(\text{CH}_2)_2]$ endgroups by ^{13}C , which corresponds to a 5% increase of the ET molecule's mass, a shift of $\Delta T_c = -(0.12 \pm 0.08)\text{K}$ has been observed. Assuming a BCS-like mass-isotope effect $T_c \propto M^{-\alpha}$ with the whole ET molecule as the relevant mass entity M , this shift corresponds to $\alpha = 0.26 \pm 0.11$. This experiment provides clear evidence that the *intermolecular* (lattice) phonon modes are strongly involved in the pairing mechanism. On the other hand, the same group demonstrated the absence of a comparable isotope effect on T_c for $\kappa\text{-(ET)}_2\text{Cu(NCS)}_2$ and $\kappa\text{-(ET)}_2\text{Cu[N(CN)}_2\text{]Br}$ upon a partial substitution of the central C=C and also a simultaneous replacement of both the central and ring C=C atoms. The same holds true for a substitution of the eight sulfur atoms, see [127] and references therein. These results indicate that the *intramolecular* C=C and C-S bond-stretching vibrational modes of the ET molecule do not provide a substantial contribution to the Cooper pairing.

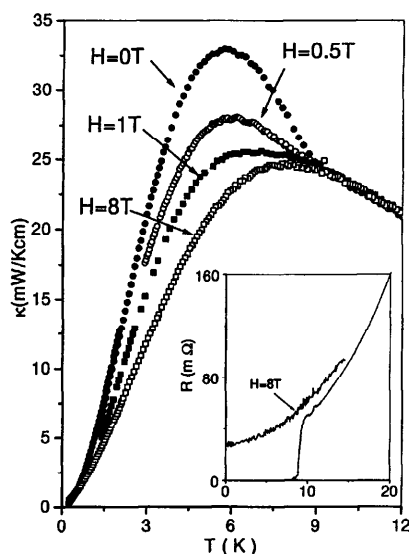


Fig. 39. Temperature dependence of the thermal conductivity of $\kappa\text{-(ET)}_2\text{Cu(NCS)}_2$ for B applied perpendicular to the planes. Inset: temperature dependence of the resistance. Taken from [61].

Further indications for a strong electron-phonon coupling have been inferred from measurements of the thermal conductivity on $\kappa\text{-(ET)}_2\text{Cu(NCS)}_2$ and $\kappa\text{-(ET)}_2\text{Cu[N(CN)}_2\text{]Br}$ [61,62,51]. As shown in Fig. 39, the thermal con-

ductivity $\kappa(T)$ of $\kappa\text{-(ET)}_2\text{Cu(NCS)}_2$ exhibits an upturn at the onset of superconductivity followed by a pronounced maximum just below T_c . It has been convincingly argued by the authors that the enhancement of $\kappa(T)$ in the superconducting state is a consequence of the condensation of electrons into Cooper pairs which strengthens the heat transport by freezing out the scattering of the main heat carriers, the phonons. By employing the Wiedemann-Franz law it has been found that just above T_c the electronic contribution amounts to only 5 % of the total thermal conductivity [61]. Figure 39 also shows $\kappa(T)$ data taken at varying fields applied perpendicular to the conducting planes. In the normal state, a magnetic field of 8 T does not affect the thermal conductivity within the resolution of the experiment but induces a sizeable decrease in the charge conductivity (see inset) which is an additional indication of lattice-dominated thermal conductivity in the vicinity of T_c . Temperature-dependent Raman scattering studies of the phonon dynamics of $\kappa\text{-(ET)}_2\text{Cu(NCS)}_2$ and $\kappa\text{-(ET)}_2\text{Cu[N(CN)}_2\text{]Br}$ substantiate the strong coupling of the superconducting charge carriers to intermolecular phonons [55–60]. The observed anomalous temperature dependence of the low-frequency phonons around and below T_c were found to be consistent with an isotropic gap $2\Delta_0$ close to 2.8 meV [59]. From the reported frequency shifts the electron-phonon coupling constants λ_i have been calculated yielding a total coupling constant of $\lambda_{tot} = 0.97 \pm 0.11$ [59].

Superconductivity-induced phonon renormalization As a consequence of the interaction of charge carriers with the phonon system, the opening of a gap in the electronic density of states below T_c induces changes in the phonon frequencies and linewidths. These effects were first observed in the classical superconductors Nb_3Sn and Nb [330,331]. The results of these studies support the generally accepted picture that superconductivity in these materials is phonon-mediated.

Inelastic neutron-scattering experiments have been performed on single crystals of $\kappa\text{-(ET)}_2\text{Cu(NCS)}_2$ on both hydrogenated and deuterated crystals [332,63]. Due to the extraordinarily large incoherent crosssection of the protons, the study of $\kappa\text{-(H}_8\text{-ET)}_2\text{Cu(NCS)}_2$ allows for a selective investigation of those vibrational modes that involve the hydrogen atoms at the terminal ethylene groups. The analysis of measurements above and below T_c suggest a substantial coupling of these modes to the superconducting charge carriers [332]. Figure 40 shows the results of inelastic neutron-scattering experiments on deuterated $\kappa\text{-(ET)}_2\text{Cu(NCS)}_2$ carried out by Pintschovius et al. [63]. The data reveal a sudden increase of the frequencies of transverse acoustic phonons upon cooling through T_c . This phonon hardening was found to be most pronounced for the wave vector $\mathbf{q} = (-0.225, 0, 0.45)$ and a phonon energy 2.4 meV. As discussed by Zeyher and Zwicknagl [333], significant changes are expected only for those phonons whose energy $\hbar\omega$ is close to the gap value 2Δ with a softening (hardening) for $\hbar\omega < 2\Delta$ ($\hbar\omega > 2\Delta$) [333]. The above results thus imply $2\Delta \simeq 2.4$ meV, i.e. $2\Delta/k_B T_c \simeq 3.1$, which is close to the

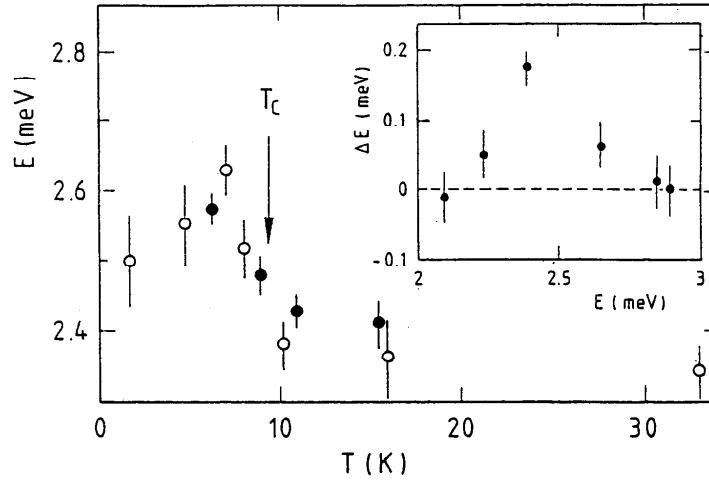


Fig. 40. Temperature dependence of the energy of the transverse acoustic phonon with wave vector $\mathbf{q} = (-0.225, 0, 0.45)$ derived from inelastic neutron scattering on two different single crystals (open and closed circles) of deuterated κ -(ET)₂Cu(NCS)₂. Inset: observed frequency shifts [$\Delta E = E(T < T_c) - E(T > T_c)$] of transverse acoustic phonons in the $[-\zeta, 0, 2\zeta]$ direction. Reproduced from [63].

BCS ratio of 3.52. The salient feature of this study is that intermolecular modes strongly couple to the superconducting charge carriers and may thus provide a substantial contribution to the pairing interaction [63].

On the order-parameter symmetry in (BEDT-TTF)₂X

Measurements of the gap anisotropy A new development in the investigation of the order-parameter symmetry is to probe the gap anisotropy directly by using orientational-dependent measurements. For the present organic superconductors, these techniques include mm-wave transmission [334], STM spectroscopy [335] and thermal conductivity [62] studies.

A *mm-wave magneto-optical technique* was used to determine the angle dependence of the high-frequency conductivity of κ -(ET)₂Cu(NCS)₂ [334,336]. The results have been interpreted to support an anisotropic gap with "X shape", i.e. with nodes along the *b*- and *c*-direction [334], consistent with a $d_{x^2-y^2}$ symmetry of the order parameter as theoretically suggested by Schmalian [307]. However, these results have been critically commented upon by other groups [337,338].

The superconducting gap structure of the same compound has been investigated using *STM spectroscopy* by Arai et al. [335]. The tunneling curves observed on the *bc*-plane (parallel to the conducting layers) in the low-energy region could be well fitted by a *d*-wave gap model. The corresponding

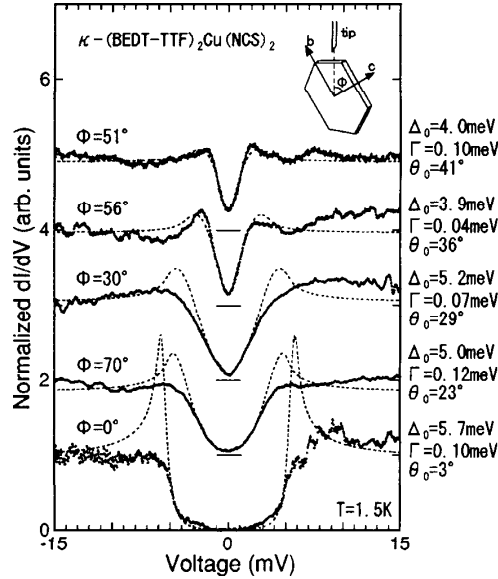


Fig. 41. dI/dV - V curves taken at 1.5 K on the lateral surfaces of κ -(ET) $_2$ Cu(NCS) $_2$ single crystals. Data have been taken along various tunneling directions at different angles ϕ as defined in the inset. The dashed line represents the calculated curve based on the d -wave gap model with a k dependent tunneling. Taken from [335].

$2\Delta_0/k_B T_c$ ratio was found to be 6.7 which is smaller than a previously reported value of 9 [339] but substantially larger than the BCS value of 3.52. In addition, the in-plane gap anisotropy was investigated, see Fig. 41. The dI/dV - V curves observed on the lateral surfaces were found to be also consistent with a d -wave gap. For this configuration a very large $2\Delta_0/k_B T_c$ ratio of $8.7 \sim 12.9$ has been obtained. The analysis of the angular dependence revealed that the direction of the line nodes of the gap is $\pi/4$ from the k_b - and k_c -axes, i.e. the gap has $d_{x^2-y^2}$ symmetry [335]. It has been noted that these orientations of the gap nodes are at variance with those inferred from the above mm-wave-transmission experiments.

The *thermal conductivity* has been used as another directional-dependent probe. When compared to STM measurements, for example, this quantity has the advantage that it is free of surface effects. The implications of the symmetry of gap zeroes on the thermal conductivity in the vortex state have been theoretically investigated by various authors, see e.g. Won and Maki [340]. Measurements have been performed for the κ -(ET) $_2$ Cu(NCS) $_2$ salt in a magnetic field rotating within the 2D superconducting plane. Figure 42 shows the angular variation of κ at a fixed field of $B = 2$ T. Θ denotes the angle between the heat current flowing along the crystallographic b direction and the magnetic field, i.e. $\Theta = 0^\circ$ for $B \parallel b$. The salient result of this study is the occurrence of a $\kappa(\theta)$ contribution with a fourfold symmetry, $\kappa_{4\theta}$, at low temperatures $T \leq 0.52$ K that adds to a predominant term with twofold symmetry. While the latter has been interpreted as being mainly phononic in origin, it is argued that the former is of a purely electronic nature and reflects the nodal gap structure [62]. Their analysis revealed that the gap

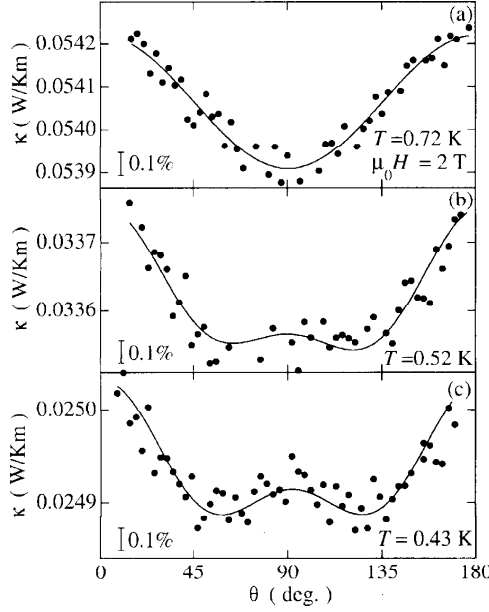


Fig. 42. Angular variation of $\kappa(B, \Theta)$ at 2 T for different temperatures where Θ denotes the angle between a rotating magnetic field in respect to the heat current flowing along the b -axis of the κ -(ET) $_2$ Cu(NCS) $_2$ crystal. The solid lines represent the results of a fit using the function $\kappa(B, \Theta) = C_0 + C_{2\Theta} \cos 2\Theta + C_{4\Theta} \cos 4\Theta$, where C_0 , $C_{2\Theta}$ and $C_{4\Theta}$ are constants. Taken from [62].

zeroes are oriented along the directions rotated by 45° relative to the b - and c -axes. It has been pointed out in [62] that this nodal structure is inconsistent with the theories based on antiferromagnetic spin fluctuation where the nodes are expected to be along the b - and c -directions. Based on this observation Izawa et al. proposed a d_{xy} symmetry (referring to the magnetic Brillouin zone, see inset of Fig. 1 in [62]) which has been theoretically suggested for a charge-fluctuation scenario [341,319].

NMR measurements A more indirect information on the symmetry of the superconducting order parameter is provided by temperature-dependent measurements of quantities which depend on the quasiparticle excitation spectrum. In this context NMR experiments, i.e. measurements of the Knight shift K_S and the spin-lattice relaxation rate $(T_1)^{-1}$ are of particular interest. The ^{13}C spin-lattice relaxation rate and Knight shift of κ -(ET) $_2$ Cu[N(CN) $_2$]Br have been investigated by various groups [142,253,342] with similar results. In these experiments single crystalline material was used where both ^{12}C atoms in the central carbon double bond of the ET molecule had been replaced by ^{13}C . For the investigation of electronic properties, these nuclei are superior since their coupling to the π -electron system is much stronger than that of the protons in the ethylene endgroups of the ET molecules. The salient results of these studies are: (i) Knight-shift measurements performed in fields aligned parallel to the conducting planes reveal a spin susceptibility that tends to zero at low temperatures. Since any contributions from the pancake vortices have been excluded for this field configuration, the above

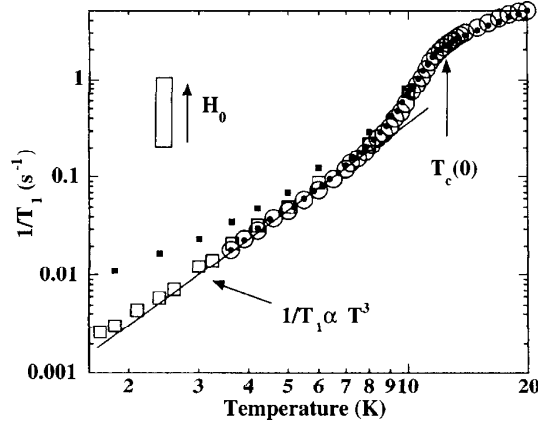


Fig. 43. Spin-lattice-relaxation rate $(T_1)^{-1}$ at fields of 5.6 T (open circles), 7.8 T (black circles) and 7 T (open squares) applied parallel to the conducting planes of κ -(ET)₂Cu[N(CN)₂]Br. Black squares correspond to a field of 7 T with a small misalignment. Taken from [253].

results have been taken as evidence for the spin-singlet character of the pairing state. (ii) The spin-lattice relaxation rate, $(T_1)^{-1}$, measured in the same parallel field configuration lacks a Hebel-Slichter peak and shows a power-law T^n behavior at low T , with n being close to 3, see Fig. 43. For the experimental conditions chosen, the authors ascribed the dominant source of relaxation to the quasiparticle excitations in the superconducting state. Consequently, the power-law temperature dependence in $(T_1)^{-1}$ has been interpreted as indicating an anisotropic pairing with nodes in the gap function [142,253,342].

Thermal conductivity Investigations of the thermal conductivity on quasi-2D organic superconductors at low temperatures have been performed first on κ -(ET)₂Cu(NCS)₂ [61] and more recently also on κ -(ET)₂Cu[N(CN)₂]Br [51]. These studies reveal that the onset of superconductivity is associated with a sudden increase of $\kappa(T)$ which can be suppressed by a moderate magnetic field. The enhancement of $\kappa(T)$ at the onset of superconductivity has been attributed to a strengthening of the phonon heat transport by reducing the scattering due to the gap formation. Their argument is based on a quantitative analysis of the data employing the Wiedemann-Franz law. It showed that just above T_c the electronic contribution amounts to only 5 % of the total thermal conductivity. A lattice-dominated thermal conductivity around T_c is also consistent with the absence of a magnetic field dependence of κ in this temperature range [61]. As for the question of the gap symmetry, the data at low temperature have been interpreted as indicating an excitation spectrum with gap zeroes: an extrapolation of the data for κ -(ET)₂Cu(NCS)₂ to $T \rightarrow 0$ revealed a finite in- T linear term which has been attributed to a residual electronic contribution [61]. The latter is expected for an unconventional superconductor due to impurity scattering of residual quasiparticles [343,344].

On the other hand, recent thermal conductivity measurements on the κ -(ET)₂Cu[N(CN)₂]Br salt showed that down to the lowest temperatures the

phonon scattering length is strongly influenced by quasiparticle scattering [51] which renders the analysis of the data on κ -(ET)₂Cu(NCS)₂ [61] as being questionable.

Magnetic penetration depth The quantity which has been studied most intensively for the κ -(ET)₂X superconductors in connection with the question on the order-parameter symmetry is the magnetic penetration depth. According to the London theory, the penetration depth λ_L in the limit $T \rightarrow 0$ is directly related to the density of superconducting electrons n_s via

$$\lambda_L(0) = \sqrt{\frac{m^* c^2}{4\pi n_s e^2}}, \quad (16)$$

where m^* is the effective mass of the superconducting carriers [204]. Employing a two-fluid model with $n_e = n_s(T) + n_n(T)$ and n_e the density of conduction electrons, the temperature dependence of $\lambda_L(T)$ provides information on the normal-conducting component $n_n(T)$, i.e. the quasiparticle excitation spectrum. Since $n_s(T \rightarrow 0) = n_e$, the low-temperature value $\lambda(T \rightarrow 0)$ is a measure of the pair condensate, i.e. $\lambda_L^2(0) \propto m^*/n_s(0)$. For a conventional weak-coupling superconductor, the BCS theory predicts a mean-field temperature dependence of λ_L around T_c and an exponentially small variation at low temperatures $T \ll T_c$ [345]:

$$\lambda_L(T) \simeq \lambda(0) \left[1 + \left(\frac{2\pi\Delta}{k_B T} \right)^{\frac{1}{2}} \exp \left(-\frac{\Delta}{k_B T} \right) \right]. \quad (17)$$

This holds true also for an anisotropic gap function without nodes, where for $k_B T \ll \Delta_{\min}$ the exponential low-temperature behavior is governed by the minimum value of the gap Δ_{\min} . In contrast, an energy gap which vanishes along lines or at points at the Fermi surface will result in a power-law dependence of $\lambda_L(T)$ for $T \ll T_c$.

For the present materials the magnetic penetration depth has been determined by a variety of different techniques including ac-susceptibility [346,262], muon-spin relaxation [263,347], dc-magnetization [264,265], surface impedance [266,260] and a related high-frequency technique using a tunnel diode oscillator [348]. The results of these studies, however, are quite inconsistent regarding both the temperature dependence as well as the absolute values of $\lambda_L(T \rightarrow 0)$ (see Table 2 in section 4.2) and have led to quite different conclusions as to the symmetry of the superconducting order parameter. Interestingly enough, these inconsistencies do not only involve results from different experimental techniques. Contradictory conclusions have been drawn also on the basis of seemingly identical experiments performed by different groups. This is the case for surface impedance studies where the penetration depth can be extracted from the complex conductivity. The latter is derived from the frequency shifts and variations of the quality factor of the resonator

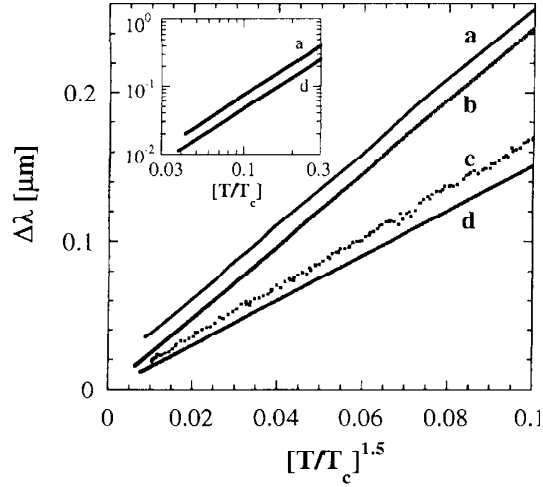


Fig. 44. Changes of the in-plane penetration depth $\Delta\lambda_{\parallel}(T)$ of κ -(ET)₂Cu[N(CN)₂]Br [two samples (a),(b)] and κ -(ET)₂Cu(NCS)₂ [(c),(d)] plotted versus $(T/T_c)^{\frac{3}{2}}$. The data have been offset. Taken from [348].

caused by the sample. While the surface impedance studies using a microwave perturbation technique on κ -(ET)₂Cu(NCS)₂ and κ -(ET)₂Cu[N(CN)₂]Br by Klein et al. [349] and Dressel et al. [260] were found to be in good agreement with the BCS predictions, other studies by Achkir et al. [266] on κ -(ET)₂Cu(NCS)₂ revealed an in- T linear behavior at low temperatures indicative of an order parameter with zeroes on the Fermi surface. Deviations from an exponential temperature dependence of $\lambda_L(T)$ for the above two κ -(ET)₂X compounds have been observed also in a more recent experiment using an rf tunnel-diode oscillator [348]. In contrast to the above measurements by Achkir et al., however, their data of the in-plane penetration depth rather follow a $T^{\frac{3}{2}}$ power law (see Fig. 44). As has been argued by the authors, the data would still be consistent with a quasi-linear variation of the superfluid density as expected for a d -wave superconductor with impurities or a small residual gap [348]. Alternatively, the authors point out that the exponent $3/2$ may arise naturally in a model proposed for short-coherence-length superconductors exhibiting a pseudogap [350].

An inconsistency exists also for μ SR experiments performed by different groups. Here λ_L can be determined by measuring the field inhomogeneities in the mixed state, i.e. the spatial variation of the local induction of the vortex lattice. This technique was first applied to κ -(ET)₂Cu(NCS)₂ by Harshman et al. [263] who could fit their data by a BCS temperature dependence. Subsequently, Le et al. [347] carried out similar experiments on the same system as well as on the κ -(ET)₂Cu[N(CN)₂]Br salt and found an in- T linear variation for the in-plane penetration depth at low temperatures $\lambda_{\parallel}(T) \approx 1 + \alpha \cdot (T/T_c)$. A power law temperature dependence of $\lambda_{\parallel}(T)$ consistent with d -wave superconductivity has been observed also by ac-susceptibility measurements performed by different groups [346,262,176]. The latter experiments as well as the surface impedance studies are operating at very small external magnetic

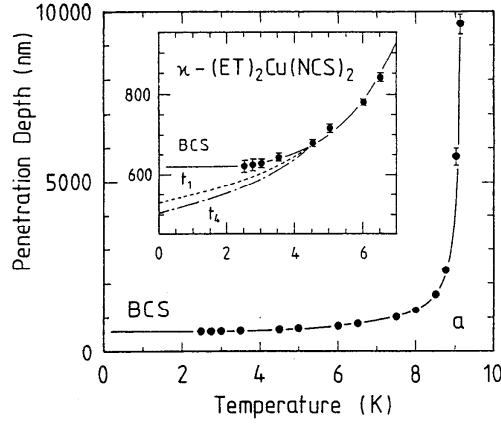


Fig. 45. In-plane penetration depth for single crystalline κ -(ET) $_2$ Cu(NCS) $_2$. The solid line represents a BCS fit. The model calculations labelled t_1 and t_4 represent those anisotropic states proposed by Hasegawa et al. [351] and used by Le et al. to explain their μ SR data [347] which have the weakest and strongest T dependences, respectively. Taken from [264].

fields ($B < B_{c1}$) attempting to probe the Meissner state. Possible difficulties in these experiments that may arise from flux-pinning-related phenomena near the surface of the superconductor, i.e. an inhomogeneous superconducting state, have been discussed in [9].

An alternative way to determine the penetration depth is to make use of the reversible mixed-state magnetization, a peculiarity of these strongly anisotropic superconductors with short coherence lengths.

According to the London model, the field dependence of the magnetization is given by

$$\frac{dM}{d(\ln H)} = \frac{\phi_0}{32\pi^2\lambda_{\text{eff}}^2}, \quad (18)$$

where $\lambda_{\text{eff}}^2 = \lambda_{\parallel}^2$ for $B \perp$ planes and $\lambda_{\text{eff}}^2 = \lambda_{\parallel}\lambda_{\perp}$ for $B \parallel$ planes. In 3D superconductors, vortex pinning usually gives rise to an inhomogeneous distribution of the vortices in the mixed state and thus to an irreversible behavior of the magnetization upon increasing and decreasing the field. This may cause substantial uncertainties in determining the penetration depth from magnetization data. On the contrary, for quasi-2D superconductors with short coherence length the magnetization is entirely reversible over an extended field range, i.e. $B_{c1} < B_{\text{irr}} < B < B_{c2}$ with B_{irr} being the temperature-dependent irreversibility line (see section 4.3). For κ -(ET) $_2$ Cu(NCS) $_2$ and κ -(ET) $_2$ Cu[N(CN) $_2$]Br a reversible magnetization has been observed over an extended range in the B - T plane which thus allows for a precise determination of the in-plane penetration depth [264,265]. The in-plane penetration depths $\lambda_{\parallel}(T)$ were determined, see Fig. 45, from the slopes $dM/d(\ln H)$ of the isotherms taken at different temperatures and using equation (18). The solid line represents a BCS fit [345] to the data. For both systems, the data reveal only a weak variation with temperature at low T consistent with an exponential temperature dependence as expected for a finite gap.

Specific heat The above variety of contradictory results on the magnetic penetration depth indicate an extraordinarily high sensitivity of this quantity to extrinsic effects such as disorder or pinning-related phenomena. As a possible source, we mention the disorder associated with the glass transition of the ethylene endgroups, see section 3.4 and [176].

A quantity which is less sensitive to the above problems but can still provide fundamental information on the gap structure is the specific heat. In case this integral thermodynamic quantity were to find a low temperature electronic quasiparticle contribution, C_{es} , that varies exponentially weakly with the temperature, the existence of gap zeroes on the Fermi surface could be definitely ruled out. On the other hand, the observation of a non-exponential temperature dependence does not necessarily prove the existence of gap zeroes as this result might originate in extraneous contributions such as impurity phases, normal-conducting regions or pair-breaking effects.

First specific heat measurements were focussing on the determination of the discontinuity at T_c which provides information on the coupling strength. From the results of Andraka et al. [352] and Graebner et al. [268] on $\kappa\text{-(ET)}_2\text{Cu(NCS)}_2$ yielding a ratio of $\Delta C/\gamma T_c > 2$ a strong-coupling behavior has been inferred for this salt. In a series of subsequent experiments, the temperature dependence of the electronic contribution, C_{es} , at lower temperatures was at the focus of the investigations. From experiments on $\kappa\text{-(ET)}_2\text{Cu[N(CN)}_2\text{]Br}$ Nakazawa et al. [353] reported a quadratic temperature

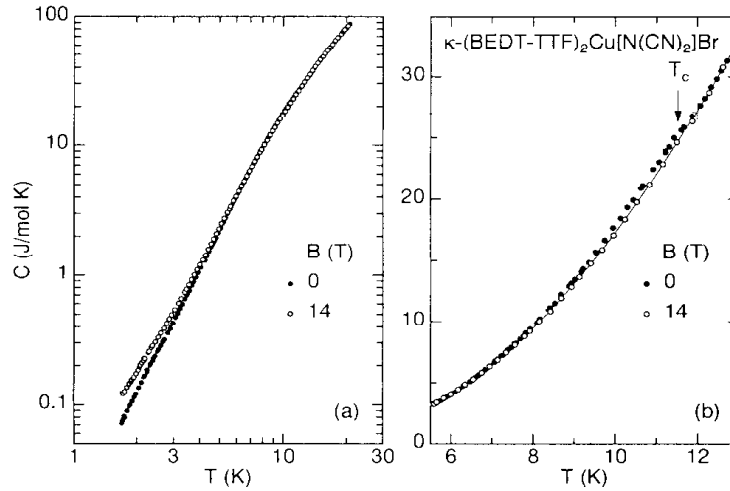


Fig. 46. Temperature dependence of the specific heat of $\kappa\text{-(ET)}_2\text{Cu[N(CN)}_2\text{]Br}$ in the superconducting ($B = 0$) and normal state ($B = 14$ T) over an extended temperature range (left panel) and in the vicinity of $T_c = 11.5$ K (right panel). The solid line is a polynomial fit to the 14 T data. Taken from [267].

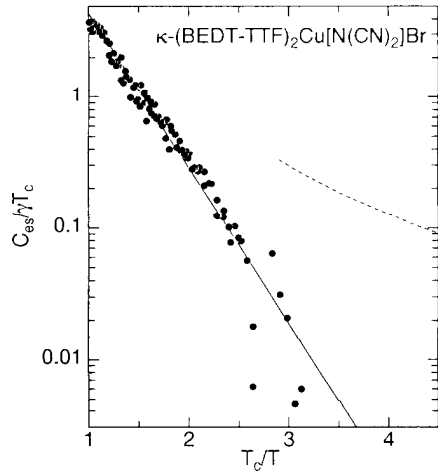


Fig. 47. A semi-logarithmic plot of $C_{es}/(\gamma T_c)$ vs T_c/T as determined from the data shown in Fig. 46. The solid line indicates the exponential variation of C_{es} . The dashed line corresponds to C_{es} as determined by Nakazawa et al. [353] (see text and [354]). Taken from [267].

dependence of C_{es} at low temperatures, which was taken as an indication for line nodes in the gap. However, recent high-resolution specific heat measurements on the same compound revealed an exponentially weak low- T electronic contribution to the specific heat implying a finite energy gap [267]. Moreover it has been shown in the latter study that the T^2 dependence in the C_{es} data by Nakazawa et al. [353] most likely originates in their incorrect determination of the phonon background [354]. Figures 46 and 47 show the results of specific heat measurements performed by Elsinger et al. [267]. The phonon contribution, which predominates the specific heat near T_c has been determined from measurements in an overcritical field. This standard procedure is valid as long as there are no magnetic contributions to the specific heat which might change with the field. From the absence of any measurable field dependence in the data above T_c this assumption appears justified. Figure 47 shows the exponential decrease of C_{es} with decreasing temperatures. The lack of a finite C_{es} for $T \rightarrow 0$ rules out the existence of zeroes in the energy gap. A similar behavior has been observed also for κ -(ET) $_2$ Cu(NCS) $_2$ [50,51]. Figure 48 shows the difference $\Delta C(T) = C(T, B = 0) - C(T, B = 8 \text{ T} > B_{c2})$ used to analyze the specific heat data. The advantage of using this quantity means that the unknown phonon contribution drops out. As Fig. 48 demonstrates, $\Delta C(T)$ deviates markedly from the weak-coupling BCS behavior in both the jump height at T_c as well as the overall temperature dependence. However, as was found also for κ -(ET) $_2$ Cu[N(CN) $_2$]Br [267], a much better description of the data is obtained by using the semi-empirical extension of the BCS formalism to strong-coupling superconductors - the so-called α -model [356]. It contains a single free parameter $\alpha \equiv \Delta_0/k_B T_c$ which scales the BCS energy gap $\Delta(T) = (\alpha/\alpha_{\text{BCS}}) \cdot \Delta_{\text{BCS}}(T)$ with $\alpha_{\text{BCS}} = 1.764$. As Fig. 48 clearly demonstrates, the strong-coupling BCS model with $\alpha = 2.8 \pm 0.1$ pro-

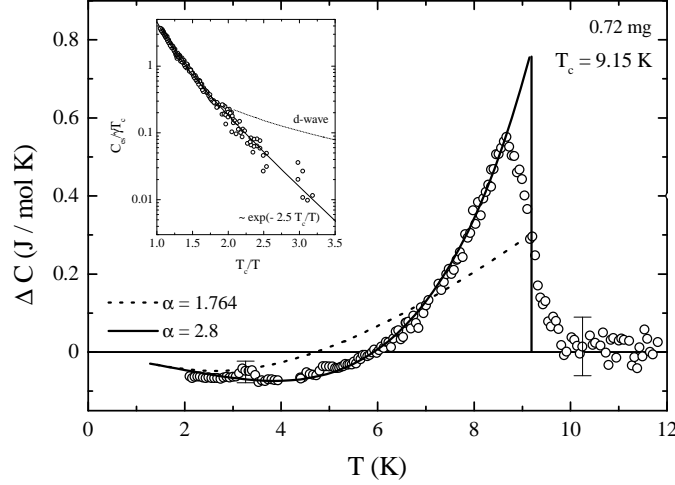


Fig. 48. Specific heat difference $\Delta C = C(0\text{ T}) - C(8\text{ T})$ of a $\kappa\text{-(ET)}_2\text{Cu(NCS)}_2$ single crystal of $m = 0.72\text{ mg}$ (main panel). The dotted and solid thick lines represent the BCS curves for weak and strong coupling, respectively. The inset shows the quasiparticle contribution to the specific heat in the superconducting state as $C_{\text{cs}}/\gamma T_c$ vs T_c/T in a semi-logarithmic representation. Here the solid line represents the strong-coupling BCS behavior while the dotted line indicates a T^2 behavior as expected for a d -wave order parameter [355]. Taken from [50,187].

vides an excellent description of the data over the entire temperature range investigated [50]. Similar to what has been found for $\kappa\text{-(ET)}_2\text{Cu[N(CN)}_2\text{]Br}$ (Fig. 47), the data for $\kappa\text{-(ET)}_2\text{Cu(NCS)}_2$ (inset of Fig. 48) are fully consistent with an exponentially small C_{cs} at low temperatures, i.e. an energy gap without zeroes at the Fermi surface. The same behavior has been previously observed for other $(\text{ET})_2\text{X}$ superconductors [357,358,51]. The above findings of an exponentially weak specific heat at low temperatures are clearly incompatible with the existence of gap zeroes as claimed by various of the above mentioned experiments. It has to be shown by future studies whether or not this controversy can be removed by taking properly into account the influence of magnetic fields even when applied parallel to the planes and other extraneous effects such as the cooling-rate-dependent disorder associated with the ethylene groups.

On the pairing state in $(\text{TMTSF})_2\text{X}$ As for the BEDT-TTF systems, the nature of superconductivity in the Bechgaard salts $(\text{TMTSF})_2\text{X}$ is still far from being understood and continues to be a controversial issue. Early suggestions of a spin-triplet ($S=1$) state were based on the proximity of superconductivity to a SDW state in the pressure-temperature phase diagram (cf. section 3.5). This situation resembles the theoretical expectation for an interacting 1D electron gas [359] where a SDW phase lies next to triplet

superconductivity. Further arguments for a spin-triplet p -wave superconductivity were derived from the observation that T_c is extremely sensitive to the introduction of nonmagnetic defects [360,361] and substitutional impurities [362,363], see also [364,365]. As discussed in section 3.5, depending on external pressure and magnetic field, the Bechgaard salts can be tuned to either a superconducting or a SDW ground state which has led to the proposal that the order parameters of both phases are not independent of each other. The superconducting properties of the Bechgaard salts have been reviewed by several authors [33,5,366]. Since these articles are comprehensive up to 1998, we shall give only a brief overview on the early results and concentrate the discussion on the more recent developments including the possibility of spin-triplet superconductivity.

Among the (TMTSF) $_2$ X superconductors, the X = PF $_6$ and ClO $_4$ salts are the most extensively studied materials although the number of experimental investigations of the superconducting properties is much less compared to that of the BEDT-TTF salts and their derivatives. The reason for this is most likely related to the low T_c values of the former systems which require extensive low-temperature equipment and, in the case of X = PF $_6$, external pressure of $p \geq 5.8$ kbar [367] to stabilize the superconducting state. For the ambient-pressure superconductor (TMTSF)ClO $_4$ it is the anion ordering which renders the experimental situation difficult (see section 3.4). By slowly cooling through the anion-ordering temperature T_{AO} at around 24 K an ambient pressure superconducting state below $T_c = (1.2 \pm 0.2)$ K can be stabilized. In this case, the anions are believed to be well ordered. On the other hand, for samples that have been cooled rapidly across T_{AO} , an insulating state forms below $T_{MI} \simeq 6.1$ K.

Early specific heat measurements on (TMTSF) $_2$ ClO $_4$ focusing on the temperature range close to T_c revealed a discontinuity at T_c , $\Delta C/\gamma T_c = 1.67$ which is in fair agreement with the BCS value of 1.43 [244]. On the other hand, deviations from a BCS-type of superconductivity have been observed in NMR measurements by Takigawa et al. [368]. These authors reported the absence of a Hebel-Schlichter peak and a T^3 dependence in the spin-lattice relaxation rate. This has led to the proposal of a d -wave order parameter with a gap that vanishes along lines on the Fermi surface [368]. These results are at variance with more recent thermal conductivity data on the same salt, showing a rapid decrease of the electronic contribution to the heat transport below T_c which indicates the absence of low-lying excitations [369]. Their results provide strong evidence for a nodeless gap function. However, as pointed out by the authors, this result is not necessarily associated with an s -wave order parameter.

By enumerating possible gap functions for quasi-1D systems, Hasegawa and Fukuyama [351] showed that besides an anisotropic spin-singlet d -wave also a spin-triplet p -wave state - in both cases the order parameters vanish along lines on the FS - is possible. The authors suggested the possibility of an an-

tiferromagnetic spin-fluctuation pairing mechanism for the Bechgaard salts. Arguments in favor of such a spin-fluctuation-mediated superconductivity with d -wave symmetry have been derived from a recent resistivity study under pressure [180,68]. According to these results, a minimum in the resistivity $\rho_a(T)$ at T_{\min} marks the onset of AF fluctuations before, at lower temperatures, an itinerant antiferromagnetic state (SDW) is stabilized. The width of the region of critical AF fluctuations in the T - p phase diagram (see Fig. 22 in section 3.5) is enhanced when the SDW ground state is approached from the high-pressure side, where the system is close to the SDW/SC border and largest where $T_c(p)$ reaches its optimum value. The correlation between the spin-fluctuation regime above the onset of superconductivity and the T_c value is taken as a strong argument for a pairing mechanism mediated by the exchange of these fluctuations [180,68].

In a recent series of papers on the upper critical fields, the discussion of a possible realization of a triplet-pairing state in the Bechgaard salts has again been raised [250,367,370]. Lee et al. examined the upper critical field $B_{c2}(T)$ and its directional dependence in $(\text{TMTSF})_2\text{PF}_6$ under pressure via resistivity measurements. The resulting magnetic field-temperature phase diagram is depicted in Fig. 49 for fields aligned along the three crystal axes [250]. While the upper-critical-field curves near T_c were found to be consistent with earlier results on the same and related compounds, which indicated a more conventional behavior (see also Fig. 32 in section 4.2) [245,248,249], the extension of the measurements to lower temperatures uncovered important new features: (i) the upper critical fields for B aligned along the a - and b -directions display

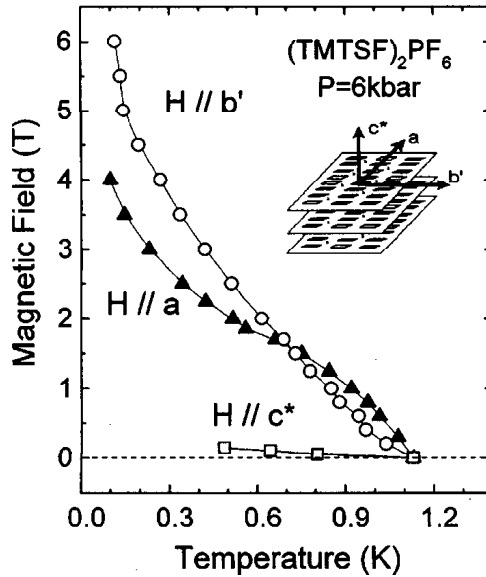


Fig. 49. B - T phase diagram of $(\text{TMTSF})_2\text{PF}_6$ at a pressure of 6 kbar for magnetic fields aligned along three perpendicular axes as defined in the inset. Taken from [250].

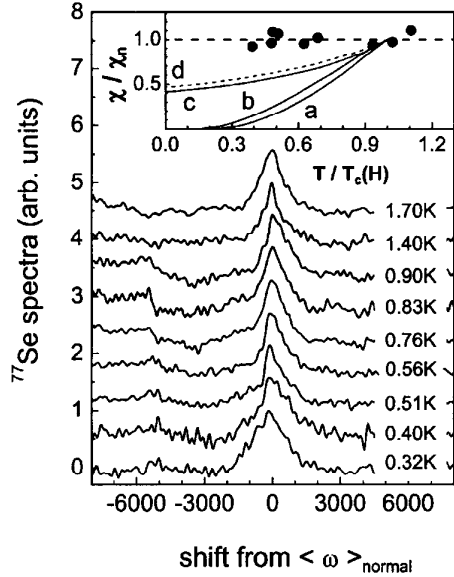


Fig. 50. ^{77}Se NMR spectra of $(\text{TMTSF})_2\text{PF}_6$ under 7 kbar at various temperatures above and below T_c which is 0.81 K at the applied field of 1.43 T aligned along the most conductive a axis. The inset shows normalized χ_{Spin} data compared with theoretical calculations. Curves a and b are for a singlet state in applied fields B/B_{c2} near zero and 0.63, respectively, as calculated by Fulde and Maki [371] while curves c and d represent a scenario where the vortex cores induce normal regions of a fraction equal to B/B_{c2} . Taken from [372].

strong positive curvatures *without* saturation. This behavior was found to be independent of the criterion used to extract B_{c2} from the resistance profiles. (ii) B_{c2}^b becomes larger than B_{c2}^a , i.e. the anisotropy inverts upon cooling, and (iii), the critical fields in both directions exceed the Pauli limiting field of $B_P = 1.84 \times T_c \simeq 2.2$ T [246,247]. In a subsequent resistivity study under fields along the b -axis and optimum pressure settings [367], the onset of superconductivity was found to persist even up to 9 T, which is more than four times B_P . The authors discussed various proposals attempting to explain an upturn in the upper critical field. Among them are strong spin-orbit scattering [373,374], a magnetic-field-induced dimensional crossover from 3D to 2D [375,376] and the formation of a spatially inhomogeneous Fulde-Ferrell-Larkin-Ovchinnikov (FFLO) state [269,270]. It has been argued by Lee et al. that, even with a field-induced dimensional crossover which greatly enhances the orbital critical field, an additional effect is required to exceed the paramagnetic limit. This could be either the formation of the FFLO state or triplet superconductivity. The fact that no indications for a first-order phase transition into the FFLO state have been observed thus points to the possibility of a spin-triplet superconducting state.

This interpretation has gained further support from recent NMR measurements of the Knight shift K_S in the superconducting state of pressurized $(\text{TMTSF})_2\text{PF}_6$ [372]. Since K_S is proportional to the spin-susceptibility χ_{Spin} , which is different for spin singlet ($\chi_{\text{Spin}} \rightarrow 0$ for $T \rightarrow 0$) and triplet (χ_{Spin} remains unchanged on cooling through T_c) superconductors, measurements of K_S provide a direct probe of the spin parity of the superconductor. Figure 50 shows that in contrast to the expectations for the various scenarios involv-

ing singlet superconductivity there is no significant change in K_S for $B \parallel a$ on cooling into the superconducting state. These observations together with similar results of a previous study for $B \parallel b$ [377] thus argue for a spin-triplet pairing. Besides K_S , the above studies included also measurements on the spin-lattice relaxation rate $1/T_1$ which exhibits a small peak near T_c . In light of the absence of such a peak in previous reports of zero field proton-NMR measurements [368] its identification with a Hebel-Schlichter peak is unclear.

5 Epilogue

Studies on superconductivity in organic charge-transfer salts have been carried out for more than twenty-years. The joint efforts of researchers from the fields of synthetic chemistry and solid-state physics have created this new class of molecular conductors which exhibits fascinating properties. Key features are a pronounced anisotropy of the electronic states spanning the whole range from quasi-1D to anisotropic 3D, a low charge carrier concentration and a strong coupling of the charge carriers to the lattice degrees of freedom. The combination of these extraordinary material parameters make the organic conductors ideal model systems for exploring the interplay of strong electron-electron and electron-phonon interactions in reduced dimensions. In fact, this material class has enriched the solid-state physics by a wealth of interesting collective phenomena such as spin-Peierls or density-wave instabilities, Mott-type metal-insulator transitions, and, above all, superconductivity. Most remarkably, these systems offer a unique opportunity to scan through the various ground states either in discrete steps by chemical means, or even in a continuous way through changes of the applied pressure.

Thanks to the intense interdisciplinary efforts from research groups in chemistry and physics, our level of understanding of these materials has progressed substantially. The basis for this development was accomplished by advances in organic and organometallic chemistry which have provided a rich and varied supply of molecules serving as building blocks for conductors and superconductors. By employing state-of-the-art preparation techniques, it is possible nowadays to synthesize crystals of unprecedented high quality which permit highly accurate measurements of their electronic parameters. In particular, these clean materials enable direct experimental access to the electronic band structure with a high level of accuracy. For the 2D materials, the various experiments agree in that the normal-state electronic properties are well described by quasiparticles within a Fermi-liquid approach. These quasiparticles reveal a considerable mass renormalization due to both electron-electron as well as electron-phonon interactions. This contrasts with the behavior found in the quasi-1D salts, where non-Fermi-liquid properties have been reported for transport and optical properties. Indeed, these results indicate the separation of spin and charge degrees of freedom - one of the hallmarks of a Luttinger liquid.

The phase diagrams of the quasi-1D and 2D materials have been mapped out in great detail utilizing a wide spectrum of experimental techniques - some of which have been applied under extreme conditions such as high magnetic fields and high pressure. These studies confirmed, on the one hand, the universal character of the phase diagrams for both families and revealed, on the other hand, intriguing new details of the interplay of the various phases. Despite such detailed information, in particular on the phase boundary between

superconductivity and magnetism, there is still no generally accepted picture on the nature of the superconducting state. The fact that both phases share a common phase boundary have led some researchers to believe that both phenomena have the same origin. In such a scenario, the attractive pairing interaction would have to be provided by the exchange of antiferromagnetic spin fluctuations. In fact, some of the experimental data seem to indicate an anisotropic pairing state compatible with such a magnetic pairing interaction. While for the quasi-2D salts a spin-singlet state with *d*-wave symmetry is the most favored one among the anisotropic states proposed, a number of experiments on the quasi-1D materials even suggest triplet superconductivity. However, for the quasi-2D salts, the notion of an anisotropic superconducting state is in clear conflict with results of other experiments - in particular specific heat measurements - which demonstrate the existence of a finite superconducting energy gap on the whole Fermi surface.

It is remarkable that despite the continuous experimental efforts to unravel the fundamental features of the superconducting state, the above controversy still persists. These efforts include the application of standard experimental techniques, some of which have been driven to an extraordinarily high resolution, as well as new, more sophisticated methods such as angular-dependent investigations of the gap functions.

An important lesson to be learnt from this controversy concerns the role of disorder, in particular the *intrinsic*-type of disorder which is inherent to many of the materials even when prepared under ideal conditions. As was recognized early on for the quasi-1D materials but has now proved to be true also for the quasi-2D systems, *intrinsic* disorder can be of crucial importance and should not be overlooked in exploring and discussing superconducting-state properties. This is of concern for all those materials where, by the symmetry, certain structural elements can adopt more than one orientation. Since these states are almost degenerate in energy, a cooling-rate dependent frozen *intrinsic* disorder will result at low temperatures which may have a severe influence on both the electronic and also the elastic properties of the sample. It is to be hoped that part of the above controversy can be removed by taking these disorder effects into account properly.

In viewing the field of organic conductors and superconductors as a whole, it is clear that these materials have provided a considerable contribution to our understanding of strongly interacting electrons in low dimensions, though important questions still remain open. This concerns, in particular, the nature of the metallic state above T_c and the role of electron-electron and electron-phonon interactions in the pairing mechanism. In light of the progress we have made in recent years, one can be optimistic that more systematic investigations on the relationship between molecular properties and crystal structure on the one hand, and the collective features of the bulk, on the other, will not only provide an answer to these questions but

also will be a guidance for the synthesis of new materials with hopefully even more fascinating properties.

References

1. D. Jérôme, A. Mazaud, M. Ribault, K. Bechgaard: *J. Physique Lett.* **41**, L95 (1980)
2. H. Akamatu, H. Inokuchi, Y. Matsunaga: *Nature* **173**, 168 (1954)
3. W.A. Little: *Phys. Rev. A* **134**, 1416 (1964)
4. R.H. McKenzie: *Science* **278**, 820 (1997); *Comments Cond. Mat. Phys.* **18**, 309 (1998)
5. T. Ishiguro, K. Yamaji, G. Saito: *Organic superconductors*, 2nd edn. (Springer, Berlin 1998)
6. The review 'Organic conductors and superconductors' by D. Jérôme and H.J. Schulz: *Adv. Phys.* **31**, 229 (1982) on the quasi-1D organic conductors has been republished in: *Adv. Phys.* **51**, 293 (2002)
7. L.N. Bulaevskii: *Adv. Phys.* **37**, 443 (1988)
8. J.-P. Farges (editor): *Organic Conductors - Fundamentals and Applications*, (M. Dekker, New York 1994)
9. M. Lang: *Quasi-Two-dimensional Organic Superconductors*, *Superconductivity Review* **2**, 1 (1996)
10. J. Singleton, C. Mielke: *Quasi-two-dimensional organic superconductors: a review*, *Contemp. Phys.* **43**, 63 (2002)
11. L.B. Coleman, M.J. Cohen, D.J. Sandman, F.G. Yamagishi, A.F. Garito, A.J. Heeger: *Solid State Commun.* **12**, 1125 (1973)
12. J. Ferraris, D.O. Cowan, V. Walatka, Jr., J.H. Perlstein: *J. Am. Chem. Soc.* **95**, 948 (1973)
13. G.C. Papavassiliou, G.A. Mousdis, J.S. Zambounis, A. Terzis, A. Hountas, B. Hilti, C.W. Mayer, J. Pfeiffer: *Synth. Met.* **27**, B379 (1988)
14. A.M. Kini, M.A. Beno, D. Son, H.H. Wang, K.D. Carlson, L.C. Porter, U. Welp, B.A. Vogt, J.M. Williams, D. Jung, M. Evain, M.-H. Whangbo, D.L. Overmyer, J.E. Schirber: *Solid State Commun.* **69**, 503 (1989)
15. M.A. Beno, H.H. Wang, A.M. Kini, K.D. Carlson, U. Geiser, W.K. Kwok, J.E. Thompson, J.M. Williams, J. Ren, M.-H. Whangbo: *Inorg. Chem.* **29**, 1599 (1990)
16. K. Bechgaard, C.S. Jacobsen, K. Mortensen, H.J. Pedersen, N. Thorup: *Solid State Commun.* **33**, 1119 (1980)
17. K. Bechgaard, K. Carneiro, M. Olsen, F.B. Rasmussen, C.S. Jacobsen: *Phys. Rev. Lett.* **46**, 852 (1981)
18. L.K. Montgomery: 'Chemical Synthesis and Crystal Growth Techniques'. In: *Organic Conductors - Fundamentals and Applications*. ed. by J.-P. Farges (M. Dekker, New York 1994) pp. 115–145
19. G. Saito, T. Enoki, K. Toriumi, H. Inokuchi: *Solid State Commun.* **42**, 557 (1982)
20. K. Oshima, H. Urayama, H. Yamochi, G. Saito: *Physica C* **153 - 155**, 1148 (1988)
21. J.M. Williams, J.R. Ferraro, R.J. Thorn, K.D. Carlson, U. Geiser, H.H. Wang, A.M. Kini, M.-H. Whangbo: *Organic Superconductors (Including Fullerenes)*. (Prentice Hall, Englewood Cliffs, N.J. 1992) chapter 2
22. R. Moret, J.P. Pouget: In: *Crystal Chemistry and Properties of Materials with Quasi-One-Dimensional Structures*. ed. by J. Rouxel (D. Reidel, Dordrecht, The Netherlands, 1986) pp. 87–143

23. T. Mori: Bull. Chem. Soc. Japan **71**, 2509 (1998); T. Mori, H. Mori, S. Tanaka: *ibid.* **72**, 179 (1999); T. Mori: *ibid.* **72**, 2011 (1999)
24. A.M. Kini, U. Geiser, H.H. Wang, K.D. Carlson, J.M. Williams, W.K. Kwok, K.D. Vandervoort, J.E. Thompson, D.L. Supka, D. Jung, M.-H. Whangbo: Inorg. Chem. **29**, 2555 (1990)
25. J.M. Williams, A.M. Kini, H.H. Wang, K.D. Carlson, U. Geiser, L.K. Montgomery, G.J. Pyrk, D.M. Watkins, J.M. Kommers, S.J. Boryschuk, A.V. Strieby Crouch, W.K. Kwok, J.E. Schirber, D.L. Overmyer, D. Jung, M.-H. Whangbo: Inorg. Chem. **29**, 3272 (1990)
26. H.H. Wang, K.D. Carlson, U. Geiser, A.M. Kini, A.J. Schultz, J.M. Williams, L.K. Montgomery, W.K. Kwok, U. Welp, K.G. Vandervoort, S.J. Boryshuk, A.V. Strieby Crouch, J.M. Kommers, D.M. Watkins, J.E. Schirber, D.L. Overmyer, D. Jung, J.J. Novoa, M.-H. Whangbo: Synth. Met. **41-43**, 1983 (1991)
27. Yu.V. Sushko, K. Andres: Phys. Rev. B **47**, 330 (1993)
28. A. Kobayashi, R. Kato, T. Naito, H. Kobayashi: Synth. Met. **56**, 2078 (1993)
29. A. Kobayashi, T. Udagawa, H. Tomita, T. Naito, H. Kobayashi: Chem. Lett. **1993**, 2179 (1993)
30. L.K. Montgomery, T. Burgin, C. Husting, L. Tilley, J.C. Huffmann, K.D. Carlson, J.D. Dudek, G.A. Yaconi, U. Geiser, J.M. Williams: Mol. Cryst. Liq. Cryst. **211**, 283 (1992)
31. H. Kobayashi, H. Akutsu, E. Arai, H. Tanaka, A. Kobayashi: Phys. Rev. B **56**, R8526 (1997)
32. S. Uji, C. Terakura, T. Terashima, T. Yakabe, Y. Terai, M. Tokumoto, A. Kobayashi, F. Sakai, H. Tanaka, H. Kobayashi: Phys. Rev. B **65**, 113101 (2002)
33. D. Jérôme: 'Organic Superconductors: From (TMTSF)₂PF₆ to Fullerenes'. In: *Organic Conductors - Fundamentals and Applications*. ed. by J.-P. Farges (M. Dekker, New York 1994) pp. 405-494
34. For a comprehensive overview on the band-structure calculations and Fermi-surface studies see [5] and references cited therein.
35. T. Mori, A. Kobayashi, Y. Sasaki, H. Kobayashi, G. Saito, H. Inokuchi: Bull. Chem. Soc. Jpn. **57**, 627 (1984)
36. M.-H. Whangbo, J.J. Novoa, D. Jung, J.M. Williams, A.M. Kini, H.H. Wang, U. Geiser, M.A. Beno, K.D. Carlson: 'Organic superconductivity'. ed. by V.Z. Kresin and W.A. Little (Plenum Press, New York 1990) p. 243
37. U. Geiser, A.J. Schultz, H.H. Wang, D.M. Watkins, D.L. Stupka, J.M. Williams, J.E. Schirber, D.L. Overmyer, D. Jung, J.J. Novoa, M.-H. Whangbo: Physica C **174**, 475 (1991)
38. P.M. Grant: J. Phys. C **15**, 847 (1983)
39. G.M. Danner, W. Kang, P.M. Chaikin: Phys. Rev. Lett. **72**, 3714 (1994)
40. J. Wosnitza: *Fermi Surfaces of Low-Dimensional Organic Metals and Superconductors*, (Springer, Berlin 1996)
41. J. Singleton: *Studies of quasi-two-dimensional organic conductors based on BEDT-TTF using high magnetic fields*, Rep. Prog. Phys. **63**, 1111 (2000)
42. K. Oshima, T. Mori, H. Inokuchi, H. Urayama, H. Yamochi, G. Saito: Phys. Rev. B **38**, 938 (1988)
43. H. Mori, S. Tanaka, M. Oshima, G. Saito, T. Mori, Y. Maruyama, H. Inokuchi: Bull. Chem. Soc. Jpn. **63**, 2183 (1990)
44. N. Harrison, E. Rzepniewski, J. Singleton, J.P. Gee, M.M. Honold, P. Day, M. Kurmoo: J. Phys.: Cond. Mat. **11**, 7227 (1999)

45. L. Onsager: Phil. Mag. **43**, 1006 (1952).
46. L.F. Lifshitz, A.M. Kosevich: Zh. Eksp. Teor. Fiz. **29**, 730 (1955); Sov. Phys. JETP **2**, 636 (1956)
47. J. Caulfield, W. Lubczynski, F.L. Pratt, J. Singleton, D.Y.K. Ko, W. Hayes, M. Kurmoo, P. Day, J. Phys.: Cond. Mat. **6**, 2911 (1994)
48. T. Sasaki, H. Sato, N. Toyota: Solid State Commun. **76**, 507 (1990)
49. T. Sasaki, H. Sato, N. Toyota: Physica C **185 - 189**, 2687 (1991)
50. J. Müller, M. Lang, R. Helfrich, F. Steglich, T. Sasaki: Phys. Rev. B **65**, R140509 (2002)
51. J. Wosnitza, S. Wanka, J. Hagel, M. Reibelt, D. Schweitzer, J.A. Schlueter: Synth. Met. (2002), in press
52. Y.-N. Xu, W.Y. Ching, Y.C. Jean, Y. Lou: Phys. Rev. B **52**, 12946 (1995)
53. J. Merino, R.H. McKenzie: Phys. Rev. B **62**, 2416 (2000)
54. J. Singleton, F.L. Pratt, M. Doporto, T.J.B.M. Janssen, M. Kurmoo, J.A.A.J. Perenboom, W. Hayes, P. Day: Phys. Rev. Lett. **68**, 2500 (1992)
55. J.E. Eldridge, Y. Xie, H.H. Wang, J.M. Williams, A.M.Kini, J.A. Schlueter: Spectrochim. Acta A **52**, 45 (1996)
56. J.E. Eldridge, Y. Xie, Y. Lin, H.H. Wang, J.M. Williams, J.A. Schlueter: Synth. Met. **86**, 2067 (1997)
57. D. Pedron, G. Visentini, R. Bozio, J.M. Williams, J.A. Schlueter: Physica C **276**, 1 (1997)
58. D. Pedron, R. Bozio, J.A. Schlueter, M.E. Kelly, A.M. Kini, J.M. Williams: Synth. Met. **103**, 2220 (1999)
59. E. Faulques, V.G. Ivanov, C. Mézière, P. Batail: Phys. Rev. B **62**, R9291 (2000)
60. A. Girlando, M. Masino, G. Visentini, A. Brillante, R.G. Della Valle, E. Venuti: Synth. Met. **109**, 13 (2000)
61. S. Belin, K. Behnia, A. Deluzet: Phys. Rev. Lett. **81**, 4728 (1998)
62. K. Izawa, H. Yamaguchi, T. Sasaki, Y. Matsuda: Phys. Rev. Lett. **88**, 027002 (2002)
63. L. Pintschovius, H. Rietschel, T. Sasaki, H. Mori, S. Tanaka, N. Toyota, M. Lang, F. Steglich: Europhys. Lett. **37**, 627 (1997)
64. H. Weiss, M.V. Kartsovnik, W. Biberacher, E. Steep, E. Balthes, A.G.M. Janssen, K. Andres, N.D. Kushch: Phys. Rev. B **59**, 12370 (1999)
65. A.-K. Klehe, R.D. McDonald, A.F. Goncharov, V.V. Struzhkin, Ho-kwang Mao, R.J. Hemley, T. Sasaki, W. Hayes, J. Singleton: J. Phys.: Cond. Mat. **12**, L247 (2000)
66. P. Wzietek, F. Creuzet, C. Bourbonnais, D. Jérôme, K. Bechgaard, P. Batail: J. Phys. I France **3**, 171 (1993)
67. T. Adachi, E. Ojima, K. Kato, H. Kobayashi: J. Am. Chem. Soc. **122**, 3238 (2000)
68. H. Wilhelm, D. Jaccard, R. Duprat, C. Bourbonnais, D. Jérôme, J. Moser, C. Carcel, J.M. Fabre: Eur. Phys. J. B **21**, 175 (2001); H. Wilhelm, D. Jaccard, D. Jérôme, J. Moser, R. Duprat, C. Bourbonnais: In: *Frontiers of High Pressure Research II: Application of High Pressure to Low-Dimensional Novel Electronic Materials*. ed. by H.D. Hochheimer et al., 423 (2001)
69. J.R. Cooper, B. Korin-Hamzić: 'Organic Metals'. In: *Organic Conductors - Fundamentals and Applications*. ed. by J.-P. Farges (M. Dekker, New York 1994) pp. 359-403
70. S. Tomonaga: Prog. Theor. Phys. **5**, 554 (1950)

71. J. Luttinger: *J. Math. Phys.* **4**, 1154 (1963)
72. H.J. Schulz: *Int. J. Mod. Phys. B* **5**, 57 (1991)
73. C. Bourbonnais, D. Jérôme: *Physics World* (September 1998) p. 41
74. V. Vescoli, L. Degiorgi, W. Henderson, G. Grüner, K.P. Starkey, L.K. Montgomery: *Nature* **281**, 1181 (1998)
75. T. Lorenz, M. Hofmann, M. Grüninger, A. Freimuth, G.S. Uhrig, M. Dumm, M. Dressel: *Nature* **418**, 614 (2002)
76. B. Dardel, D. Malterre, M. Grioni, P. Weibel, Y. Baer, J. Voit, D. Jérôme: *Europhys. Lett.* **24**, 687 (1993)
77. V. Vescoli, F. Zwick, W. Henderson, L. Degiorgi, M. Grioni, G. Gruner, L.K. Montgomery: *Eur. Phys. J. B* **13**, 503 (2000)
78. J. Moser, M. Gabay, P. Auban-Senzier, D. Jérôme, K. Bechgaard, J.M. Fabre: *Eur. Phys. J. B* **1**, 39 (1998)
79. K. Murata, M. Tokumoto, H. Anzai, Y. Honda, N. Kinoshita, T. Ishiguro, N. Toyota, T. Sasaki, Y. Muto: *Synth. Met* **27**, A263 (1988)
80. H. Sato, T. Sasaki, N. Toyota: *Physica C* **185-189**, 2679 (1991)
81. J.E. Schirber, D.L. Overmyer, K.D. Carlson, J.M. Williams, A.M. Kini, H.H. Wang, H.A. Charlier, B.J. Love, D.M. Watkins, G.A. Yaconi: *Phys. Rev. B* **44**, 4666 (1991)
82. M. Oshima, H. Mori, G. Saito, K. Oshima: 'The physics and chemistry of organic superconductors'. ed. by G. Saito, S. Kagoshima (Springer, Berlin, Heidelberg 1990) p. 257
83. K. Kikuchi, Y. Honda, Y. Ishikawa, K. Saito, I. Ikemoto, K. Murata, H. Anzai, T. Ishiguro: *Solid State Commun.* **66**, 405 (1988)
84. K. Yamaji: *Synth. Met. A* **27**, 115 (1988)
85. S. Gärtner, E. Gogu, I. Heinen, H.J. Keller, T. Klutz, D. Schweitzer: *Solid State Commun.* **65**, 1531 (1998)
86. N. Toyota, T. Sasaki, H. Sato, Y. Watanabe: *Physica C* **178**, 339 (1991)
87. I.D. Parker, R.H. Friend, M. Kurmoo, P. Day, C. Lenoir, P. Batail: *J. Phys. Cond. Mat.* **1**, 4479 (1989)
88. M. Kund, H. Müller, W. Biberacher, K. Andres: *Physica C* **191**, 274 (1993)
89. M.A. Tanatar, T. Ishiguro, T. Kondo, G. Saito: *Phys. Rev. B* **59**, 3841 (1999)
90. N.L. Wang, B.P. Clayman, H. Mori, S. Tanaka: *J. Phys.: Cond. Mat.* **12**, 2867 (2000)
91. B. Thoma: Diploma Thesis, Stuttgart University (1996), unpublished
92. L.K. Montgomery, R.M. Vestal, K.P. Starkey, B.W. Fravel, M.J. Samide, D.G. Peters, C.H. Mielke, J.D. Thompson, *Synth. Met.* **103**, 1878 (1999)
93. K. Murata, M. Ishibashi, Y. Honda, N.A. Fortune, M. Tokumoto, N. Kinoshita, H. Anzai: *Solid State Commun.* **76**, 377 (1990)
94. Y.V. Sushko, V.A. Bondarenko, R.A. Petrosov, N.D. Kushch, E.B. Yagubskii: *J. Phys. I France* **1**, 1375 (1991)
95. K. Kanoda: *Hyperfine Int.* **104**, 235 (1997)
96. K. Kanoda: *Physica C* **282 - 287**, 299 (1997)
97. J. Müller, M. Lang, F. Steglich, J.A. Schlueter, A.M. Kini, T. Sasaki: *Phys. Rev. B* **65**, 144521 (2002)
98. M. Lang, J. Müller, F. Steglich, J.A. Schlueter, A.M. Kini, T. Sasaki: *Synth. Met.* (2002), in press
99. T. Sasaki, N. Yoneyama, A. Matsuyama, N. Kobayashi: *Phys. Rev. B* **65**, 060505 (2002)

100. M. Weger, M. Tittelbach, E. Balthes, D. Schweitzer, H.J. Keller: J. Phys.: Cond. Mat. **5**, 8569 (1993)
101. M. Weger, M. Kaveh, H. Gutfreund: Solid State Commun. **37**, 421 (1981)
102. M. Weger, D. Schweitzer: Synth. Met. **70**, 889 (1995)
103. M. Weger: Acta Physica Polonica A **87**, 723 (1995)
104. L.I. Buravov, A.V. Zvarykina, N.D. Kushch, V.N. Laukhin, V.A. Merzhanov, A.G. Khomenko, E.B. Yagubskii: Sov. Phys. JETP **68**, 182 (1989)
105. R.H. McKenzie, P. Moses: Phys. Rev. Lett. **81**, 4492 (1998)
106. J. Singleton, P.A. Goddard, A. Ardavan, N. Harrison, S.J. Blundell, J.A. Schlueter, A.M. Kini: Phys. Rev. Lett. **88**, 037001 (2002)
107. C.S. Jacobsen: In: *Low-Dimensional Conductors and Superconductors*. ed. by D. Jérôme and L.G. Caron (Plenum Press, New York 1987) p. 253
108. A. Graja: 'Optical Properties'. In: *Organic Conductors, Fundamentals and Applications*. ed. by J.-P. Farges (M. Dekker, New York 1994) pp. 229–267
109. M. Dressel: Synth. Met. **85**, 1503 (1997)
110. L. Degiorgi, V. Vescoli, W. Henderson, G. Gruner, L.K. Montgomery: J. Phys. IV France **10**, Pr3-103 (2000)
111. M. Dressel: 'Optical properties of layered organic superconductors'. In: *Studies of High Temperature Superconductors*, Vol. **34**. (Nova Science, New York 2000)
112. J.E. Eldridge, Y. Lin, H.H. Wang, J.M. Williams, A.M. Kini: Phys. Rev. B **57**, 597 (1998)
113. Y. Lin, J.E. Eldridge, J.A. Schlueter, H.H. Wang, A.M. Kini: Phys. Rev. B **64**, 024506 (2001)
114. C.S. Jacobsen, D.B. Danner, K. Bechgaard: Phys. Rev. Lett. **46**, 1142 (1981); Phys. Rev B **28**, 7019 (1983); C.S. Jacobsen, K. Mortensen, M. Weger, K. Bechgaard: Solid State Commun. **38**, 423 (1981)
115. D. Pedron, R. Bozio, M. Meneghetti, C. Pecile: Phys. Rev B **49**, 10893 (1994)
116. F. Zwick, S. Brown, G. Margaritondo, C. Merlic, M. Onellion, J. Voit, M. Grioni: Phys. Rev. Lett. **79**, 3982 (1997)
117. F. Zwick, D. Jérôme, G. Margaritondo, M. Onellion, J. Voit, M. Grioni: Phys. Rev. Lett. **81**, 2974 (1998)
118. K. Kornelsen, J.E. Eldridge, H.H. Wang, J.M. Williams: Phys. Rev. B **44**, 5235 (1991)
119. K. Kornelsen, J.E. Eldridge, H.H. Wang, H.A. Charlier, J.M. Williams: Solid State Commun. **81**, 343 (1992)
120. N.O. Lipari, M.J. Rice, C.B. Duke, R. Bozio, A. Girlando, C. Pecile: Int. Quantum Chem. Symp. **11**, 583 (1977)
121. Important references are [118,122,55,123], see [9,111] for both earlier and more recent citations.
122. J.E. Eldridge, C.C. Homes, J.M. Williams, A.M. Kini, H.H. Wang: Spectrochim. Acta A **51**, 947 (1995)
123. G. Visentini, M. Masino, C. Bellitto, A. Girlando: Phys. Rev. B **58**, 9460 (1998)
124. M.E. Kozlov, K.I. Pokhodnia, A.A. Yurchenko: Spectrochim. Acta A **43**, 323 (1987)
125. M.E. Kozlov, K.I. Pokhodnia, A.A. Yurchenko: Spectrochim. Acta A **45**, 437 (1989)
126. M. Meneghetti, R. Bozio, C. Pecile: J. Phys. **47**, 1377 (1986)

127. A.M.Kini, K.D. Carlson, H.H. Wang, J.A. Schlueter, J.D. Dudek, S.A. Sirchio, U. Geiser, K.R. Lykke, J.M. Williams: *Physica C* **264**, 81 (1996); A.M.Kini, K.D. Carlson, J.D. Dudek, U. Geiser, H.H. Wang, J.M. Williams: *Synth. Met.* **85**, 1617 (1997)
128. A. Nowack, M. Weger, D. Schweitzer, H. Keller: *Solid State Commun.* **60**, 199 (1986)
129. A. Nowack, U. Poppe, M. Weger, D. Schweitzer, H. Schenk: *Z. Phys. B* **68**, 41 (1987)
130. S. Sugai, H. Mori, H. Yamochi, G. Saito: *Phys. Rev. B* **47**, 14374 (1993)
131. K.I. Pokhodnia, A. Graja, M. Weger, D. Schweitzer: *Z. Phys. B* **90**, 127 (1993)
132. M. Dressel, J.E. Eldridge, J.M. Williams, H.H. Wang: *Physica C* **203**, 247 (1992)
133. A. Andrieux, D. Jérôme, K. Bechgaard: *J. Phys. (Paris) Lett.* **42**, L87 (1981)
134. E. Barthel, G. Quirion, P. Wzietek, D. Jérôme, J.B. Christensen, M. Jorgensen, K. Bechgaard: *Europhys. Lett.* **21**, 87 (1993)
135. K. Mortensen, Y. Tomkiewicz, K. Bechgaard: *Phys. Rev. B* **25**, 3319 (1982)
136. R.L. Greene, E.M. Engler: *Phys. Rev. Lett.* **45**, 1587 (1980)
137. D. Jérôme: *Science* **252**, 1509 (1991)
138. H. Mayaffre, P. Wzietek, C. Lenoir, D. Jérôme, P. Batail: *Europhys. Lett.* **28**, 205 (1994)
139. H. Mayaffre, P. Wzietek, S. Charfi-Kaddour, C. Lenoir, D. Jérôme, P. Batail: *Physica B* **206 & 207**, 767 (1995)
140. A. Kawamoto, K. Miyagawa, Y. Nakazawa, K. Kanoda: *Phys. Rev. Lett.* **74**, 3455 (1995)
141. A. Kawamoto, K. Miyagawa, Y. Nakazawa, K. Kanoda: *Phys. Rev. B* **52**, 15522 (1995)
142. S.M. De Soto, C.P. Slichter, A.M. Kini, H.H. Wang, U. Geiser, J.M. Williams: *Phys. Rev. B* **52**, 10364 (1995)
143. P. Wzietek, H. Mayaffre, D. Jérôme, S. Brazovskii: *J. Phys. I France* **6**, 2011 (1996)
144. V. Kataev, G. Winkel, D. Khomskii, D. Wohlleben, W. Crump, K.F. Tebbe, J. Hahn: *Solid State Commun.* **83**, 435 (1992)
145. K. Frikach, M. Poirier, M. Castonguay, K.D. Truong: *Phys. Rev. B* **61**, R6491 (2000)
146. T. Shimizu, N. Yoshimoto, M. Nakamura, M. Yoshizawa: *Physica B* **281 & 282**, 896 (2000)
147. Y. Lin, J.E. Eldridge, H.H. Wang, A.M. Kini, J.M. Williams, J.A. Schlueter: *Phys. Rev. B* **58**, R599 (1998)
148. J. Merino, R.H. McKenzie: *Phys. Rev. B* **62**, 16442 (2000)
149. J. Merino, R.H. McKenzie: *Phys. Rev. B* **61**, 7996 (2000)
150. M. Kund, K. Andres, H. Müller, G. Saito: *Physica B* **203**, 129 (1994)
151. J. Müller, M. Lang, F. Steglich, J.A. Schlueter, A.M. Kini, U. Geiser, J. Mottasham, R.W. Winter, G.L. Gard, T. Sasaki, N. Toyota, *Phys. Rev. B* **61**, 11739 (2000)
152. U. Welp, S. Fleshler, W.K. Kwok, G.W. Crabtree, K.D. Carlson, H.H. Wang, U. Geiser, J.M. Williams, V.M. Hitsman: *Phys. Rev. Lett.* **69**, 840 (1992)
153. K. Miyagawa, A. Kawamoto, Y. Nakazawa, K. Kanoda: *Phys. Rev. Lett.* **75**, 1174 (1995)
154. M. Pinterić, M. Miljak, N. Biškup, O. Milat, I. Aviani, S. Tomić, D. Schweitzer, W. Strunz, I. Heinen: *Eur. Phys. J B* **11**, 217 (1999)

155. K. Miyagawa, A. Kawamoto, K. Uchida, K. Kanoda: *Physica B* **284** - **288**, 1589 (2000)
156. H. Posselt, H. Müller, K. Andres, G. Saito: *Phys. Rev. B* **49**, 15849 (1994)
157. M.A. Tanatar, T. Ishiguro, H. Ito, M. Kubota, G. Saito: *Phys. Rev. B* **55**, 12529 (1997)
158. M. Tokumoto, H. Anzai, K. Murata, K. Kajimura, T. Ishiguro: *Japan J. Appl. Phys.* **26** Suppl. 26-3, 1977 (1987)
159. J.P. Pouget, S. Ravy: *J. Phys. I France* **6**, 1501 (1996)
160. S. Ravy, R. Moret, J.P. Pouget: *Phys. Rev. B* **38**, 4469 (1988)
161. S. Tomic et al.: *J. Phys. C3* **44**, 1083 (1983)
162. H. Schwenk, K. Andres, F. Wudl: *Phys. Rev. B* **29**, 500 (1984)
163. T. Takahashi, D. Jérôme, K. Bechgaard: *J. Physique Lett.* **43**, L565 (1982)
164. K. Mortensen, C.S. Jacobsen, A. Lindegaard-Andersen, K. Bechgaard: *J. Physique* **44**, C3-963 (1983)
165. H. Yang, J.C. Lasjaunias, P. Monceau: *J. Phys.: Cond. Mat.* **12**, 7183 (2000)
166. K. Saito, H. Akutsu, M. Sorai: *Solid State Commun.* **111**, 471 (1999)
167. H. Akutsu, K. Saito, M. Sorai: *Phys. Rev. B* **61**, 4346 (2000)
168. A. Sato, H. Akutsu, K. Saito, M. Sorai: *Synth. Met.* **120**, 1035 (2001)
169. For a review, see e.g.: R.W. Cahn (editor): 'Glasses and Amorphous Materials'. In: *Materials Science and Technology* Vol. **9** (Verlag Chemie, Weinheim 1991) p. 137; W. Kauzmann: *The nature of the glassy state and the behavior of liquids at low temperatures*, *Chem. Rev.* **43**, 219 (1948)
170. M.A. deBolt, A.J. Easteal, P.B. Macedo, and C.T. Moynihan: *J. Am. Ceram. Soc.* **59**, 16 (1976)
171. P. Nagel, V. Pasler, C. Meingast, A.I. Rykov, S. Tajima, *Phys. Rev. Lett.* **85**, 2376 (2000)
172. Y. Watanabe, H. Sato, T. Sasaki, N. Toyota: *J. Phys. Soc. Japan* **60**, 3608 (1991)
173. X. Su, F. Zuo, J.A. Schlueter, M.E. Kelly, J.M. Williams: *Phys. Rev. B* **57**, R14056 (1998)
174. X. Su, F. Zuo, J.A. Schlueter, M.E. Kelly, and J.M. Williams: *Solid State Commun.* **107**, 731 (1998)
175. A. Aburto, L. Fruchter, C. Pasquier: *Physica C* **303**, 185 (1998)
176. M. Pinterić, S. Tomić, M. Prester, D. Drobac, K. Maki: *cond-mat/0206574* (2002)
177. A. Kawamoto, K. Miyagawa, K. Kanoda: *Phys. Rev. B* **55**, 14140 (1997)
178. H. Ito, T. Ishiguro, T. Kondo, G. Saito: *Phys. Rev. B* **61**, 3243 (2000)
179. L. Balicas, K. Behnia, W. Kang, E. Canadell, P. Auban-Senzier, D. Jérôme, M. Ribault, J.M. Fabre: *J. Phys. I France* **4**, 1539 (1994)
180. D. Jaccard, H. Wilhelm, D. Jérôme, J. Moser, C. Carcel, J.M. Fabre: *J. Phys.: Cond. Mat.* **13**, L1 (2001)
181. F. Guo, K. Murata, A. Oda, Y. Mizuno, H. Yoshino: *J. Phy. Soc. Japan*, **69**, 2164 (2000)
182. H. Hirai, R. Kondo, M. Maesato, T. Shibata, S. Kagoshima: *Synth. Met.* **120**, 963 (2001)
183. M. Miyazaki, K. Kishigi, Y. Hasegawa: *J. Phy. Soc. Japan*, **69**, 997 (2000)
184. A. Kawamoto, H. Taniguchi, K. Kanoda: *J. Am. Chem. Soc.* **120**, 10984 (1998)
185. H. Taniguchi, A. Kawamoto, K. Kanoda: *Phys. Rev. B* **59**, 8424 (1999); *Physica B* **284-288**, 519 (2000)

186. Y. Nakazawa, H. Taniguchi, A. Kawamoto, and K. Kanoda: *Phys. Rev. B* **61**, R16295 (2000)
187. J. Müller: *Thermodynamische Untersuchungen an quasi-zweidimensionalen organischen Supraleitern*. PhD Thesis, Dresden University, Dresden (2001), (Shaker Verlag, Aachen 2002)
188. J.E. Schirber, E.L. Venturini, A.M. Kini, H.H. Wang, J.R. Witworth, J.M. Williams: *Physica C* **152**, 157 (1988)
189. J.E. Schirber, D.L. Overmyer, J.M. Williams, A.M. Kini, H.H. Wang: *Physica C* **170**, 231 (1990)
190. H. Ito, T. Ishiguro, M. Kubota, G. Saito: *J. Phys. Soc. Japan* **65**, 2987 (1996)
191. S. Lefebvre, P. Wzietek, S. Brown, C. Bourbonnais, D. Jérôme, C. Mézière, M. Fourmigué, P. Batail: *Phys. Rev. Lett.* **85**, 5420 (2000)
192. A. Sato, E. Ojima, H. Akutsu, H. Kobayashi, A. Kobayashi, P. Cassoux: *Chem. Lett.* **1998**, 673 (1998)
193. F. Goze, V.N. Laukhin, L. Brossard, A. Audouard, J.P. Ulmet, S. Azkenazy, T. Naito, H. Kobayashi, A. Kobayashi, M. Tokumoto, P. Cassoux: *Physica B* **211**, 290 (1995)
194. L. Brossard, R. Clerac, C. Coulon, M. Tokumoto, T. Ziman, D.K. Petrov, V.N. Laukhin, M.J. Naughton, A. Audouard, F. Goze, A. Kobayashi, H. Kobayashi, P. Cassoux: *Eur. Phys. J. B* **1**, 439 (1998)
195. C. Hotta, H. Fukuyama: *J. Phys. Soc. Japan* **69**, 2577 (2000)
196. A.F. Hebard, M.J. Rosseinsky, R.C. Haddon, D.W. Murphy, S.H. Glarum, T.T.M. Palstra, A.P. Ramirez, A.R. Kortan: *Nature (London)* **350**, 600 (1991)
197. V.G. Kogan: *Phys. Rev. B* **24**, 1572 (1981)
198. W.E. Lawrence, S. Doniach: In: *Proceedings to the Twelfth International Conference on Low-Temperature Physics*, Kyoto 1970. ed. E. Kanada (Keigaku, Tokyo 1971) p. 361
199. R. Kleiner, F. Steinmeyer, G. Kunkel, P. Müller: *Phys. Rev. Lett.* **68**, 2394 (1992)
200. P. Müller: *Advances in Solid State Physics* **34** (Vieweg-Verlag, Braunschweig 1994)
201. U. Geiser, J.A. Schlueter, H.H. Wang, A.M. Kini, J.M. Williams, P.P. Sche, H.I. Zakowicz, M.L. VanZile, J.D. Dudek, P.G. Nixon, R.W. Winter, G.L. Gard, J. Ren, M.-H. Whangbo: *J. Am. Chem. Soc.* **118**, 9996 (1996)
202. J.A. Schlueter, U. Geiser, J.M. Williams, J.D. Dudek, M.E. Kelly, J.P. Flynn, R.R. Wilson, H.I. Zakowicz, P.P. Sche, D. Naumann, T. Roy, P.G. Nixon, R.W. Winter, G.L. Gard, *Synth. Met.* **85**, 1453 (1997)
203. T.P. Orlando, E.J. McNiff, Jr., S. Foner, M.R. Beasley: *Phys. Rev. B* **19**, 4545 (1979)
204. M. Tinkham: *Introduction to Superconductivity*, 2nd edn. (McGraw-Hill, New York 1996)
205. M. Lang, F. Steglich, N. Toyota, T. Sasaki: *Phys. Rev. B* **49**, 15227 (1994)
206. D.E. Farrell, C.J. Allen, R.C. Haddon, S.V. Chichester: *Phys. Rev. B* **42**, 8694 (1990)
207. S. Kawamata, K. Okuda, T. Sasaki, N. Toyota: *Solid State Commun.* **89**, 955 (1994)
208. J.C. Martinez, S.H. Brongersma, A. Koshelev, B. Ivlev, P.H. Kes, R.P. Griessen, D.G. de Groot, Z. Tarnavski, A.A. Menovsky: *Phys. Rev. Lett.* **69**, 2276 (1992)

209. Y. Matsuda, Marat B. Gaifullin, K. Kumagai, M. Kosugi, K. Hirata: Phys. Rev. Lett. **78**, 1972 (1997)
210. W.J. Skocpol, M. Tinkham: Rep. Prog. Phys. **38**, 1049 (1975)
211. U. Welp, S. Fleshler, W.K. Kwok, R.A. Klemm, V.M. Vinokur, J. Downey, B. Veal, G.W. Crabtree, Phys. Rev. Lett. **67**, 3180 (1991)
212. V. Pasler: PhD Thesis, Karlsruhe University, Karlsruhe (2000)
213. G. Bergmann: Z. Phys. **225**, 430 (1969)
214. P.A. Lee, S.R. Shenoy: Phys. Rev. Lett. **28**, 1025 (1972)
215. R. Ikeda, T. Ohmi, T. Tsuneto: J. Phys. Soc. Japan **59**, 1397 (1990)
216. S. Ullah, A.T. Dorsey: Phys. Rev. B **44**, 262 (1991)
217. Q. Li: In: *Physical Properties of High-Temperature Superconductors* Vol. **V**. ed. by D.M. Ginsberg (World Scientific, Singapore 1996)
218. S. Friemel, C. Pasquier, Y. Loirat, D. Jérôme: Physica C **259**, 181 (1996)
219. H. Ito, M. Watanabe, Y. Nogami, T. Ishiguro, T. Komatsu, G. Saito, N. Hosoi: Jpn. J. Appl. Phys. Series **7**, 419 (1992)
220. J.S. Brooks, X. Chen, S.J. Klepper, S. Valfells, G.J. Athas, Y. Tanaka, T. Kinoshita, N. Kinoshita, M. Tokumoto, H. Anzai, C.C. Agosta: Phys. Rev. B **52**, 14457 (1995)
221. D. Chasseau, J. Gaultier, M. Rahal, L. Ducasse, M. Kurmoo, P. Day: Synth. Met. **41-43**, 2039 (1991)
222. M. Rahal, D. Chasseau, J. Gaultier, L. Ducasse, M. Kurmoo, P. Day: Acta Cryst. B **53**, 159 (1997)
223. G. Gladstone, M.A. Jensen, J.R. Schrieffer: In: *Superconductivity* Vol. **2**. ed. by R.D. Parks (M. Dekker, New York 1969) p. 655
224. C. Meingast, B. Blank, H. Bürkle, B. Obst, T. Wolf, H. Wühl, V. Selvamannickam, K. Salama: Phys. Rev. B **41**, 11299 (1990)
225. H. Kusunohara, Y. Sakata, Y. Ueba, K. Tada, M. Kaji, T. Ishiguro: Solid State Commun. **74**, 251 (1990)
226. C.E. Campos, J.S. Brooks, P.J.M. van Bentum, J.A.A.J. Perenboom, S.J. Klepper, P.S. Sandhu, S. Valfells, Y. Tanaka, T. Kinoshita, N. Kinoshita, M. Tokumoto, H. Anzai: Phys. Rev. B **52**, R7014 (1995)
227. S. Kagoshima, M. Maesato, R. Kondo, T. Shibata, H. Hirai: Synth. Met. **120**, 683 (2001); M. Maesato, Y. Kaga, R. Kondo, H. Hirai, S. Kagoshima: Synth. Met. **120**, 941 (2001)
228. E.S. Choi, J.S. Brooks, S.Y. Han, L. Balicas. J.S. Qualls: Phil. Mag. B **81**, 399 (2001)
229. M. Kund, H. Veith, H. Müller, K. Andres, G. Saito: Physica C **221**, 119 (1994)
230. M. Kund, J. Lehrke, W. Biberacher, A. Lerf, K. Andres: Synth. Met. **70**, 949 (1995)
231. S. Sadewasser, C. Looney, J.S. Schilling, J.A. Schlueter, J.M. Williams, P.G. Nixon, R.W. Winter, G.L. Gard: Solid State Commun. **102**, 571 (1997)
232. T. Biggs, A.-K. Klehe, J. Singleton, D. Bakker, J. Symington, P. Goddard, A. Ardavan, W. Hayes, J.A. Schlueter, T. Sasaki, M. Kurmoo: J. Phys.: Cond. Mat. **14**, L495 (2002)
233. J. Müller, M. Lang, J.A. Schlueter, U. Geiser, D. Schweitzer: Synth. Met. **120**, 855 (2001)
234. P.B. Allen, R.C. Dynes: Phys. Rev. B **12**, 905 (1975)
235. H. Kino, H. Fukuyama: J. Phys. Soc. Japan **65**, 2158 (1996)
236. H. Kondo, T. Moriya: Physica B **281 & 282**, 940 (2000)

237. A. Painelli, A. Girlando, A. Fortunelli: *Phys. Rev. B* **64**, 054509 (2001)
238. A.M. Kini, J.A. Schlueter, B.H. Ward, U. Geiser, H.H. Wang, *Synth. Met.* **120**, 713 (2001)
239. J.A. Schlueter, A.M. Kini, B.H. Ward, U. Geiser, H.H. Wang, J. Mohtasham, R.W. Winter, G.L. Gard: *Physica C* **351**, 261 (2001)
240. Y. Watanabe, T. Shimazu, T. Sasaki, N. Toyota: *Synth. Met.* **86**, 1917 (1997)
241. J.M. Williams, A.J. Schultz, U. Geiser, K.D. Carlson, A.M. Kini, H.H. Wang, W.K. Kwok, M.-H. Whangbo, J.E. Schirber: *Science* **252**, 1501 (1991)
242. R.S. Edwards, A. Narduzzo, J. Singleton, A. Ardavan, J.A. Schlueter: *cond-mat/0208086* (2002)
243. D. Mailly, M. Ribault, K. Bechgaard: *J. Physique* **44**, C3-1037 (1983)
244. P. Garoche, R. Brusetti, D. Jérôme, K. Bechgaard: *J. Physique Lett.* **43**, L147 (1982)
245. K. Murata, M. Tokumoto, H. Anzai, K. Kajimura, T. Ishiguro: *Jpn. J. Appl. Phys.* **26**, Suppl. 26-3, 1367 (1987)
246. A.M. Clogston: *Phys. Rev. Lett.* **9**, 266 (1962)
247. B.S. Chandrasekhar: *Appl. Phys. Lett.* **1**, 7 (1962)
248. R.L. Greene, P. Haen, S.Z. Huang, E.M. Engler, M.Y. Choi, P.M. Chaikin: *Mol. Cryst. Liq. Cryst.* **79**, 539 (1982)
249. P.M. Chaikin, M.Y. Choi, R.L. Greene: *J. Magn. Magn. Mater.* **31**, 1268 (1983)
250. I.J. Lee, M.J. Naughton, G.M. Danner, P.M. Chaikin: *Phys. Rev. Lett.* **78**, 3555 (1997)
251. H. Schwenk, K. Andres, F. Wudl, E. Aharon-Shalom: *Solid State Commun.* **45**, 767 (1983)
252. Y. Shimojo, A.E. Kovalev, S. Kamiya, E. Ohmichi, T. Ishiguro, H. Yamochi, G. Saito, A. Ayari, P. Monceau: *Physica B* **294-295**, 427 (2001)
253. H. Mayaffre, P. Wzietek, D. Jérôme, C. Lenoir, P. Batail: *Phys. Rev. Lett.* **75**, 4122 (1995)
254. C. Mielke, J. Singleton, M.-S. Nam, N. Harrison, C.C. Agosta, B. Fravel, L.K. Montgomery: *J. Phys.: Cond. Mat.* **13**, 8325 (2001)
255. T. Kawasaki, M.A. Tanatar, T. Ishiguro, H. Tanaka, A. Kobayashi, H. Kobayashi: *Synth. Met.* **120**, 771 (2001)
256. F. Zuo, J.S. Brooks, R.H. McKenzie, J.A. Schlueter, J.M. Williams: *Phys. Rev. B* **61**, 750 (2000)
257. J. Singleton, J.A. Symington, M.S. Nam, A. Ardavan, M. Kurmoo, P. Day: *J. Phys.: Cond. Mat.* **12**, L641 (2001)
258. M.A. Tanatar, T. Ishiguro, H. Tanaka, A. Kobayashi, H. Kobayashi: *J. Supercond.* **12**, 511 (1999)
259. J. Hagel, S. Wanka, D. Beckmann, J. Wosnitza, D. Schweitzer, W. Strunz, M. Thumfart: *Physica C* **291**, 213 (1997)
260. M. Dressel, O. Klein, G. Grüner, K.D. Carlson, H.H. Wang, J.M. Williams: *Phys. Rev. B* **50**, 13603 (1994)
261. P.A. Mansky, P.M. Chaikin, R.C. Haddon: *Phys. Rev. B* **50**, 15929 (1994)
262. M. Pinterić, S. Tomić, M. Prester, D. Drobac, O. Milat, K. Maki, D. Schweitzer, I. Heinen, W. Strunz: *Phys. Rev. B* **61**, 7033 (2000)
263. D.R. Harshman, R.N. Kleiman, R.C. Haddon, S.V. Chichester-Hicks, M.L. Kaplan, L.W. Rupp Jr., T. Pfiz, D.L. Williams, D.B. Mitzi: *Phys. Rev. Lett.* **64**, 1293 (1990)

264. M. Lang, N. Toyota, T. Sasaki, H. Sato: Phys. Rev. Lett. **69**, 1443 (1992)
265. M. Lang, N. Toyota, T. Sasaki, H. Sato: Phys. Rev. B **46**, 5822 (1992)
266. D. Achkir, M. Poirier, C. Bourbonnais, G. Quirion, C. Lenoir, P. Batail, D. Jérôme: Phys. Rev. B **47**, 11595 (1993)
267. H. Elsinger, J. Wosnitza, S. Wanka, J. Hagel, D. Schweitzer, W. Strunz: Phys. Rev. Lett. **84**, 6098 (2000)
268. J.E. Graebner, R.C. Haddon, S.V. Chichester, S.H. Glarum: Phys. Rev. B **41**, 4808 (1990)
269. P. Fulde, R.A. Ferrell: Phys. Rev. **135**, A550 (1964)
270. A.I. Larkin, Y.N. Ovchinnikov: Sov. Phys. JETP **20**, 762 (1965)
271. J.A. Symington, J. Singleton, M.-S. Nam, A. Ardavan, M. Kurmoo, P. Day: Physica B **294-295**, 418 (2001)
272. T. Ishiguro: J. Phys. IV France **10**, Pr3-139 (2000)
273. G. Blatter, M.V. Feigel'man, V.B. Geshkenbein, A.I. Larkin, V.M. Vinokur: Rev. Mod. Phys. **66**, 1125 (1994)
274. E. Zeldov, D. Majer, M. Konczykowski, V.B. Geshkenbein, V.M. Vinokur, H. Shtrikman: Nature **375**, 373 (1995)
275. S. Schilling, R.A. Fisher, N.E. Phillips, U. Welp, D. Dasgupta, W.K. Kwok, G.W. Crabtree: Nature **382**, 791 (1996)
276. J.R. Clem: Phys. Rev. B **43**, 7837 (1991)
277. T. Sasaki, W. Biberacher, K. Neumaier, W. Hehn, K. Andres, T. Fukase: Phys. Rev. B **56**, 10889 (1998)
278. M. Inada, T. Sasaki, T. Nishizaki, N. Kobayashi, S. Yamada, T. Fukase: J. Low Temp. Phys. **117**, 1423 (1999)
279. S.L. Lee, F.L. Pratt, S.J. Blundell, C.M. Aegerter, P.A. Pattenden, K.H. Chow, E.M. Forgan, T. Sasaki, W. Hayes, H. Keller: Phys. Rev. Lett. **79**, 1563 (1997)
280. L.Ya. Vinnikov, T.L. Barkov, M.V. Kartsovnik, N.D. Kushch: Phys. Rev. B **61**, 14358 (2000)
281. T. Nishizaki, T. Sasaki, T. Fukase, N. Kobayashi: Phys. Rev. B **54**, R3760 (1996)
282. M.M. Mola, J.T. King, C.P. McRaven, S. Hill, J.S. Qualls, J.S. Brooks: Phys. Rev. B **62**, 5965 (2000)
283. M.M. Mola, S. Hill, J.S. Brooks, J.S. Qualls: Phys. Rev. Lett. **86**, 2130 (2001)
284. T. Shibauchi, M. Sato, S. Ooi, T. Tamegai: Phys. Rev. B **57**, R5622 (1998)
285. N. Yoneyama, A. Higashihara, T. Sasaki, N. Kobayashi, S. Yamada: Synth. Met. (2002), in press
286. L. Fruchter, A. Aburto, C. Pham-Phu: Phys. Rev. B **56**, R2936 (1997)
287. F. Steinmeyer, R. Kleiner, P. Müller, H. Müller, K. Winzer: Europhys. Lett. **25**, 459 (1994)
288. H. Shimahara: J. Phys. Soc. Japan **66**, 541 (1997)
289. H. Shimahara: J. Phys. Soc. Japan **67**, 1872 (1998)
290. H. Shimahara: Phys. Rev. B **50**, 12760 (1994)
291. M. Tachiki, S. Takahashi, P. Gegenwart, M. Weiden, M. Lang, C. Geibel, F. Steglich, R. Modler, C. Paulsen, Y. Ōnuki: Z. Phys. B **100**, 369 (1996)
292. P. Gegenwart, M. Deppe, M. Köppen, F. Kromer, M. Lang, R. Modler, M. Weiden, C. Geibel, F. Steglich, T. Fukase, N. Toyota: Ann. Physik **5**, 307 (1996)
293. S. Uji, H. Shinagawa, T. Terashima, T. Yakabe, Y. Terai, M. Tokumoto, A. Kobayashi, H. Tanaka, H. Kobayashi: Nature, **410**, 908 (2001)

294. L. Balicas, J.S. Brooks, K. Storr, S. Uji, M. Tokumoto, H. Tanaka, H. Kobayashi, A. Kobayashi, V. Barzykin, L.P. Gor'kov: Phys. Rev. Lett. **87**, 0670021 (2001)
295. S. Uji, C. Terakura, T. Terashima, T. Yakabe, Y. Imanaka, Y. Terai, S. Yasuzuka, M. Tokumoto, F. Sakai, A. Kobayashi, H. Tanaka, H. Kobayashi, L. Balicas, J.S. Brooks: Synth. Met. (2002), in press
296. J. Bardeen, L.N. Cooper, J.R. Schrieffer: Phys. Rev. **108**, 1175 (1957)
297. F. Steglich, J. Aarts, C.D. Bredl, W. Lieke, D. Meschede, W. Franz, H. Schäfer: Phys. Rev. Lett. **43**, 1892 (1979)
298. J.G. Bednorz, K.A. Müller: Z. Phys. B **64**, 189 (1986)
299. Y. Maeno, H. Hashimoto, K. Yoshida, D. Nishizaki, T. Fujita, J.G. Bednorz, F. Lichtenberg: Nature **372**, 532 (1994)
300. S. Mazumdar: Solid State Commun. **66**, 427 (1988)
301. Y.J. Uemura, L.P. Le, G.M. Luke, B.J. Sternlieb, W.D. Wu, J.H. Brewer, T.M. Riseman, C.L. Seaman, M.B. Maple, M. Ishikawa, D.G. Hinks, J.D. Jorgensen, G. Saito, H. Yamochi: Phys. Rev. Lett. **66**, 2665 (1991)
302. W.A. Little: 'Organic Conductors: An Overview'. In: *Organic Conductors, Fundamentals and Applications*. ed. by J.-P. Farges (M. Dekker, New York 1994) pp. 1–24
303. K. Yamaji: Solid State Commun. **61**, 413 (1987)
304. A. Girlando, M. Masino, A. Brillante, R.G. Della Valle, E. Venuti: Phys. Rev. B **66**, 100507(R) (2002)
305. A. Girlando, M. Masino, G. Visentini, R.G. Della Valle, A. Brillante, E. Venuti: Phys. Rev. B **62**, 14476 (2000)
306. G. Varelogiannis: Phys. Rev. Lett. **88**, 117005 (2002)
307. J. Schmalian: Phys. Rev. Lett. **81**, 4232 (1998)
308. E. Demiralp, W.A. Goddard III: Phys. Rev. B **56**, 11907 (1997)
309. H. Kondo, T. Moriya: J. Phys. Soc. Japan **67**, 3695 (1998)
310. H. Kondo, T. Moriya: J. Phys.: Cond. Mat. **11**, L363 (1999)
311. H. Kondo, T. Moriya: J. Phys. Soc. Japan **68**, 3170 (1999)
312. H. Kino, H. Kontani: J. Phys. Soc. Japan **67**, 3691 (1998)
313. M. Vojta, E. Dagotto: Phys. Rev. B **59**, R713 (1999)
314. K. Kuroki, H. Aoki: Phys. Rev. B **60**, 3060 (1999)
315. T. Jujo, K. Yamada: J. Phys. Soc. Japan **68**, 1331 (1999)
316. H. Kino, H. Kontani: J. Phys. Soc. Japan **68**, 1481 (1999)
317. T. Jujo, K. Yamada: J. Phys. Soc. Japan **68**, 2198 (1999)
318. R. Louati, S. Charfi-Kaddour, A. Ben Ali, R. Bennaceur, M. Héritier: Phys. Rev. B **62**, 5957 (2000)
319. J. Marino, R.H. McKenzie: Phys. Rev. Lett. **87**, 237002 (2001)
320. K. Maki: In: *Superconductivity* Vol. **2**. ed. by R.D. Parks (M. Dekker, New York 1969) p. 1035
321. A.A. Abrikosov, L.P. Gor'kov: Sov. Phys. JETP **12**, 1243 (1969)
322. H. Keiber, C. Geibel, B. Renker, H. Rietschel, H. Schmidt, H. Wühl, G.R. Stewart: Phys. Rev. B **30**, 2542 (1984)
323. B. Lüthi, M. Herrmann, W. Assmus, H. Schmidt, H. Rietschel, H. Wühl, U. Gottwick, G. Sparn, F. Steglich: Z. Phys. B. **60**, 387 (1985)
324. M. Jourdan, M. Huth, H. Adrian: Nature **398**, 47 (1999)
325. N.K. Sato, N. Aso, K. Miyake, S. Shiina, P. Thalmeier, G. Varelogiannis, C. Geibel, F. Steglich, P. Fulde, T. Komatsubara: Nature **410**, 340 (2001)

326. C.C. Tsuei, J.R. Kirtley, C.C. Chi, Lock See Yu-Jahnes, A. Gupta, T. Shaw, J.Z. Sun, M.B. Ketchen: Phys. Rev. Lett. **73**, 593 (1994)
327. D.J. van Harlingen: 'Phase-sensitive tests of the symmetry of the pairing state in the high-temperature superconductors - Evidence for $d_{x^2-y^2}$ symmetry', Rev. Mod. Phys. **67**, 515 (1995)
328. P. Auban-Senzier, C. Bourbonnais, D. Jérôme, C. Lenoir, P. Batail, E. Canadell, J.P. Buisson, S. Lefrant: J. Phys. I France **3**, 871 (1993)
329. K.D. Carlson, J.N. Williams, U. Geiser, A.M. Kini, H.H. Wang, R.A. Klemm, S.K. Kumar, J.A. Schlueter, J.R. Ferraro, K.R. Lykke, P. Wurz, D.H. Parker, J.D.M. Sutin: Inorg. Chem. **114**, 10069 (1992)
330. J.D. Axe, G. Shirane: Phys. Rev. B **8**, 1965 (1973)
331. S.M. Shapiro, G. Shirane: Phys. Rev. B **12**, 4899 (1975)
332. N. Toyota, M. Lang, S. Ikeda, T. Kajitani, T. Shimazu, T. Sasaki, K. Shibata: Synth. Met. **86**, 2009 (1997)
333. R. Zeyher, G. Zwicknagl: Z. Phys. B **78**, 175 (1990)
334. J.M. Schrama, E. Rzepniewski, R.S. Edwards, J. Singleton, A. Ardavan, M. Kurmoo, P. Day: Phys. Rev. Lett. **83**, 3041 (1999)
335. T. Arai, K. Ichimura, K. Nomura, S. Takasaki, J. Yamada, S. Nakatsuji, H. Anzai: Phys. Rev. B **63**, 104518 (2001); Solid State Commun. **116**, 679 (2000)
336. J.M. Schrama, J. Singleton: Phys. Rev. Lett. **86**, 3453 (2001)
337. S. Hill, N. Harrison, M. Mola, J. Wosnitzer: Phys. Rev. Lett. **86**, 3451 (2001)
338. T. Shibauchi, Y. Matsuda, M.B. Gaifullin, T. Tamegai: Phys. Rev. Lett. **86**, 3452 (2001)
339. H. Bando, S. Kashiwaya, H. Tokumoto, H. Anzai, N. Kinoshita, K. Kajimura: J. Vac. Sci. Technol. A **8**, 479 (1990)
340. H. Won, K. Maki: Physica B **312-313**, 44 (2002)
341. D.J. Scalapino, E. Loh, Jr., J.E. Hirsch: Phys. Rev. B **35**, 6694 (1987)
342. K. Kanoda, K. Miyagawa, A. Kawamoto, Y. Nakazawa: Phys. Rev. B **54**, 76 (1996)
343. M.J. Graf, S.K. Yip, J.A. Sauls, D. Rainer : Phys. Rev. B **53**, 15147 (1996)
344. M.R. Norman, P.J. Hirschfeld: Phys. Rev. B **53**, 5706 (1996)
345. B. Mühlischlegel: Z. Phys. **155**, 313 (1959)
346. K. Kanoda, K. Akiba, K. Suzuki, T. Takahashi, G. Saito: Phys. Rev. Lett. **65**, 1271 (1990)
347. L.P. Le, G.M. Luke, B.J. Sternlieb, W.D. Wu, Y.J. Uemura, J.H. Brewer, T.M. Riseman, C.E. Stronach, G. Saito, H. Yamochi, H.H. Wang, A.M. Kini, K.D. Carlson, J.M. Williams: Phys. Rev. Lett. **68**, 1923 (1992)
348. A. Carrington, I.J. Bonalde, R. Prozorov, R.W. Giannetta, A.M. Kini, J.A. Schlueter, H.H. Wang, U. Geiser, J.M. Williams: Phys. Rev. Lett. **83**, 4172 (1999)
349. O. Klein, K. Holczer, G. Grüner, J.J. Chang, F. Wudl: Phys. Rev. Lett. **66**, 655 (1991)
350. I. Kosztin, Q.J. Chen, B. Janko, K. Levin: Phys. Rev. B **58**, R5936 (1998); Q.J. Chen, I. Kosztin, B. Janko, K. Levin: Phys. Rev. Lett. **81**, 4708 (1998); Q. Chen, I. Kosztin, K. Levin: Phys. Rev. Lett. **85**, 2801 (2000)
351. Y. Hasegawa, H. Fukuyama: J. Phys. Soc. Japan **56**, 877 (1987)
352. B. Andraka, J.S. Kim, G.R. Stewart, K.D. Carlson, H.H. Wang, J.M. Williams, Phys. Rev. B **40**, 11345 (1989)
353. Y. Nakazawa, K. Kanoda: Phys. Rev. B **55**, R8670 (1997)

354. In [353] the lattice specific heat of κ -(ET)₂Cu[N(CN)₂]Br was estimated by measuring a second, deuterated sample after quench cooling to suppress superconductivity. The data analysis in [353] is based on the assumption that by this procedure the lattice specific heat remains unaffected and is identical to that of the hydrogenated superconducting compound. In [267] it has been shown, however, that the so-derived phonon background differs substantially from that determined in an overcritical field. The reason for this might be related to the glass-like transition at T_g observed in this system [97], see section 3.4.
355. N. Momono, M. Ido: *Physica C* **264**, 311 (1996)
356. H. Padamsee, J.E. Neighbor, C.A. Shiffman, J. Low Temp. Phys. **12**, 387 (1973)
357. J. Wosnitza, X. Liu, D. Schweitzer, H.J. Keller: *Phys. Rev. B* **50**, 12747 (1994)
358. S. Wanka, J. Hagel, D. Beckmann, J. Wosnitza, J.A. Schlueter, J.M. Williams, P.G. Nixon, R.W. Winter, G.L. Gard, *Phys. Rev. B* **57**, 3084 (1998)
359. J. Solyom: *Adv. Phys.* **28**, 201 (1979)
360. M.Y. Choi, P.M. Chaikin, S.Z. Huang, P. Haen, E.M. Engler, R.L. Greene: *Phys. Rev. B* **25**, 6208 (1982)
361. S. Bouffard, M. Ribault, R. Brusetti, D. Jérôme, K. Bechgaard: *J. Phys. C* **15**, 2951 (1982)
362. C. Coulon, P. Delhaes, J. Amiell, J.P. Manceau, J.M. Fabre, L. Giral: *J. Phys. (Paris)* **43**, 1721 (1982)
363. S. Tomić, D. Jérôme, D. Mailly, M. Ribault, K. Bechgaard: *J. Phys. (Paris) Colloq.* **44**, C3-1075 (1983)
364. A.A. Abrikosov: *J. Low Temp. Phys.* **53**, 359 (1983)
365. L.P. Gor'kov, D. Jérôme: *J. Phys. (Paris) Lett.* **46**, L643 (1985)
366. M. Dressel: *Physica C* **317-318**, 89 (1999)
367. I.J. Lee, P.M. Chaikin, M.J. Naughton: *Phys. Rev. B* **62**, R14669 (2000)
368. M. Takigawa, H. Yasuoka, G. Saito: *J. Phys. Soc. Jpn.* **56**, 873 (1987)
369. S. Belin, K. Behnia: *Phys. Rev. Lett.* **79**, 2125 (1997)
370. I.J. Lee, P.M. Chaikin, M.J. Naughton: *Phys. Rev. B* **65**, 180502 (2002)
371. P. Fulde, K. Maki: *Phys. Rev.* **139**, A788 (1965)
372. I.J. Lee, S.E. Brown, W.G. Clark, M.J. Strouse, M.J. Naughton, W. Kang, P.M. Chaikin: *Phys. Rev. Lett.* **88**, 017004 (2002)
373. R.A. Klemm, A. Luther, M.R. Beasley: *Phys. Rev. B* **12**, 877 (1975)
374. X. Huang, K. Maki: *Phys. Rev. B* **39**, 6459 (1989)
375. A.G. Lebed': *JETP Lett.* **44**, 114 (1986); L.I. Burlachkov, L.P. Gor'kov, A.G. Lebed': *Europhys. Lett.* **4**, 941 (1987)
376. N. Dupuis, G. Montambaux, C.A.R. Sá de Melo: *Phys. Rev. Lett.* **70**, 2613 (1993)
377. I.J. Lee, D.S. Chow, W.G. Clark, J. Strouse, M.J. Naughton, P.M. Chaikin, S.E. Brown: *cond-mat/0001332*, (2000)

Index

- activation energy, 33, 34
- anion ordering, 32, 80
- anisotropic order parameter (see order parameter)
- anisotropy parameter, 43, 44, 58
- antiferromagnetic order, 30, 37, 41
- antiferromagnetic spin fluctuations, 20, 25–27, 63, 66

- band filling, 13, 14
- band structure, 5, 13, 50, 65
- bandwidth, 5, 16, 38, 66
- BCS
 - model, 63, 66, 75, 79
 - ratio, 52, 54, 71, 72, 79, 80
 - relation, 50
- Bechgaard salts, 6–8, 31, 80, 81
- BEDT-TSF, 5, 41, 42
- BEDT-TTF, 5–7, 41, 42, 51, 68
- BETS, 5, 12, 20, 41, 54
- B_{c1} , 52, 55, 56
- B_{c2} , 43, 52–56, 58, 60, 62, 81
- B_{cth} , 45, 52, 55–57

- carrier concentration, 5, 21, 42, 45
- charge transfer, 5, 13, 14
- coherence length, 43, 45, 53, 54, 56, 57, 76, 77
- cooling-rate dependence, 33–35, 40, 80
- crystal growth, 7

- density of states, 15, 24, 27, 38, 50, 55, 70
- density wave, 6, 20, 25, 30, 37, 40, 50, 66
- dimerization, 7–9, 13, 14, 16, 38
- Dingle temperature, 15
- disorder, 7, 9, 20, 31–33, 35, 40, 77, 80

- d*-wave superconductivity, 65–67, 72, 75, 76, 81

- eclipsed conformation, 9
- effective masses, 16, 17, 22, 43, 54
- electron-electron interaction/correlations, 16, 17, 21, 37, 63
- electron-intermolecular-phonon interaction/coupling (see also electron-phonon interaction), 23, 24, 70, 71
- electron-molecular-vibration (EMV) coupling (see also electron-phonon interaction), 23, 24, 68
- electron-phonon
 - coupling constant, 24, 50, 70
 - interaction/coupling, 16, 17, 22, 23, 37, 67, 69
- ET, 5, 8, 9, 20
- ethylene conformation, 9, 34, 40
- ethylene endgroups, 9, 20, 28, 33, 34, 40, 68, 70, 73, 77

- Fermi liquid, 13, 14, 19, 20, 22, 27
- Fermi surface, 13, 14, 16, 21, 22, 25, 27, 29, 31, 37, 39, 40, 51, 54, 63, 65, 66
- Fulde-Ferrell-Larkin-Ovchinnikov (FFLO) state, 55, 60, 82

- Ginzburg number, 45
- Ginzburg-Landau coherence length (see coherence length)
- glass-like transition, 28, 33, 39, 77

- half-filled band (see band filling)
- H-bonding, 9, 51
- highest occupied molecular orbital (HOMO), 13, 14, 23, 24, 50

- impurities, 31
- irreversibility line, 57–59, 77
- isotope effect, - substitution, 34, 50, 51, 68
- Josephson
 - coupling, 57
 - effect, 43
 - vortices, 57, 60
- Little’s model, 3, 64
- lock-in transition, 58
- London penetration depth (see penetration depth)
- lower critical field (see B_{c1})
- lowest unoccupied molecular orbital (LUMO), 13
- Luttinger liquid, 19, 22
- many-body effects, 16
- mean-field transition temperature, 45, 46, 53
- Mott-Hubbard insulating state, 31, 37, 65, 66
- nesting, 13, 25, 27, 31, 37, 38, 51, 66
- non-centrosymmetric anion, 7, 31
- order parameter, 42, 53, 55, 57, 60, 63, 64, 67, 68, 72, 75, 79–81
- overlap/transfer integral, 13, 18, 21, 22, 24, 36, 50, 54
- packing, 5, 8, 9, 51
- pancake vortices, 57, 58, 74
- Pauli-limiting field B_P , 52–55, 60, 62, 81
- penetration depth, 35, 43, 53, 56, 57, 67, 74–77
- pinning, 56, 58–60, 76, 77
- π -electrons, -orbital, 5, 6, 10, 13, 37, 50, 73
- resistance maximum, 19, 20, 31
- scaling behavior, 46
- spin fluctuations (see antiferromagnetic spin fluctuations)
- spin-singlet state, 52, 55, 60, 63, 74, 81
- spin-triplet state, 53, 80–82
- staggered conformation, 9
- superconducting fluctuations, 44, 45, 53
- s -wave superconductivity, 81
- σ -electrons, -orbital, 5, 13
- TCNQ, 5
- terminal ethylene groups (see ethylene endgroups)
- thermodynamic critical field (see $B_{c_{th}}$)
- TMTSF, 5, 6, 42
- TMTTF, 5
- TTF, 5, 6
- upper critical field (see B_{c2})
- van der Waals radius, 7, 8